

A YIELD FUNCTION TO SIMULATE EARING IN THE DEEP DRAWING OF ALUMINIUM

BY

G. D. THOMAS

A thesis submitted in partial fulfillment of the requirements for
the degree of Master of Science in Engineering

Department of Mechanical Engineering
University of Cape Town
Rondebosch 7700
South Africa

July 1996

The University of Cape Town has been given
the right to reproduce this thesis in whole
or in part. Copyright is held by the author.

The copyright of this thesis vests in the author. No quotation from it or information derived from it is to be published without full acknowledgement of the source. The thesis is to be used for private study or non-commercial research purposes only.

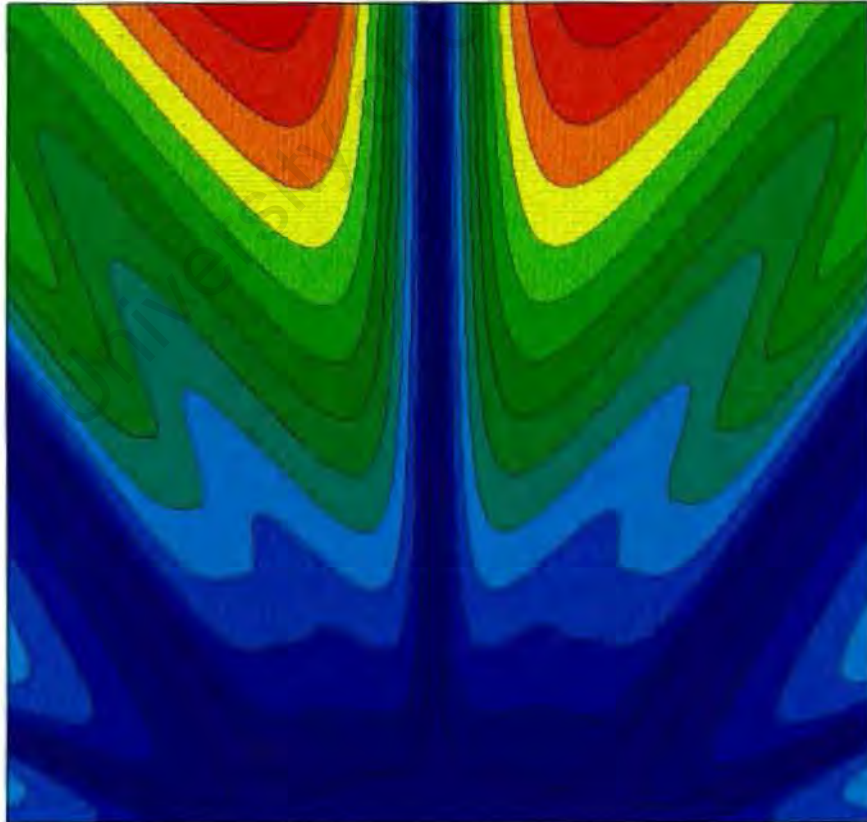
Published by the University of Cape Town (UCT) in terms of the non-exclusive license granted to UCT by the author.

"The fairest thing we can experience is the mysterious. It is the fundamental emotion which stands at the cradle of true art and true science. He who knows it not and can no longer wonder, no longer feel amazement, is as good as dead, a snuffed out candle."

Albert Einstein

"Science is not technology, it is not gadgetry, it is not some mysterious cult, it is not a great mechanical monster. Science is an adventure of the human spirit. It is an essentially artistic enterprise, stimulated largely by curiosity, served largely by disciplined imagination, and based largely on faith in the reasonableness, order, and beauty of the universe of which man is a part."

*Warren Weaver
Ex-President of the Sloan
Foundation*



University of Cape Town

Figure on previous page:
Iso-error plot of plastic integration
algorithm utilised in the constitutive
model presented in this work.

DECLARATION

This is to certify that the results, calculations and other work presented in this thesis are essentially my own, and that no part of it has been submitted for a degree at this or any other university.

Signed by candidate

Signature Removed

G. D. Thomas

July 1996

University of Cape Town

ACKNOWLEDGEMENTS

I would like to express my sincere thanks to the following people for their guidance and support during my studies:-

- My supervisor, Dr Greg Mitchell.
- My colleagues and friends at CERECAM, in particular Hellmut Bowles, Greg Starke and Jean Irving.
- My parents, family and friends for their unconditional support.

I would also like to thank the FRD, CERECAM and Hulett Aluminium (Pty) Ltd for their financial support.

SYNOPSIS

Deep drawing of metal sheeting is a commercially significant manufacturing process and as with all metal forming processes is subject to geometric defects. One defect of particular concern, termed *earing*, is characterised by an uneven edge to the drawn article. This work covers the implementation of a suitable constitutive model in a general purpose finite element code ABAQUS Version 5.4 to simulate this earing phenomenon in aluminium can body stock.

Earing is caused by plastic anisotropy of the blank material and anisotropy induced during the drawing process. It is the result of crystallographic textures or preferred grain orientations that develop during the sheet rolling process. In polycrystalline materials it may be modelled via either crystallographic texture models or phenomenological yield surface models. Crystallographic models have the advantage over phenomenological ones in that they are able to describe both initial *and* evolving anisotropy. However, they are very demanding in terms of computational power and are reported to over predict the plastic strain ratios in anisotropic materials.

A phenomenological yield surface model proposed by Karafillis and Boyce was consequently selected as a suitable constitutive model to investigate the earing phenomenon. This model can describe the elasto-plastic behaviour of both isotropic and anisotropic three dimensional polycrystalline materials. It is a pressure independent yield surface which is convex in stress space and assumes an associated flow rule. It was implemented in ABAQUS as a FORTRAN 77 User-Material Subroutine. An Euler Backward integration scheme was adopted and a consistent tangent modulus used.

Four axisymmetric cupping operations were simulated: two with the model's parameters set to represent the aluminium alloy under consideration and two to investigate the effect of the yield surface on earing. For comparison purposes, a fifth case was run using the Hill (1948) anisotropic material model.

It was found that the Hill criterion is more suited to earing simulation in this material and that a contracted yield surface in stress space results in larger ears. Both constitutive models were found to under predict the degree of earing as compared to laboratory drawn cups. This may be improved by modelling the tool geometry more accurately and by implementing an accurate material hardening routine in the material model subroutine.

This work partially investigated the suitability of the Karafillis-Boyce constitutive model for simulating the anisotropic elasto-plastic behaviour of polycrystalline metals. Further investigation should include the simulation of cupping operations for various *face centered cubic* and *body centered cubic* materials with different degrees of planar anisotropy.

TABLE OF CONTENTS

	<u>Page</u>
Acknowledgements	i
Synopsis	ii
List of Figures	v
List of Tables	vii
CHAPTER 1: Introduction	1
1.1 Basic Deep Drawing Procedures	1
1.2 Deep Drawing: Material Considerations	3
1.3 Deep Drawing: Tooling and Friction Effects	6
1.4 Geometric Defects of Deep Drawing	7
1.5 Earing	9
CHAPTER 2: Anisotropic Constitutive Models	11
2.1 Crystallographic Constitutive Models	11
2.2 Phenomenological Yield Surface Models	13
2.2.1 Basic Rate Equations of Classical Plasticity	13
2.2.2 Stress Return and Consistent Tangent Modulus	15
2.2.2.1 Stress Calculation	15
2.2.2.2 Consistent Tangent Modulus	17
2.2.3 Isotropic Yield Surfaces	18
2.2.4 Anisotropic Yield Surfaces	20
2.3 Constitutive Model Selection	24
CHAPTER 3: The Karafillis-Boyce Anisotropic Constitutive Model	26
3.1 Generic Isotropic Yield Surface	27
3.2 Transformation Weighting Tensor	30
3.3 Parameter Evaluation: Orthotropic Symmetry	31
CHAPTER 4: Implementation of Constitutive Model	37
4.1 Flow Vector and Flow Vector Derivative	37
4.1.1 Modified Yield Function and Derivatives	38
4.1.2 Derivation of Flow Tensor	39
4.1.3 Flow Tensor Derivative	41
4.1.4 Flow Tensor: Vector Form	43
4.1.5 Flow Tensor Derivative: Matrix Form	44

4.2	Equivalent Plasticity and Linear Hardening	44
4.3	Reduced Order Yield Function	46
4.4	Mapping Between Anisotropic and Isotropic Spaces	48
CHAPTER 5: User-Material Verification		51
5.1	Yield Surface Position in Stress Space	51
5.2	von Mises Case	53
5.3	Integration Algorithm Iso-Error Plots	54
CHAPTER 6: Finite Element Earing Simulation		59
6.1	Deep Drawing Cupping Operation	59
6.2	Material Model Parameters	61
6.3	Finite Element Model	64
6.4	Results	64
6.5	Discussion of Results	65
CHAPTER 7: Conclusion and Recommendations		74
7.1	Conclusion	74
7.2	Recommendations	74
REFERENCES		76
APPENDIX A: Principal Deviatoric Stresses		78
APPENDIX B: Mathcad Document: Yield Function Derivatives		80
APPENDIX C: Deviatoric Stress Invariant Derivatives		85
APPENDIX D: Derivation of Flow Tensor Derivative		89
APPENDIX E: Reordering of Flow Tensor Derivative		94
APPENDIX F: FORTRAN 77 Listing: Material Model Parameters		97
APPENDIX G: FORTRAN 77 Listing: ABAQUS User-Material		101
APPENDIX H: FORTRAN 77 Listing: Iso-Error Routine		117
APPENDIX I: FORTRAN 77 Listing: ABAQUS V5.4 Input File: Deep Drawing Problem		121

LIST OF FIGURES

<u>Figure</u>	<u>Page</u>
1.1 Tool and Blank Set-up for Deep Drawing Operation	2
1.2 Tool and Blank Set-up for Direct Redrawing Operation	2
1.3 Tool and Blank Set-up for Reverse Redrawing Operation	3
1.4 Single Stroke Drawing, Redrawing and Ironing of Cup	4
1.5 R-value Test for Strip Tensile Specimen	5
1.6 Failure of Drawn Cups by Necking	7
1.7 Wrinkling in Partially Drawn Cups	8
1.8 Stress Corrosion Cracking of Cups	8
1.9 Typical Earing Profiles of Deep Drawn Cups	8
1.10 Correlation Between ΔR and Earing Profile	9
2.1 Elastic Predictor-Plastic Return	16
2.2 Depiction of von Mises and Tresca Yield Surfaces in the π -Plane	19
3.1 Mapping Between IPE and Anisotropic Materials	26
3.2 Upper Bound, Lower Bound and von Mises Yield Surfaces	27
3.3 Generic Yield Function: von Mises Case	28
3.4 Generic Yield Function: Tresca Approximation	29
3.5 Generic Yield Function: Upper Bound Approximation	29
3.6 Shear and Uniaxial Yield Stresses on Generic Yield Surface	35
4.1 Stress Path for Strain Hardening Material	46
5.1 Generic Yield Surface Position in Principal Stress Space	52
5.2 Iso-Error Axes on Yield Surface	54
5.3 Cantilever Beam Mesh	55
5.4 Iso-Error Plot: Lower Bound at (Y, Y, 0)	55
5.5 Iso-Error Plot: Lower Bound at (Y, 0, 0)	56
5.6 Iso-Error Plot: Lower Bound at (0.5117Y, -0.5117Y, 0)	56
5.7 Iso-Error Plot: Upper Bound at (Y, Y, 0)	57
5.8 Iso-Error Plot: Upper Bound at (Y, 0, 0)	57
5.9 Iso-Error Plot: Upper Bound at (0.6514Y, -0.6517Y, 0)	58
6.1 Blank and Tool Geometries	60
6.2 Iso-Error Plot: $k = 3$, $c = 0.3513$ at (Y, Y, 0)	62
6.3 Iso-Error Plot: $k = 12$, $c = 0.9174$ at (Y, Y, 0)	63
6.4 Blank Mesh: Eight Noded (C3D8) Brick Elements	67
6.5 Earing Profile: Hill	68
6.6 Total Equivalent Plasticity: Hill	68

List of Figures

6.7	Earing Profile: $k = 1, c = 0$	69
6.8	Total Equivalent Plasticity: $k = 1, c = 0$	69
6.9	Earing Profile: $k = 3, c = 0.3513$	70
6.10	Total Equivalent Plasticity: $k = 3, c = 0.3513$	70
6.11	Earing Profile: $k = 12, c = 0.9174$	71
6.12	Total Equivalent Plasticity: $k = 12, c = 0.9174$	71
6.13	Earing Profile: $k = 6, c = 0.0075$	72
6.14	Total Equivalent Plasticity: $k = 6, c = 0.0075$	72
6.15	Punch Force/Time Profile	73

University of Cape Town

LIST OF TABLES

<u>Table</u>	<u>Page</u>
3.1 Material Symmetries	31
5.1 Force Residuals: von Mises Case	53
6.1 A3004-H19 Material Properties	59
6.2 Isotropic Yield Surface Parameters for A3004-H19	61
6.3 IPE Mapping Matrix Parameters	61
6.4 Alternative Yield Surface Parameters	62
6.5 CPU Time and Number of Increments	64
6.6 Cup Geometry Results and Earing	65

University of Cape Town

CHAPTER ONE

INTRODUCTION

Increased consumer specification and competition within the metal forming industry require the production of high quality products. The acceptable limits on product geometry, surface finish and mechanical properties, which are largely microstructure dependent, are becoming increasingly demanding.

One manufacturing process which is commercially significant is deep drawing. This is a forming operation in which a blank metal sheet is forced through a die by a punch to produce an article of the desired shape. This process is used to produce items such as vacuum and pressure vessels, zinc batteries, torches, ammunition cartridge cases, cooking pots and beverage cans.

As with all metal forming processes deep drawing is subject to geometric defects which result in added material and machining costs. A defect of particular interest, termed *earing*, is identified by an uneven edge to the drawn article. This defect is the subject of this study where attention will be given to simulating earing in a cup drawn from aluminium alloy.

In this chapter the basics of deep drawing will be presented in order to give an overview of the origin of some common geometrical defects, with special attention being paid to earing. This introduction will serve as a basis for following chapters which detail the implementation and application of a suitable anisotropic constitutive model for earing simulation in a general purpose finite element code.

1.1 Basic Deep Drawing Procedures

Figure 1.1 illustrates the tooling arrangement involved in a basic deep drawing, or radial cupping operation. The blank material, which is circular for axisymmetric products, is allowed to slip along the die and hold-down clamp surfaces as the punch forces it through the die. Tensile stresses are the dominant stresses in this operation. Compressive stresses are, however, established in the hoop direction in the blank material between the tool surfaces (termed the *flange*) as the material moves inward. The principal strains in the plane of the blank material are therefore positive in the radial direction and negative in the hoop direction.

This type of single drawing operation will not usually produce a cup deep enough for most applications and a second drawing, or *redrawing*, process may be necessary to increase the cup depth. In direct redrawing the cup from the initial draw is reduced in

diameter in an operation using a smaller diameter die and punch. This process is illustrated in Figure 1.2. An alternative approach, termed reverse redrawing, also uses a smaller diameter die and punch in the second draw. However, in this case, the draw occurs in the opposite direction to the initial one. This is illustrated in Figure 1.3.

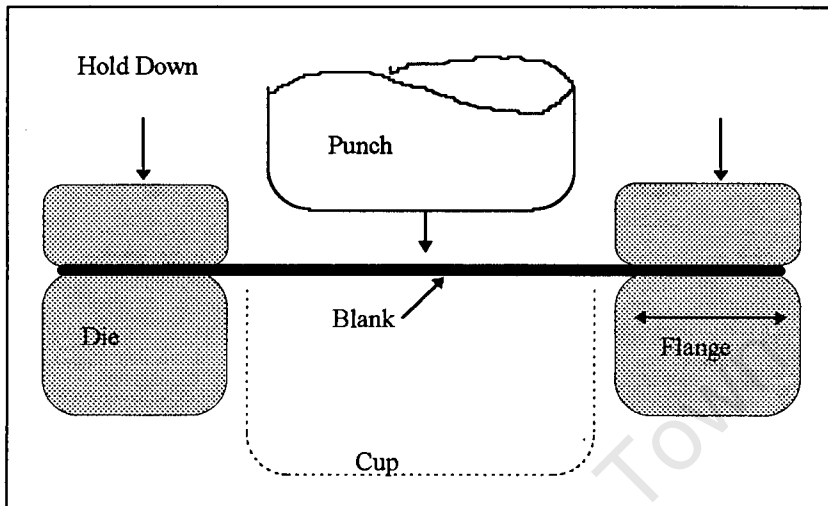


Figure 1.1. Tool and Blank Set-up for Deep Drawing Operation

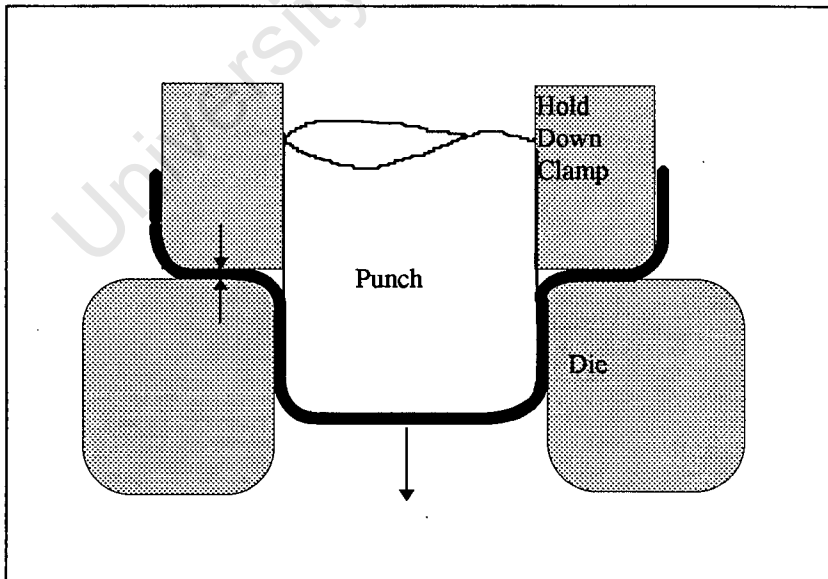


Figure 1.2. Tool and Blank Set-up for Direct Redrawing Operation

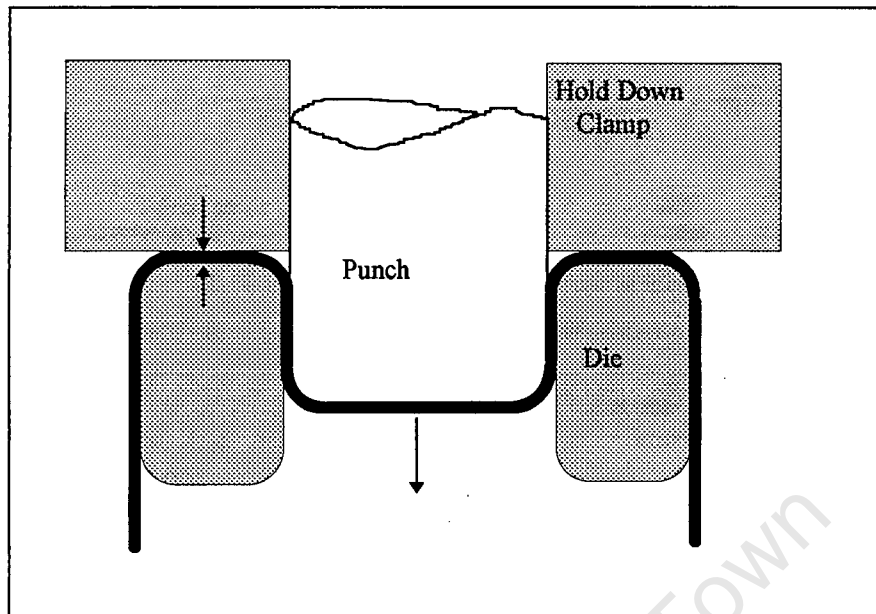


Figure 1.3. Tool and Blank Set-up for Reverse Redrawing Operation

Generally, as a result of unequal plastic flow during drawing, these procedures result in products with non-uniform wall thickness. This problem may be minimised by forcing the drawn article through a ring which is dimensioned to compress and thin the cup wall between it and the punch. In addition to a more uniform wall thickness, this *ironing* process results in increased cup height and improved surface finish. Figure 1.4 is an illustration of tooling for making deep cups using a continuous stroke with concentric punches, direct redrawing and ironing.

As with all metal forming operations the success of a particular drawing operation depends on material properties, process parameters, tooling and lubrication. These will now be discussed in more detail.

1.2 Deep Drawing: Material Considerations

There are two main regions of interest in a workpiece during the drawing process; the flange where most of the plastic deformation occurs and the wall which must be able to transmit sufficient force from the punch to cause deformation in the flange.

As a material point in the flange moves along the die upper surface it is subject to a tensile stress in the radial direction, a compressive stress in the hoop direction and a compressive stress in the axial direction. For normal deep drawing operating parameters the compressive stress has the net affect of thickening the wall and the tensile stress of thinning the wall. Typically the sum of these effects results in only small wall thickness strains in the flange.

A material point in the cup wall which is moving in an axial direction is in a state of plane stress with tensile stresses in both the axial and hoop directions. These stresses result in thinning of the cup wall as the draw proceeds.

If the blank is too large, in relation to the desired cup diameter, the forces the cup wall must transmit from the punch to the flange may result in a wall stress greater than the material yield stress. This may lead to a common form of failure: tensile failure due to large plastic strains. Thus the Limiting Draw Ratio, defined as the maximum permissible ratio of the blank to cup diameters, will be reached when localised necking occurs at the wall. For relatively isotropic metals this ratio is typically 2.1 to 2.2.

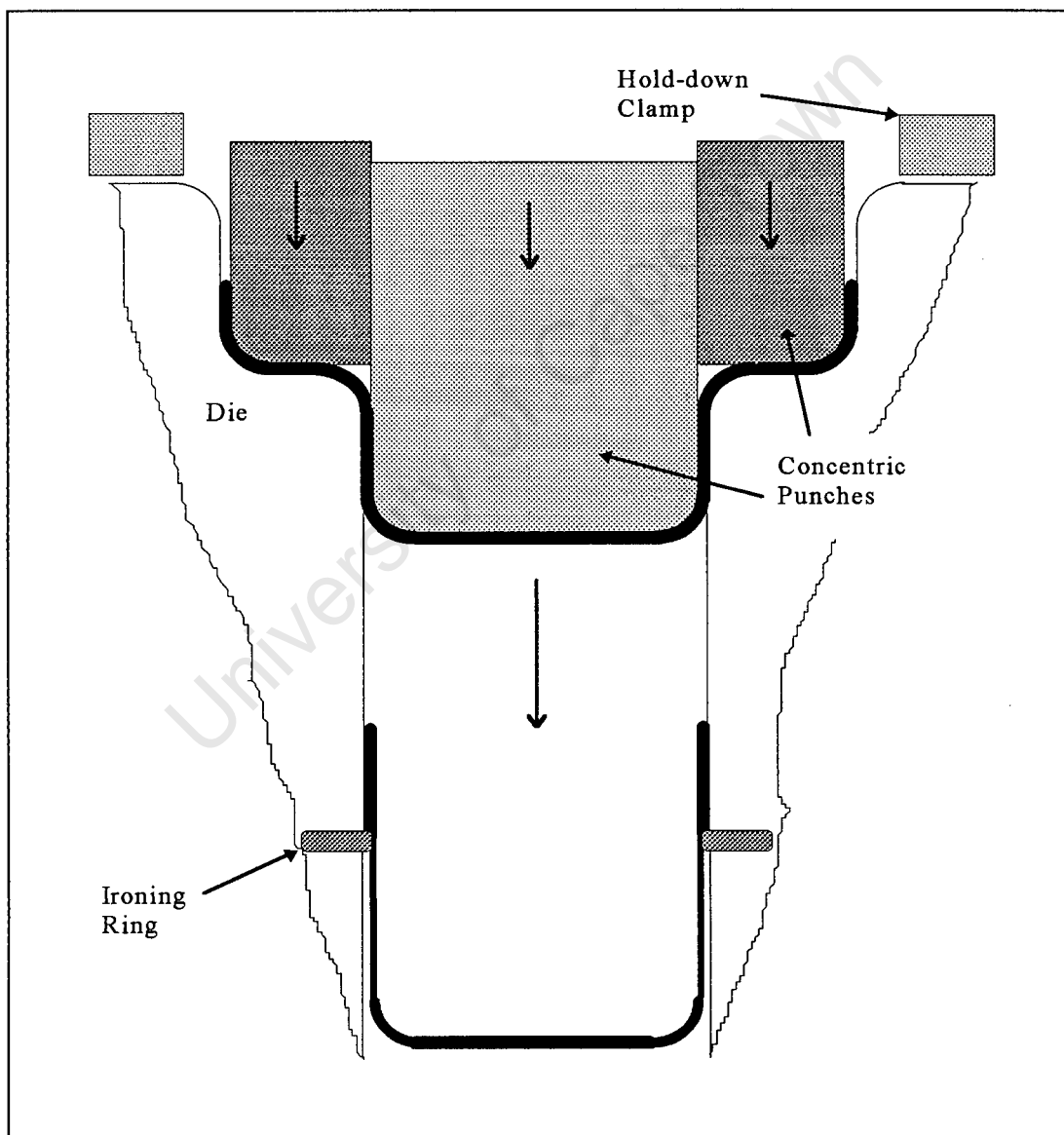


Figure 1.4. Single Stroke Drawing, Redrawing and Ironing of Cup

Hosford and Caddell [1] report that the Limiting Draw Ratio (LDR) may be determined from:-

$$\ln(\text{LDR}) = \eta\beta \quad \dots(1.1)$$

with η - the deformation deficiency factor which accounts for frictional and bending work.
Typically $0.74 \leq \eta \leq 0.79$

and
$$\beta = \left(\frac{2\bar{R}}{\bar{R} + 1} \right)^{0.27} \quad \dots(1.2)$$

where \bar{R} is the average plastic strain ratio defined as:-

$$\bar{R} = \frac{R_0 + 2R_{45} + R_{90}}{4} \quad \dots(1.3)$$

R_0 , R_{45} and R_{90} are the R-values measured at 0, 45 and 90 degrees to the sheet rolling direction. These are defined as the ratio of the transverse plastic strain ϵ_w^p to normal plastic strain ϵ_t^p for material strip samples strained in the above directions i.e.:-

$$R_\theta = \frac{\epsilon_w^p}{\epsilon_t^p} \quad \dots(1.4)$$

This is illustrated in Figure 1.5. Isotropic sheet metals have unity R-values for all directions.

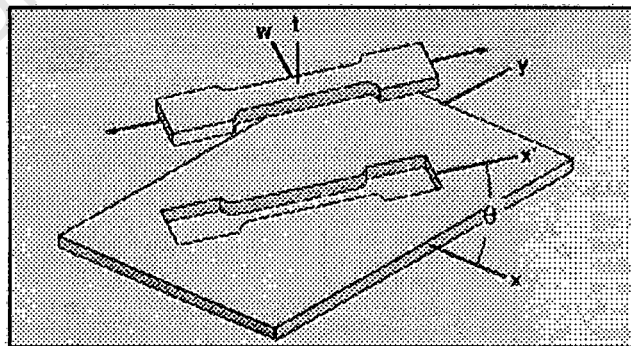


Figure 1.5. R-value Test for Strip Tensile Specimen [1]

Since localised necking followed by tearing is the most common mode of failure for deep drawn articles it would seem that the LDR should be affected by the material strain hardening properties. However, Hosford and Caddell [1] show that this effect is

minor for the normal range of material hardening encountered in most drawable sheet metals.

Some materials exhibit strain rate and hence draw speed dependence. For example, certain metastable austenitic stainless steels such as type 304, exhibit a change in phase from austenite to martensite during plastic straining. Ward [2] shows that greater draw speeds result in greater localisation of the martensite in the final product. The extent of this phase transformation is influenced by the level of plastic strain and the material temperature.

The effect of varying the deep drawing process parameters, such as draw speed and blank temperature, is therefore strongly dependent on the material type.

1.3 Deep Drawing: Tooling and Friction Effects

Tooling and lubrication also play an important role in the drawability of a particular product. Varying the die lip radius, the punch nose radius or the friction between the tooling and the workpiece, while keeping all other parameters constant, directly effects the magnitude of the cup wall stresses and thus the LDR.

The work expended in bending and unbending the sheet as it flows over the die lip increases as the ratio of the sheet thickness to die lip radius increases. This means that for a given job decreasing the die radius will require a greater punch force which results in greater wall stresses and therefore a lower LDR.

The failure site of an unsuccessful draw is usually at the point where the radiused portion at the bottom of the cup meets the wall as this is where the least amount of work hardening has occurred and is therefore the weakest point on the wall. Increasing the punch nose radius has the effect of moving this necking point upward into the work hardened region of the wall. Failure will therefore occur at a greater wall stress and consequently an increased punch nose radius results in an increased LDR. For the case where the friction between the punch and blank is very low the failure point tends to move onto the punch radius as shown on the right of Figure 1.6. This figure also illustrates failure at the point where the cup wall and radiused portion meet.

As noted earlier, most of the plastic work in a drawing operation takes place in the flange region. The force to do this work must be transmitted from the punch to the flange via the cup wall. The chances of localised failure at the interface between the radiused portion at the bottom of the cup and the cup wall may be decreased by increasing the frictional forces between the punch side and the wall, thereby transferring some of the required drawing force to the sides of the punch. This has the effect of transmitting the punch force to the cup wall over a larger area, thus decreasing localised stresses in the wall and increasing the LDR. In practice, this may be achieved by using roughened punches, a suitable lubricant or no lubricant at all, or by pressurising the die cavity in order to force the cup wall onto the punch side.



Figure 1.6. Failure of Drawn Cups by Necking [1]

In order to maximise efficiency, it is desirable that the force transmitted to the flange only does work on the flange material in the form of plastic deformation. However, this is not possible as some energy will be absorbed in frictional work done at the flange and tooling interfaces. Decreasing this frictional work will decrease the required punch force for a particular tooling geometry and therefore increase the LDR. Frictional forces may be minimised by selecting a suitable lubricant or by using as small a hold-down force as possible. This hold-down force must, however, be sufficiently large to prevent wrinkling of the flange. This is a common geometric defect of deep drawing and is discussed in the next section.

1.4 Geometric Defects of Deep Drawing

During drawing the compressive hoop stress developed in the flange may reach a sufficient magnitude to cause buckling in the flange if the hold-down force is not high enough. This results in the *wrinkling* defect and is depicted in Figure 1.7.

This defect may be eliminated by increasing the hold-down force or by decreasing the draw ratio. Aluminium pie dishes are examples of partially drawn cups produced without any hold-down, hence the severe wrinkling and folding which characterises their walls.

As the blank flows over the die lip during a draw the consequent bending and unbending of the material causes tension on the outside and compression on the inside of the cup wall, in the radial direction. These stresses, which are largest near the lip of the cup, induce a bending moment in the wall which is in turn balanced by hoop tension in the wall. This residual hoop stress may be sufficiently large to cause splitting of the cup walls by stress-corrosion cracking unless the cups are stress relieved. Examples of this defect are illustrated in Figure 1.8.



Figure 1.7. Wrinkling in Partially Drawn Cups [1]



Figure 1.8. Stress Corrosion Cracking of Cups [1]

Almost without exception, all rolled sheet metal displays planar anisotropic behavior. Although heat treatment may alleviate this problem, it is rarely eliminated. This anisotropy and any further anisotropy induced during deep drawing causes uneven plastic strain in the cup which, in turn, results in an undulating cup lip, termed *earing*. This phenomenon, illustrated in Figure 1.9, will be discussed in more detail in the following section.



Figure 1.9. Typical Earing Profiles of Deep Drawn Cups [1]
Arrow indicates rolling direction

1.5 Earing

Plastic anisotropy in metal sheeting is primarily the result of crystallographic textures, or preferred grain orientations that develop during the sheet rolling process. Planar anisotropy is generally quantified either by X-ray diffraction methods [3], resulting in pole diagrams, or by measuring the uniaxial yield strengths at various angles to the rolling direction together with the plastic strain ratios (R-values) in the same angles [1]. These R-values display a greater variation than the yield strengths for a given anisotropic state.

It is well established in metal forming literature [1], [3] that ear height and position correlate with the parameter ΔR defined by:-

$$\Delta R = \frac{R_0 + R_{90} - 2R_{45}}{2} \quad \dots(1.5)$$

Figure 1.10 illustrates this correlation, where it may be noted that a negative ΔR results in ears at 45° and a positive one at 90° .

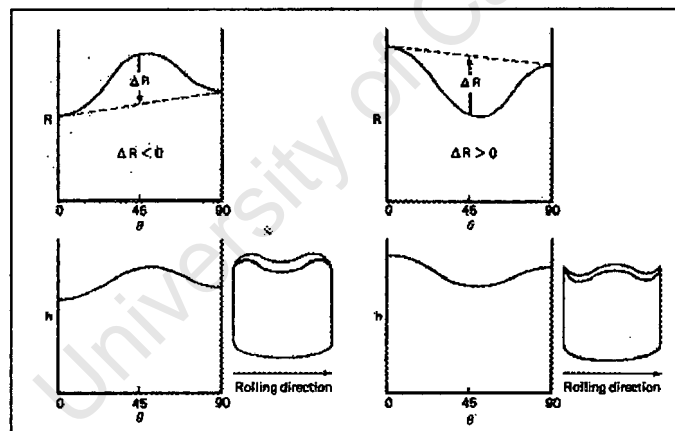


Figure 1.10. Correlation Between ΔR and Earing Profile [1]

The degree of earing is commonly expressed as a percentage of the mean ear height relative to the mean cup height [3] i.e.

$$\text{Percentage earing} = \frac{\Delta h}{\bar{h}} \times 100 \quad \dots(1.6)$$

with $\Delta h = (h_0 + h_{90}) / 2 - h_{45}$

$$\bar{h} = (h_0 + 2h_{45} + h_{90}) / 4$$

where h_{0° , h_{45° and h_{90° are the cup heights at the indicated directions.

Qualitative prediction of earing from pole figures may be accomplished by determining the type of texture represented by the pole figure and thereby the earing profile. Naoyuki *et al* [3] report that four-fold earing symmetry may be expected at $0-90^\circ$ for cube texture and at 45° for rolling texture. Malin and Chen [4] confirm this for the aluminium alloy A3004. They report further that two small but significant components of earing in this material exhibit two-fold and six-fold symmetries. The former is widely believed to be caused by crystallographic Goss texture and the latter by asymmetry of the R-values relative to the sheet rolling direction.

In A3004 alloys mechanical anisotropy is controlled in principle by balancing the cube texture formed during annealing (recrystallisation) with the rolling texture produced during subsequent cold rolling [4]. Thus, under optimum conditions, the earing profile exhibits eight small ears.

It is clear from this introduction that earing can only be successfully simulated in a finite element code if the material constitutive model accurately describes the material anisotropy. The following chapter will select, from various anisotropic constitutive models presented, one which is suited to modelling the earing phenomena.

CHAPTER TWO

ANISOTROPIC CONSTITUTIVE MODELS

A constitutive model describes a material's response to a prescribed deformation or loading. Within the context of this thesis this means that for a given strain at a material point the constitutive model must determine the resultant stress, plastic strain and material tangent modulus. The tangent modulus may be loosely understood as the "slope" of the material's stress-strain curve at the strain point in question.

The modelling of anisotropic polycrystalline materials such as aluminium may be accomplished via either crystallographic texture models or phenomenological yield surface models. In this chapter both types of models will be introduced and discussed and the most suitable constitutive model selected for modelling earing in A3004-H19 can body stock.

2.1 Crystallographic Constitutive Models

Crystallographic texture models describe anisotropic elastic and plastic deformation by monitoring crystal lattice rotation and deformation which occurs during loading. These models are able to model both initial and evolving anisotropy. Becker *et al* [5] maintain that evolving anisotropy is important during the drawing process.

An example of a crystallographic constitutive model for a face centered cubic (*fcc*) material such as aluminium is presented by Becker *et al* [5]. Here the parameters of concern are the velocity and velocity gradient for any material point in a single crystal. For a body defined in a Cartesian coordinate system the velocity gradient is decomposed additively into elastic and plastic parts:-

$$\frac{\partial \dot{\underline{x}}}{\partial \underline{x}} = \underline{\underline{L}}^e + \underline{\underline{L}}^p \quad \dots(2.1)$$

where \underline{x} denotes the current position of the material point $(x_1 \ x_2 \ x_3)^T$

$\dot{\underline{x}}$ denotes the velocity $(\dot{x}_1 \ \dot{x}_2 \ \dot{x}_3)^T$

$\underline{\underline{L}}^e$ denotes the elastic velocity gradient

and $\underline{\underline{L}}^p$ denotes the plastic velocity gradient

The elastic part of the velocity gradient, $\underline{\underline{L}}^e$, is related to stress via elastic moduli in the standard way. For a *fcc* crystal plastic deformation occurs by slip on 12 slip systems. The plastic deformation kinematics of a crystal are therefore related to the slip rates on the individual slip systems. The plastic part of the velocity gradient can therefore be expressed as:-

$$\underline{\underline{L}}^p = \sum_{\alpha=1}^{12} \dot{\gamma}^{\alpha} \underline{s}_{\alpha} \underline{m}_{\alpha} \quad \dots(2.2)$$

where $\dot{\gamma}$ is the slip rate in a slip system
 α indicates one of the slip systems
 \underline{s}_{α} denotes the current slip direction
 \underline{m}_{α} denotes the slip plane normal

Whether slip will occur in a particular system or not depends on the resolved shear stresses in the plane and the strength of the crystal in that plane. The resolved shear stress on the slip system is given in terms of the principal Cauchy stress, $\underline{\underline{\sigma}}^p = (\sigma_1 \ \sigma_2 \ \sigma_3)^T$, and the slip system geometry by:-

$$\tau^{\alpha} = \underline{m}_{\alpha} (\underline{\underline{\sigma}}^p)^T \underline{s}_{\alpha} \quad \dots(2.3)$$

Thus the slip rate on a slip system is given by:-

$$\dot{\gamma}^{\alpha} = F(\tau^{\alpha}, q(\gamma)) \quad \dots(2.4)$$

where $q(\gamma)$ is the slip system strength or hardness
 and γ is the accumulated slip for all slip systems given by:-

$$\gamma = \int_0^t \sum_{\alpha=1}^{12} \dot{\gamma}^{\alpha} dt' \quad \dots(2.5)$$

As noted the above equations model the anisotropic deformation of a single crystal and are therefore not directly applicable to polycrystalline materials. Becker *et al* extend their model to the macroscopic level by firstly determining the volume fractions of the textured components of a material from pole diagrams and then apportioning these volume fractions to each material integration point in the finite element model. Clearly not all the material at a given point may be textured in a polycrystalline material. Becker *et al* therefore use a von Mises model to characterise the background isotropic material. In their study they posit an 80% background material volume fraction for the aluminium alloy they were modelling.

Derivation of the incremental formulations for the tangent modulus and final stress for this constitutive model are detailed by Smelser and Becker [6] and are not presented here.

2.2 Phenomenological Yield Surface Models

The notion of the phenomenological yield surface is well documented in constitutive modelling literature. Essentially these are hypothetical surfaces in stress space which bound all allowable stress states that a material may assume. The mathematical functions which describe these surfaces may be functions of stress, in which case they are termed *yield functions*, or of plastic strain rates, in which case they are called *strain-rate potentials*.

In this section it will be shown how a general yield function may be used in the basic rate equations of plasticity to describe the elasto-plastic behavior of a material. It will then be demonstrated how these equations may be used in the incremental formulation of the stress and tangent modulus algorithms using an Euler Backward (fully implicit) integration scheme. Two of the more commonly used isotropic yield functions will then be presented followed by a section discussing yield functions which may be used to model the planar anisotropic behavior of aluminium sheeting.

2.2.1 Basic Rate Equations of Classical Plasticity

The total strain increment at a material point is assumed to be divisible into elastic and plastic components [7], i.e.

$$\underline{\dot{\epsilon}} = \underline{\dot{\epsilon}}^e + \underline{\dot{\epsilon}}^p \quad \dots(2.6)$$

where $\underline{\dot{\epsilon}}$ is the total strain rate vector $(\dot{\epsilon}_{11} \quad \dot{\epsilon}_{22} \quad \dot{\epsilon}_{33} \quad 2\dot{\epsilon}_{12} \quad 2\dot{\epsilon}_{13} \quad 2\dot{\epsilon}_{23})^T$
 $\underline{\dot{\epsilon}}^e$ is the elastic strain rate component vector
 and $\underline{\dot{\epsilon}}^p$ is the plastic strain rate component vector

The material stress is a result of the elastic strain alone and may simply be calculated from:-

$$\underline{\dot{\sigma}} = \underline{\underline{D}} \underline{\dot{\epsilon}}^e \quad \dots(2.7)$$

where $\underline{\dot{\sigma}}$ is the stress rate vector due to the elastic strain rate
 and $\underline{\underline{D}}$ is the standard elastic constitutive matrix

In order to quantify the plastic strain rate a relationship between it and the stress vector must be determined. This is achieved by assuming that the plastic strain rate is proportional to the stress gradient of a function termed the *plastic potential* [7], i.e.

$$\underline{\dot{\epsilon}}^p = \dot{\lambda} \frac{\partial g}{\partial \underline{\sigma}} \quad \dots(2.8)$$

where $\underline{\dot{\epsilon}}^p$ is the plastic strain rate

$\dot{\lambda}$ is a proportionality constant termed the *plastic multiplier*

g is the plastic potential, which is a function of stress

and $\underline{\sigma}$ is the stress vector

A yield surface f that bounds all elastic stress states must also be given. This yield surface is defined as the surface in stress space for which the yield function, $f = f(\underline{\sigma}, \kappa)$, has a value of zero. As a special case this yield function may be used for the plastic potential in Equation (2.8) giving:-

$$\underline{\dot{\epsilon}}^p = \dot{\lambda} \frac{\partial f}{\partial \underline{\sigma}} \quad \dots(2.9)$$

This is termed the *normality condition* as the vector $\partial f / \partial \underline{\sigma}$ (labelled the flow vector by Owen and Hinton [7]) has a direction normal to the yield surface at the stress point under consideration. Equation (2.8) is called the *flow rule* as it governs the plastic flow after yielding. Equation (2.9) is a special case of this rule termed *associated flow*.

The conditions for plastic loading or unloading of a material point, in terms of the yield function and plastic multiplier, can be given by [8] :-

$$\begin{aligned} f &\leq 0 \\ \dot{\lambda} &\geq 0 \\ \text{and } f \dot{\lambda} &= 0 \end{aligned} \quad \dots(2.10a)$$

Most yield functions are functions of both stress $\underline{\sigma}$ and a hardening parameter κ . This hardening parameter, which may be a function of plastic strain or plastic work, has the effect of shifting the yield surface in stress space to make allowance for material strain or work hardening. To ensure that the stresses during plastic loading remain on the yield surface the plastic consistency condition therefore requires:-

$$\dot{f} = \frac{\partial f}{\partial \underline{\sigma}} \underline{\dot{\sigma}} + \frac{\partial f}{\partial \kappa} \dot{\kappa} = 0 \quad \dots(2.10b)$$

A yield function is required to be *convex* in stress space as it is essential that the function's normals do not intersect. Lubliner [8] also shows that this convexity requirement is a consequence of the principle of maximum plastic dissipation.

2.2.2 Stress Return and Consistent Tangent Modulus

Equations (2.6), (2.7), (2.9) and (2.10) are the rate equations of classical plasticity for an associated flow rule. The incremental formulation of these equations are summarised below, noting that integration of the plastic strains for an increment [n-1,n] is carried out using an Euler Backward scheme, Mitchell [9]:-

$$\Delta \underline{\underline{\epsilon}}_n = \Delta \underline{\underline{\epsilon}}_n^e + \Delta \underline{\underline{\epsilon}}_n^p \quad \dots(2.11)$$

$$\Delta \underline{\underline{\sigma}}_n = \underline{\underline{D}} \Delta \underline{\underline{\epsilon}}_n^e \quad \dots(2.12)$$

$$\Delta \underline{\underline{\epsilon}}_n^p = \dot{\lambda} \underline{\underline{a}}_n \quad \text{with} \quad \underline{\underline{a}}_n = \left. \frac{\partial f}{\partial \underline{\underline{\sigma}}} \right|_n \quad \dots(2.13)$$

The stress and strain quantities at the end of increment n are given by:-

$$\underline{\underline{\epsilon}}_n = \underline{\underline{\epsilon}}_{n-1} + \Delta \underline{\underline{\epsilon}}_n \quad \dots(2.14)$$

$$\underline{\underline{\epsilon}}_n^p = \underline{\underline{\epsilon}}_{n-1}^p + \Delta \underline{\underline{\epsilon}}_n^p \quad \dots(2.15)$$

$$\text{and} \quad \underline{\underline{\sigma}}_n = \underline{\underline{\sigma}}_{n-1} + \underline{\underline{D}}(\Delta \underline{\underline{\epsilon}}_n - \Delta \underline{\underline{\epsilon}}_n^p) \quad \dots(2.16)$$

These formulae will now be used to obtain expressions for the stress update and tangent modulus derived in a manner consistent with a Newton-Raphson solution procedure.

2.2.2.1 Stress Calculation

The *elastic predictor-plastic corrector* method may be used to solve Equations (2.15) and (2.16). This is a two step procedure which assumes that the total strain increment $\Delta \underline{\underline{\epsilon}}_n$ is initially elastic. If the stress state calculated from this strain falls inside the yield surface then this assumption is correct and the final stress has been determined. However, if this stress state, or *elastic predictor* as it is called, falls outside the yield surface then it is not a permissible stress state and a *plastic corrector* step must follow. This involves returning the elastic predictor to the correct stress point on the yield surface. Figure 2.1 illustrates this for an arbitrary yield surface in stress space.

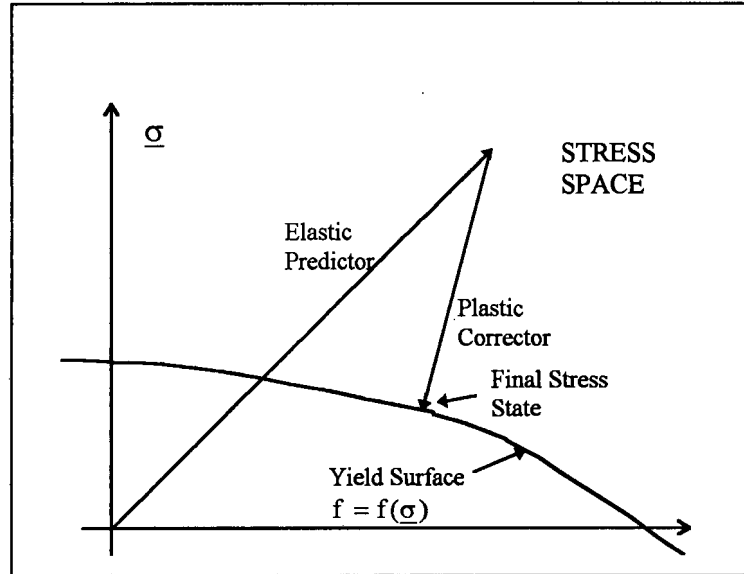


Figure 2.1. Elastic Predictor-Plastic Return

The elastic predictor at the beginning of an increment n is given by:-

$$\underline{\sigma}_n^E = \underline{D}(\underline{\varepsilon}_n - \underline{\varepsilon}_{n-1}^p) \quad \dots(2.17)$$

and the stress return by:-

$$\Delta \underline{\sigma}_n = -\dot{\lambda} \underline{D} \underline{a}_n \quad \dots(2.18)$$

In general an iterative stress return is necessary. In order to achieve this Mitchell [9] shows that the yield function $f(\underline{\sigma}_n, \kappa_n)$ can be linearised around the current values of $\underline{\sigma}_n^i$ and κ_n^i at each iteration i , giving:-

$$f_n^{i+1} = f_n^i + \underline{a}_n^{i T} \Delta \underline{\sigma}_n^i - \dot{\lambda}^i H_n^i \quad \dots(2.19)$$

where H_n^i is the slope of the equivalent plastic strain-stress curve. Now set $f_n^{i+1} = 0$, substitute Equation (2.18) into (2.19) and solve for $\dot{\lambda}^i$:-

$$\dot{\lambda}^i = \frac{f_n^i}{\underline{a}_n^{i T} \underline{D} \underline{a}_n^i + H_n^i} \quad \dots(2.20)$$

The stress is therefore updated according to:-

$$\underline{\sigma}_n^{i+1} = \underline{\sigma}_n^i - \dot{\lambda}^i \underline{D} \underline{a}_n^i \quad \dots(2.21)$$

The above scheme is formally discussed by Simo and Ortiz [19].

2.2.2.2 Consistent Tangent Modulus

Using an Euler backward scheme [9] the stress at any increment n during the solution procedure may be written as:-

$$\underline{\underline{\sigma}}_n = \underline{\underline{D}}(\underline{\underline{\varepsilon}}_n - \underline{\underline{\varepsilon}}_{n-1}^p - \dot{\lambda} \underline{\underline{a}}_n) \quad \dots(2.22)$$

Differentiating (2.22) gives:-

$$d\underline{\underline{\sigma}}_n = \underline{\underline{D}}d\underline{\underline{\varepsilon}}_n - d\dot{\lambda}\underline{\underline{D}}\underline{\underline{a}}_n - \dot{\lambda}\underline{\underline{D}}\frac{\partial \underline{\underline{a}}}{\partial \underline{\underline{\sigma}}}\Big|_n d\underline{\underline{\sigma}}_n$$

Which can be written as:-

$$d\underline{\underline{\sigma}}_n = \underline{\underline{D}}^*(d\underline{\underline{\varepsilon}}_n - d\dot{\lambda}\underline{\underline{a}}_n) \quad \dots(2.23)$$

$$\text{with } \underline{\underline{D}}^* = \left(\underline{\underline{I}} + \dot{\lambda}\underline{\underline{D}}\underline{\underline{b}}_n\right)^{-1} \underline{\underline{D}} \quad \text{and} \quad \underline{\underline{b}}_n = \frac{\partial \underline{\underline{a}}}{\partial \underline{\underline{\sigma}}}\Big|_n \quad \dots(2.24)$$

Now the yield function may be written as :-

$$f = \Phi(\underline{\underline{\sigma}}) - k(\kappa) = 0$$

so differentiating at step n gives:-

$$df_n = \frac{\partial f}{\partial \underline{\underline{\sigma}}}\Big|_n d\underline{\underline{\sigma}}_n + \frac{\partial f}{\partial \kappa}\Big|_n d\kappa_n = 0$$

$$\text{i.e. } \underline{\underline{a}}_n^T d\underline{\underline{\sigma}}_n - H_n d\dot{\lambda}_n = 0 \quad \text{with} \quad H_n = -\frac{1}{d\dot{\lambda}} \frac{\partial f}{\partial \kappa}\Big|_n d\kappa_n \quad \dots(2.25)$$

Now substitute (2.22) into (2.24) and rearrange:-

$$d\dot{\lambda} = \frac{\underline{\underline{a}}_n^T \underline{\underline{D}}^* d\underline{\underline{\varepsilon}}_n}{\underline{\underline{a}}_n^T \underline{\underline{D}}^* \underline{\underline{a}}_n + H_n} \quad \dots(2.26)$$

and substitute (2.25) into (2.23) and rearrange:-

$$d\underline{\underline{\sigma}}_n = \hat{\underline{\underline{D}}}_n d\underline{\underline{\varepsilon}}_n \quad \dots(2.27)$$

where $\underline{\underline{\hat{D}}}_n = \underline{\underline{D}}_n^* - \frac{\underline{\underline{D}}_n^* \underline{\underline{a}}_n \underline{\underline{a}}_n^T \underline{\underline{D}}_n^*}{\underline{\underline{a}}_n^T \underline{\underline{D}}_n^* \underline{\underline{a}}_n + H_n}$ is the consistent tangent modulus ... (2.28)

2.2.3 Isotropic Yield Surfaces

Two of the simplest and most widely used yield functions are the *von Mises* criterion (1913) and the *Tresca* criterion (1864) [7]. The von Mises criterion defines yielding to occur when J_2 , the second deviatoric stress invariant, reaches a critical value. i.e.

$$f(\underline{\underline{\sigma}}, \kappa) = \sqrt{3J_2} - \tilde{k}(\kappa) = 0 \quad \dots(2.29)$$

with $J_2 = s_{12}^2 + s_{23}^2 + s_{13}^2 - s_{11}s_{22} - s_{22}s_{33} - s_{11}s_{33}$... (2.30)

$$\underline{\underline{s}} = \begin{pmatrix} \sigma_{11} - \sigma_v \\ \sigma_{22} - \sigma_v \\ \sigma_{33} - \sigma_v \\ \tau_{12} \\ \tau_{13} \\ \tau_{23} \end{pmatrix} \quad \dots \text{deviatoric stress vector}$$

$$\sigma_v = \frac{1}{3}(\sigma_{11} + \sigma_{22} + \sigma_{33}) \quad \dots \text{volumetric stress}$$

Typically for linear strain hardening $\tilde{k}(\kappa) = Y + H\bar{\epsilon}^p$

where $\bar{\epsilon}^p$ is the equivalent plastic strain calculated from the principal plastic strain vector:-

$$\bar{\epsilon}^p = \int \sqrt{\frac{2}{3}(\dot{\epsilon}_1^p{}^2 + \dot{\epsilon}_2^p{}^2 + \dot{\epsilon}_3^p{}^2)} dt$$

Y is the initial uniaxial yield strength

H is the slope of the yield strength/equivalent plastic strain curve

The von Mises yield function depends only on J_2 as a criterion for yielding and is therefore a member of a class of yield functions termed J_2 - Plasticity. An alternative interpretation of the von Mises criterion is that yielding will occur when the *octahedral shear stress* τ_{oct} reaches a critical value. This is the shear stress on the plane of a regular octahedron which has its apices on the principal axes of stress. The value of τ_{oct} is related to J_2 by [7]:-

$$\tau_{\text{oct}} = \sqrt{\frac{2}{3}J_2}$$

The Tresca yield criterion assumes that plastic deformation occurs when the maximum shear stress over all planes attains a critical value, namely, the value of the current yield stress in shear, denoted by $k(\kappa)$. This yield function may therefore be represented by [8]:-

$$f(\underline{\sigma}, \kappa) = \frac{1}{2} \max(|\sigma_1 - \sigma_2|, |\sigma_2 - \sigma_3|, |\sigma_3 - \sigma_1|) - \hat{k}(\kappa) \quad \dots(2.31)$$

where σ_1 , σ_2 and σ_3 are the principal Cauchy stresses.

Equation (2.31) may be expressed in the following analytical form:-

$$f(\underline{\sigma}, \kappa) = 4J_2^3 - 27J_3^2 - 36\hat{k}^2(\kappa)J_2^2 + 96\hat{k}^4(\kappa)J_2 - 64\hat{k}^6(\kappa) \quad \dots(2.32)$$

where it is clear that the Tresca criterion is not part of J_2 - Plasticity theory as it is also a function of J_3 , the third deviatoric stress invariant defined by:-

$$J_3 = s_{11}s_{22}s_{33} + 2s_{12}s_{13}s_{23} - s_{11}s_{23}^2 - s_{22}s_{13}^2 - s_{33}s_{12}^2 \quad \dots(2.33)$$

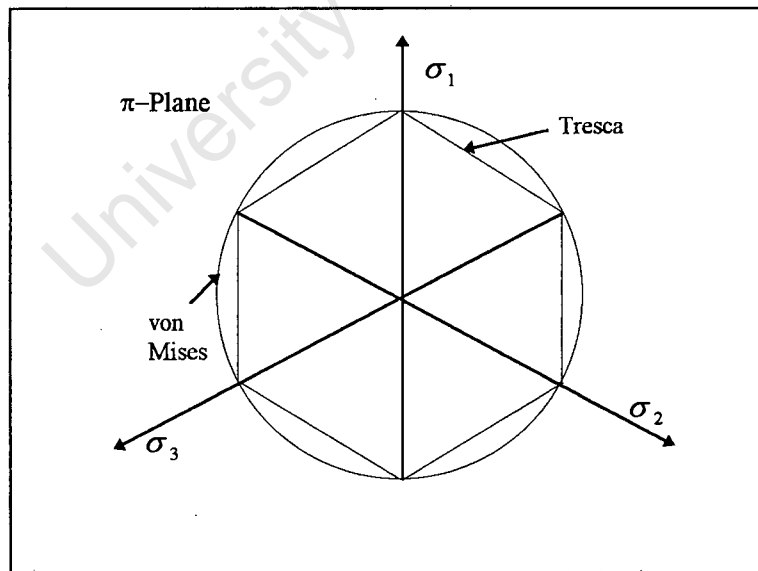


Figure 2.2. Depiction of von Mises and Tresca Yield Surfaces in π -Plane.

Figure 2.2 depicts the von Mises and Tresca yield surfaces in the π -plane. This is a plane in stress space perpendicular to the line defined by $\sigma_1 = \sigma_2 = \sigma_3$. Strictly speaking these are a family of parallel planes. However the yield surfaces under

consideration are pressure independent and are therefore independent of their position on this line. Their geometries, which are therefore identical on all planes, can be captured by sampling a single plane. In Figure 2.2 the values for $\tilde{k}(\kappa)$ and $\hat{k}(\kappa)$ have been chosen such that both surfaces exhibit the same uniaxial yield strength.

2.2.4 Anisotropic Yield Surfaces

The most widely used anisotropic yield criterion is the one proposed by Hill in 1948 [10]. This criterion, like all existing anisotropic yields surfaces, cannot model evolving anisotropy. The Hill criterion is a quadratic function of the form:-

$$f(\underline{\sigma}) = \left[F(\sigma_{22} - \sigma_{33})^2 + G(\sigma_{33} - \sigma_{11})^2 + H(\sigma_{11} - \sigma_{22})^2 + 2L\tau_{23}^2 + 2M\tau_{31}^2 + 2N\tau_{12}^2 \right]^{1/2} \quad \dots(2.34)$$

where F, G, H, L, M and N are material constants. The x, y, and z axes are called the principal axis of anisotropy which for rolled sheets and plates are conventionally taken as the rolling, transverse and thickness directions, respectively. The material constants are defined as :-

$$F = \frac{1}{2} \left(\frac{1}{\bar{\sigma}_{22}} + \frac{1}{\bar{\sigma}_{33}} - \frac{1}{\bar{\sigma}_{11}} \right) \quad \dots(2.35)$$

$$G = \frac{1}{2} \left(\frac{1}{\bar{\sigma}_{33}} + \frac{1}{\bar{\sigma}_{11}} - \frac{1}{\bar{\sigma}_{22}} \right)$$

$$H = \frac{1}{2} \left(\frac{1}{\bar{\sigma}_{11}} + \frac{1}{\bar{\sigma}_{22}} - \frac{1}{\bar{\sigma}_{33}} \right)$$

$$L = \frac{3}{2\bar{\tau}_{23}} \quad M = \frac{3}{2\bar{\tau}_{13}} \quad N = \frac{3}{2\bar{\tau}_{12}}$$

where the stresses $\bar{\sigma}$ and $\bar{\tau}$ represent the yield strengths on the indicated planes and directions.

If $F = G = H$ and $L = M = N = 3F$ there is complete isotropy and Equation (2.34) reduces to the von Mises criterion. Hosford [11] has shown that for this criterion the permissible variation of the R-value (plastic strain ratio) over the range 0° to 90° for a given variation of yield strength follows the relation:-

$$R_{\theta} = \frac{H + (2N - F - G - 4H) \sin^2 \theta \cos^2 \theta}{F \sin^2 \theta + G \cos^2 \theta} \quad \dots(2.36)$$

This means that if there is a minimum in R between 0 and 90° then there *must* be a maximum in the yield strength in this range and vice versa. A consequence of this is that the Hill criterion is not able to model the so called “anomalous” behaviour of materials which display a biaxial-uniaxial yield stress ratio greater than one and an average plastic strain ratio \bar{R} (Equation (1.3)) less than one.

In order to accommodate this material behaviour Hill [11] proposed his 1979 general non-quadratic criterion of the form:-

$$\begin{aligned} f|\sigma_2 - \sigma_3|^m + g|\sigma_3 - \sigma_1|^m + h|\sigma_1 - \sigma_2|^m + a|2\sigma_1 - \sigma_2 - \sigma_3|^m \\ + b|2\sigma_2 - \sigma_3 - \sigma_1|^m + c|2\sigma_3 - \sigma_1 - \sigma_2|^m = 1 \end{aligned} \quad \dots(2.37)$$

Here subscripts 1, 2 and 3 represent both the axes of symmetry and the principal stresses. The Hill 1948 criterion is a special case of Equation (2.19) with $m = 2$ and $a = b = c = 0$. Hosford [11] however, reports that this function is concave for many combinations of m and the plastic strain ratios. Only one case exists where this is not a problem i.e. $a = b = f = g = 0$, but here planar anisotropy is no longer described.

In 1977 Gotoh [11] proposed the plane stress criterion:-

$$\begin{aligned} f = A_0(\sigma_{11} + \sigma_{22})^2 + A_1\sigma_{11}^4 + A_2\sigma_{11}^3\sigma_{22} + A_3\sigma_{11}^2\sigma_{22}^2 + A_4\sigma_{11}\sigma_{22}^3 \\ + A_5\sigma_{22}^4 + (A_6\sigma_{11}^2 + A_7\sigma_{11}\sigma_{22} + A_8\sigma_{22}^2)\tau_{12}^2 + A_9\tau_{12}^4 \end{aligned} \quad \dots(2.38)$$

This criterion can accommodate a wider range of planar anisotropy than the Hill 1948 model and may therefore be more suitable for modelling earing in deep drawing. However, it cannot accommodate the anomalous material behaviour mentioned above.

Hosford [11] states that polycrystalline material yield loci calculated from crystallographic analyses tend not to be elliptical and therefore disagrees with the surface proposed by Hill in 1948. He consequently proposed a yield surface in 1979 which is a special case of Hill's 1979 criterion, namely:-

$$F|\sigma_{22} - \sigma_{33}|^a + G|\sigma_{33} - \sigma_{11}|^a + H|\sigma_{11} - \sigma_{22}|^a = 1 \quad \dots(2.39)$$

where a is a constant larger than two.

From crystallographic considerations he further reports that values of $a = 8$ and $a = 6$ fit experimental data for *fcc* and *bcc* metals respectively. This yield criteria is only valid for normal loading, i.e. loading restricted to $\sigma_{11}, \sigma_{22}, \sigma_{33}$ with $\tau_{12} = \tau_{13} = \tau_{23} = 0$, in

other words the principal stress axes must coincide with the material symmetry axes. Furthermore it cannot accommodate the material biaxial anomaly.

In order to address the requirement that the material symmetry axes and principal stress axes coincide Hosford proposed a modification to Equation (2.39) in 1985. Here he suggested that the yield criterion be expressed in terms of the principal stress axes rather than the stress components along the material symmetry axes [11].i.e.:-

$$R_{\theta}\sigma_{\theta+90}^a + R_{\theta+90}\sigma_{\theta}^a + R_{\theta}R_{\theta+90}(\sigma_{\theta} - \sigma_{\theta+90})^a = R_{\theta+90}(R_{\theta} + 1)X_{\theta}^a \quad \dots(2.40)$$

where σ_{θ} and $\sigma_{\theta+90}$ are the principal stresses
 R_{θ} and $R_{\theta+90}$ are the plastic strain ratios measured in these directions
 and X_{θ} is the measured yield strength in the θ direction

This modification to Equation (2.39), while removing a limitation to the model, does not resolve its' inability to deal with the biaxial anomaly.

In an attempt to account for shear loading in Equation (2.39) Barlat and Lian [11] proposed a generalisation to Hosford's 1979 criterion. Their criterion has the form:-

$$2\bar{\sigma}^M = a|K_1 + K_2|^M + a|K_1 - K_2|^M + (2-a)|2K_2|^M \quad \dots(2.41)$$

with $K_1 = \frac{(\sigma_{11} + h\sigma_{22})}{2}$

$$K_2 = \left\{ \left[\frac{(\sigma_{11} - h\sigma_{22})}{2} \right]^2 + p^2\tau_{12}^2 \right\}^{1/2}$$

and $\bar{\sigma}$ the effective stress

This criterion reduces to the isotropic case when $h = p = 0$. This yield function also cannot model the biaxial anomaly.

Zhou [11] posed a non-quadratic anisotropic yield function which reduces to the Hill 1948 criterion for $m = 2$ and to Hosford's 1979 criterion for $\tau_{12} = 0$:-

$$\bar{\sigma}^m = \left[\left(\frac{3}{2} \right) / (F + G + H) \right] \left\{ \begin{array}{l} F(\sigma_{22}^2 + 3\tau_{12}^2)^{m/2} + G(\sigma_{11}^2 + 3\tau_{12}^2)^{m/2} \\ + H[(\sigma_{11} - \sigma_{22})^2 + 4\tau_{12}^2]^{m/2} + 2N(\tau_{12}^2)^{m/2} \end{array} \right\} \dots(2.42)$$

Zhou found that this function, with a value of $m = 8$, can fit the experimental variation of the R-values and the yield strength in several titanium and aluminium alloys. However, once again this criterion cannot model the biaxial anomaly.

Montheillet *et al* [12] have recommended an anisotropic yield function which can be written as:-

$$|a\sigma_1 + b\sigma_2|^m + h|\sigma_1 - \sigma_2|^m = \sigma_b^m \quad \dots(2.43)$$

where $m > 1$, $h > 0$ and $a + b = 1$
 and σ_b is the yield stress under in-plane equibiaxial tension

This function *can* model the biaxial anomaly. However, in 1993 Hill [12] pointed out that it, like all yield criterion existent at the time, fails one important test; it is not capable of representing any response where the yield stresses at 0 and 90° are of similar magnitude, while the R-values are significantly different.

In 1993 Karafillis and Boyce [13] proposed a general three dimensional anisotropic yield criterion which has a significantly different form to those discussed so far. Their proposed yield criterion, which is pressure independent, can describe both isotropic and anisotropic polycrystalline materials. The isotropic surface can be reduced to either a von Mises surface or an approximation to the Tresca surface. If appropriate, it can also capture the yield behavior of materials, such as aluminium, which do not fall into either category. The Bauschinger effect can be approximated via the introduction of a “backstress” state variable which results in different yield stresses in tension and compression. Anisotropy is described by a set of irreducible tensorial state variables that map between anisotropic and isotropic stress and plastic strain spaces.

The isotropic yield criterion has the form:-

$$f(\underline{s}) = (1 - c)\Phi_1(\underline{s}) + c \frac{3^{2k}}{2^{2k-1} + 1} \Phi_2(\underline{s}) - 2Y^{2k} \quad \dots(2.44)$$

with $\Phi_1(\underline{s}) = (S_1 - S_2)^{2k} + (S_2 - S_3)^{2k} + (S_3 - S_1)^{2k}$

$$\Phi_2(\underline{s}) = S_1^{2k} + S_2^{2k} + S_3^{2k}$$

S_1 , S_2 , and S_3 the principal deviatoric stresses

Y - uniaxial yield strength

k - integer with $1 \leq k \leq \infty$

and c - real with $0.0 \leq c \leq 1.0$

The parameters k and c are chosen such that the yield function accurately models the isotropic behavior of the material under consideration.

Mapping between isotropic and anisotropic spaces is accomplished via the tensor L_{ijkl} .

This fourth order tensor may be contracted to matrix form, thereby enabling the following mapping between *vector* spaces:-

$$\underline{s} = \underline{\underline{L}} \underline{\sigma} \quad \dots(2.45)$$

$$\underline{\varepsilon}^p = \underline{\underline{L}} \underline{e}^p \quad \dots(2.46)$$

with $\underline{\sigma}$ - full anisotropic stress vector

$\underline{\varepsilon}^p$ - anisotropic plastic strain vector

\underline{s} - deviatoric isotropic stress vector

\underline{e}^p - isotropic plastic strain vector

In this constitutive model all the anisotropic information is contained in the mapping matrix $\underline{\underline{L}}$ and all stress calculations are carried out in isotropic space. Therefore unlike previous models described in this work the anisotropic and stress information are uncoupled. This means that this constitutive model can, in theory, deal with any combination of yield strengths and R-values measured at 0° , 45° and 90° to the rolling direction. Thus, this model is not subject to the criticism Hill raised in 1993.

However, a requirement of this model is that the material yield strength in biaxial tension must be the same as that in uniaxial tension. The ratio of these two yield strengths is therefore always equal to one, thus this model is unable to model the biaxial anomaly.

2.3 Constitutive Model Selection

As stated before crystallographic texture models have the advantage over phenomenological yield surface models in that they are able to describe both initial *and* evolving anisotropy. These models are, however, very demanding in terms of computational power [5], [13]. Furthermore Karafillis and Boyce assert that the well known Taylor polycrystalline model (1938) has been found to over predict the R-values for some directions in anisotropic materials. It is thus considered expeditious to select a yield surface model for this study as the finite element deep drawing problem is computationally demanding, even for simple material models.

From the above discussion of phenomenological material models and from further considerations the following criteria may be set for selecting the most suitable model:-

- 1) The model must be able to deal with the biaxial anomaly i.e. it must be able to describe materials which display a biaxial-uniaxial yield stress ratio greater than one and an average plastic strain ratio \bar{R} less than one.

- 2) In order to describe the most general case of anisotropy the model must be reducible to the isotropic case.
- 3) The model must be capable of modeling a material where the yield stresses at 0 and 90° are of similar magnitude, while the R-values are significantly different (i.e. Hill's 1993 requirement).
- 4) The model must be able to describe fcc polycrystalline materials. Experimental evidence [13] suggests that polycrystalline materials with *fcc* or *bcc* microstructures cannot be successfully described by quadratic yield surfaces.

Clearly no single model is able to satisfy all of these requirements. Hill's 1948 model, which is probably the most widely used anisotropic constitutive model for this type of problem, is the least suitable candidate as it only satisfies criterion (2). His 1979 criteria is also unsuitable as it is concave in stress space for many combinations of its exponent and R-values.

The yield criteria described by Equations (2.38) to (2.42) are all unable to satisfy criteria (1) and (3) and are therefore considered unsuitable for this study. The yield criterion proposed by Montheillet *et al* does not satisfy criterion (3) and the model proposed by Karafillis and Boyce fails to satisfy criterion (1). Of these two criteria it is felt that the flexibility offered by the Karafillis and Boyce model, in that it can describe the most general anisotropy (triclinic) and that the R-values and yield stresses need not be coupled, make it the more attractive one for implementation in a general finite element code for describing the anisotropic behavior of A3004-H19 can body stock.

The Karafillis-Boyce constitutive model will be discussed in detail in the following chapter.

CHAPTER THREE

THE KARAFILLIS-BOYCE ANISOTROPIC CONSTITUTIVE MODEL

The Karafillis-Boyce anisotropic constitutive model can describe the elasto-plastic behaviour of both isotropic and anisotropic three dimensional polycrystalline materials. It is a pressure independent, phenomenological yield surface which is convex in stress space and assumes an associated flow rule. The model consists of two parts: a generic isotropic yield surface and a transformation weighting tensor which describes material anisotropy.

All stress and plastic strain calculations are performed on a virtual Isotropic Plasticity Equivalent (IPE) material, the elasto-plastic behaviour of which is described by a generic isotropic yield surface. As depicted in Figure 3.1 the anisotropic material state is determined by mapping the stress and plastic strain tensors between it and the IPE material via a mapping tensor L_{ijkl} .

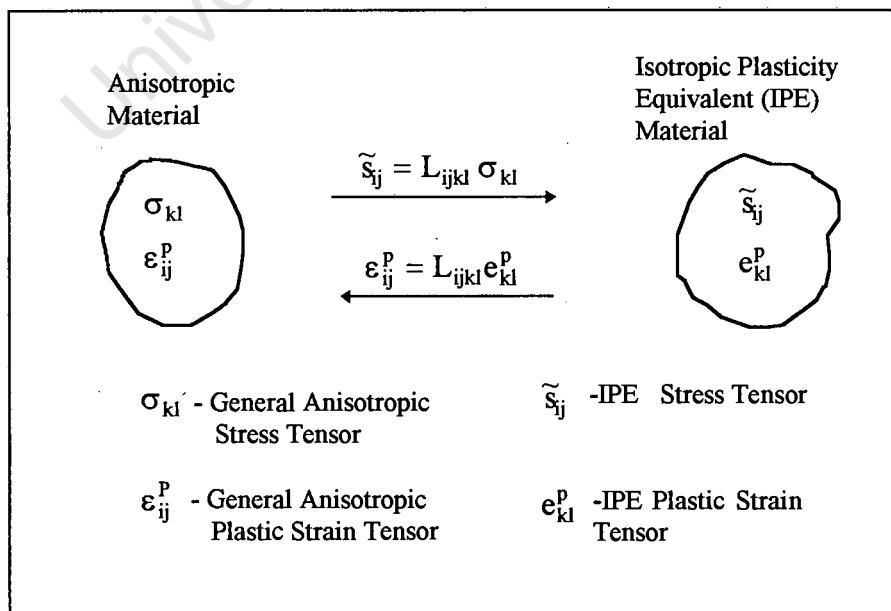


Figure 3.1. Mapping Between IPE and Anisotropic Materials

3.1 Generic Isotropic Yield Surface

Karafilis and Boyce [13] report that Mendelson [14] established the existence of bounds in the isotropic yield surfaces of materials with fixed yield stresses in uniaxial tension. These bounds were derived from symmetry and convexity considerations. The lower bound is described by Tresca's yield criterion and the upper bound by a similarly shaped hexagon surface in stress space. These bounds, together with the von Mises yield surface, are depicted in Figure 3.2.

The isotropic yield surfaces lying between the lower bound and the von Mises surface may be described by a yield function proposed by Hosford in 1972 [13] which is a modification of the von Mises case where an exponent other than two is used:-

$$\Phi_1(\underline{s}) = (S_1 - S_2)^{2k} + (S_2 - S_3)^{2k} + (S_3 - S_1)^{2k} = 2Y^{2k} \quad \dots(3.1)$$

where S_1 , S_2 , and S_3 are the principal deviatoric stresses

Y - the uniaxial yield strength

and k - an integer with $1 \leq k \leq \infty$

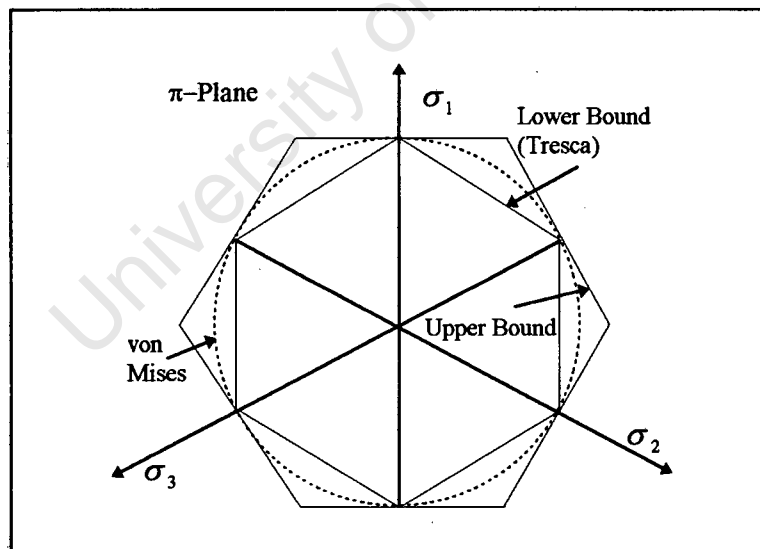


Figure 3.2. Upper Bound, Lower Bound and von Mises Yield Surfaces

This yield surface predicts equal yield strengths in tension and compression as the exponent is even for all allowable values of k . When $k = 1$ Equation (3.1) reduces to the von Mises case and when $k \rightarrow \infty$ it corresponds to the Tresca yield criterion.

Similarly the yield surfaces between the von Mises surface and the upper bound may be described by the function:-

$$\Phi_2(\underline{s}) = S_1^{2k} + S_2^{2k} + S_3^{2k} = \frac{2^{2k} + 2}{3^{2k}} Y^{2k} \quad \dots(3.2)$$

In this case when $k = 1$ the von Mises criterion is recovered and when $k \rightarrow \infty$ the upper bound is recovered.

A generic isotropic yield surface must be able to describe all surfaces between the lower and upper bound. Karafillis and Boyce achieve this by mathematically mixing Equations (3.1) and (3.2) to establish the following convex yield function:-

$$f(\underline{s}) = \Phi(\underline{s}) - 2Y^{2k} \quad \dots(3.3)$$

with $\Phi(\underline{s}) = (1 - c)\Phi_1(\underline{s}) + c \frac{3^{2k}}{2^{2k-1} + 1} \Phi_2(\underline{s})$

and c - real with $0.0 \leq c \leq 1.0$

Figure 3.3 is a contour plot of this yield function, in $\sigma_1 - \sigma_2$ space, with $Y = 100$, for the von Mises case ($k = 1$). Similarly Figure 3.4 is a plot of the generic yield function's approximation to the Tresca criterion ($k = 15$ and $c = 0$) and Figure 3.5 to the upper bound criterion ($k = 15$ and $c = 1$). The yield surfaces in these figures are depicted by those loci in $\sigma_1 - \sigma_2$ space for which the yield function assumes a zero value.

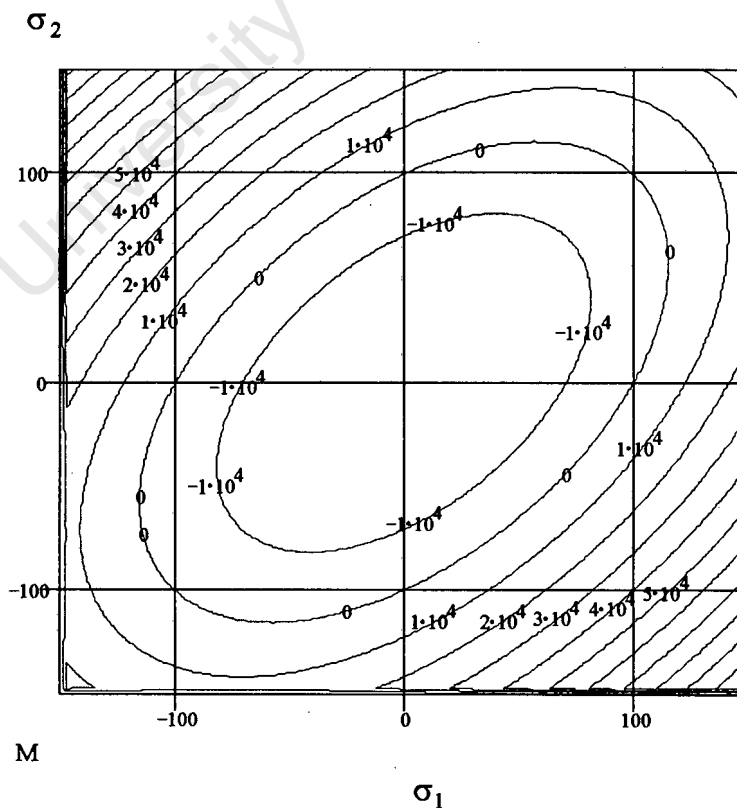


Figure 3.3. Generic Yield Function: von Mises Case

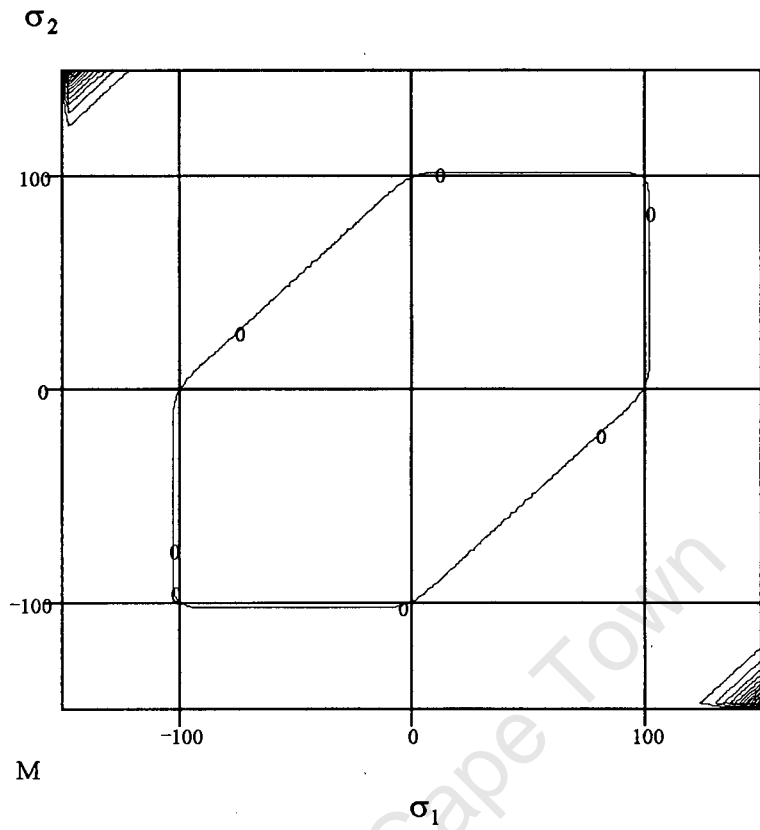


Figure 3.4. Generic Yield Function: Tresca Approximation

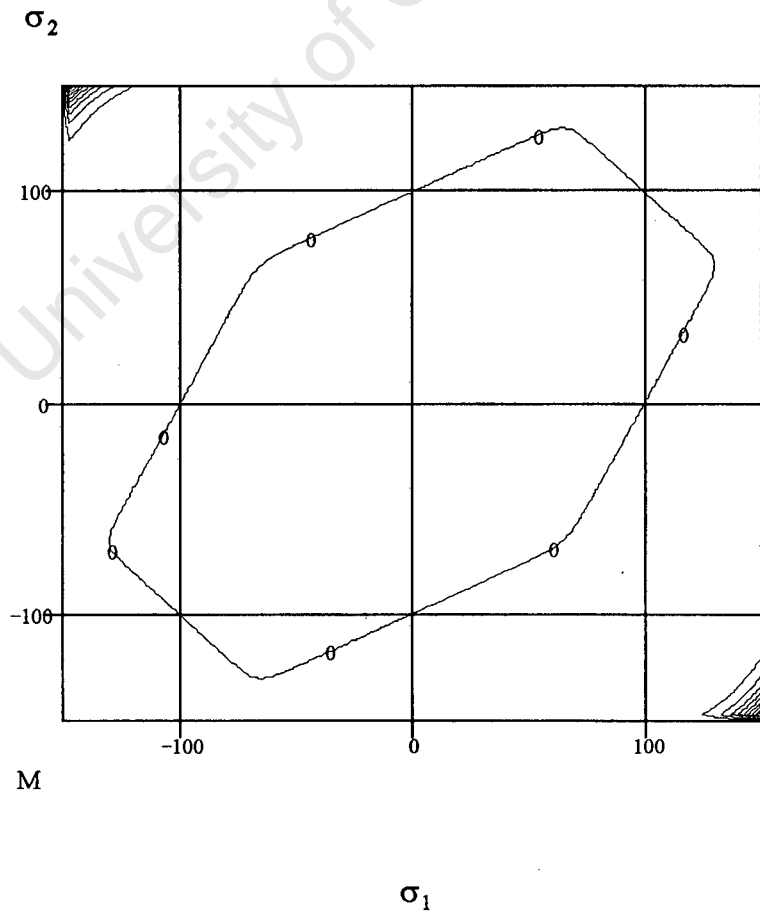


Figure 3.5. Generic Yield Function: Upper Bound Approximation

3.2 Transformation Weighting Tensor

Simulation of anisotropy in this material model is effected by a linear transformation tensor L_{ijkl} which maps the actual stress tensor acting on the anisotropic material to deviatoric isotropic stress space. This stress tensor, which Karafillis and Boyce label the “isotropy plasticity equivalent (IPE) deviatoric stress tensor”, is then used as the argument in Equation (3.3) to determine the stress and plastic strain on the IPE material. Here, the same equivalent yield stresses are assigned to both the isotropic and anisotropic materials. The “IPE stress transformation” thus operates as :-

$$\tilde{s}_{ij} = L_{ijkl} \sigma_{kl} \quad \dots(3.4a)$$

where \tilde{s}_{ij} is the IPE stress tensor

and σ_{kl} is the actual stress tensor acting on the anisotropic material

Equation (3.4a) may be written in vector and matrix form as:-

$$\underline{\tilde{s}} = \underline{L} \underline{\sigma} \quad \dots(3.4b)$$

Karafillis and Boyce report that the tensor L_{ijkl} , which represents an affine transformation and therefore preserves yield surface convexity, must exhibit some internal symmetries and must be traceless. Furthermore, they state that it can be shown, using group theory, that the components of L_{ijkl} can be associated with material symmetries which range from isotropic to triclinic.

The symmetries required of L_{ijkl} are:-

$$L_{ijkl} = L_{jikl} = L_{jilk} \quad \text{from the symmetry of } \tilde{s}_{ij} \text{ and } \sigma_{kl}$$

and $L_{ijkl} = L_{klij}$

Furthermore, the following restraint is required to ensure mapping from full to deviatoric space:-

$$L_{ijkk} = 0$$

These requirements render L_{ijkl} a traceless, partially symmetric fourth order tensor. Table 3.1 lists the rotations which leave L_{ijkl} invariant against different material symmetries together with the corresponding number of independent tensor components. Here R_i^ϕ denotes rotation about the i -axis by the angle ϕ .

Table 3.1. Material Symmetries[13]

Material symmetry	Rotations which leave L_{ijkl} invariant	Number of independent elements of L_{ijkl}
Triclinic	No rotation	15
Monoclinic	R_2^π	8
Orthotropic	R_1^π, R_2^π	6
Trigonal	$R_3^{2\pi/3}, R_1^\pi$	4
Tetragonal	$R_3^{\pi/2}, R_1^\pi$	4
Transversely isotropic	all R_3^ϕ, R_1^π	3
Cubic	$R_1^{\pi/2}, R_2^{\pi/2}, R_3^{\pi/2}$	2
Isotropic	All rotations	1

A similar mapping to that defined by Equation (3.4) may be derived for mapping the plastic strain of the IPE material to anisotropic strain space [13]. This mapping is a consequence of the normality rule, the symmetry and constraint requirements stated above, and the requirement that the plastic dissipation rate for the IPE material and the anisotropic material must be equal. It is given by:-

$$\varepsilon_{ij}^p = L_{ijkl} e_{kl}^p \quad \dots(3.5a)$$

where e_{kl}^p is the isotropic "IPE material" plastic strain
and ε_{ij}^p is the anisotropic material plastic strain

Equation (3.5a) may be written in vector and matrix form:-

$$\underline{\varepsilon}^p = \underline{L} \underline{e}^p \quad \dots(3.5b)$$

Equations (3.3), (3.4) and (3.5) thus form the basis of the Karafillis-Boyce constitutive model.

3.3 Parameter Evaluation: Orthotropic Symmetry

This section will demonstrate a method to evaluate the generic yield function and mapping tensor parameters for a material displaying orthotropic symmetry such as rolled aluminium sheeting

It is computationally more effective to write Equations (3.4) and (3.5) in matrix form. To this end Karafillis and Boyce report:-

$$\underline{\underline{L}} = C \begin{bmatrix} 1 & \beta_1 & \beta_2 & \cdot & \cdot & \cdot \\ \beta_1 & \alpha_1 & \beta_3 & \cdot & \cdot & \cdot \\ \beta_2 & \beta_3 & \alpha_2 & \cdot & \cdot & \cdot \\ \cdot & \cdot & \cdot & \gamma_1 & \cdot & \cdot \\ \cdot & \cdot & \cdot & \cdot & \gamma_2 & \cdot \\ \cdot & \cdot & \cdot & \cdot & \cdot & \gamma_3 \end{bmatrix} \quad \dots(3.6)$$

with $\beta_1 = \frac{\alpha_2 - \alpha_1 - 1}{2}$

$$\beta_2 = \frac{\alpha_1 - \alpha_2 - 1}{2}$$

and $\beta_3 = \frac{1 - \alpha_1 - \alpha_2}{2}$

As per Table 3.1 it is clear that six independent parameters must be evaluated to define this mapping matrix $\underline{\underline{L}}$.

For an isotropic material, we have:-

$$C = \frac{2}{3}$$

$$\alpha_1 = \alpha_2 = 1$$

and $\gamma_1 = \gamma_2 = \gamma_3 = \frac{3}{2}$

Evaluation of $\underline{\underline{L}}$ and the yield function parameters k and c may be accomplished from experimentally determined values for the material uniaxial yield strengths, shear yield strengths and R-values measured at 0° , 45° and 90° to the sheet rolling direction.

To this end Equation (3.5b) may be used to obtain expressions for the R-values in terms of the matrix components. For example, for R_0 this equation may be written in the form:-

$$\underline{\underline{\epsilon}}^p = \underline{\underline{L}} \underline{\underline{e}}^p = \dot{\lambda} \underline{\underline{L}} \underline{\underline{a}}$$

with $\underline{\underline{a}} = (2 \quad -1 \quad -1 \quad 0 \quad 0 \quad 0)^T$ the deviatoric flow vector for $\dots(3.7)$

a strip strained in the 0° direction

and $\dot{\lambda}$ an arbitrary magnitude.

The R-value is then obtained by determining the ratio $\frac{\epsilon_{22}^p}{\epsilon_{33}^p}$ from $\underline{\epsilon}^p$ giving:-

$$R_0 = \frac{2\beta_1 - \alpha_1 - \beta_3}{2\beta_2 - \beta_3 - \alpha_2} \quad \dots(3.8)$$

Similarly for R_{90} :-

$$R_{90} = \frac{-1 + 2\beta_1 - \beta_2}{-\beta_2 + 2\beta_3 - \alpha_2} \quad \dots(3.9)$$

To obtain an expression for R_{45} it is necessary to define a mapping matrix $\underline{\underline{M}}$ which maps the plastic strain vector from the global set of axes defined by the sheet rolling direction, to a local set of axes set at 45° to these axes. Here the sheet rolling direction is taken as the x direction for the global axes and the direction 45° to these axes, the x' direction for the local axes. Thus:-

$$\underline{\epsilon}^{p'} = \underline{\underline{M}} \underline{\epsilon}^p \quad \dots(3.10a)$$

$$\text{and } \underline{\epsilon}^p = \underline{\underline{M}}^{-1} \underline{\epsilon}^{p'} \quad \dots(3.10b)$$

$$\text{with } \underline{\underline{M}} = \begin{bmatrix} \frac{1}{2} & \frac{1}{2} & 0 & \frac{1}{2} & 0 & 0 \\ \frac{1}{2} & \frac{1}{2} & 0 & -\frac{1}{2} & 0 & 0 \\ 0 & 0 & 1 & 0 & 0 & 0 \\ -1 & 1 & 0 & 0 & 0 & 0 \\ 0 & 0 & 0 & 0 & \frac{1}{\sqrt{2}} & \frac{1}{\sqrt{2}} \\ 0 & 0 & 0 & 0 & -\frac{1}{\sqrt{2}} & \frac{1}{\sqrt{2}} \end{bmatrix}$$

Now, when strained in the x' direction, the IPE material produces an isotropic, deviatoric plastic strain of the form:-

$$\underline{\epsilon}^{p'} = \dot{\lambda} (2 \quad -1 \quad -1 \quad 0 \quad 0 \quad 0)^T$$

Mapping this strain to the global axis using Equation (3.10b) gives:-

$$\underline{\epsilon}^p = \dot{\lambda} \left(\frac{1}{2} \quad \frac{1}{2} \quad -1 \quad 3 \quad 0 \quad 0 \right)^T \quad \dots(3.11)$$

As required Equation (3.11) is a deviatoric strain. It is now substituted into Equation (3.5b) to produce an anisotropic plastic strain, which is a function of the $\underline{\underline{L}}$

components and $\dot{\lambda}$, relative to the global axes. We, however, require this anisotropic strain relative to the local set of axes as the experimental value for R_{45} is determined relative to these axis. This anisotropic strain is therefore rotated back to the local set of axes using Equation (3.10a), where it is now possible to produce an expression for R_{45} in terms of α_2 and γ_1 only.:-

$$R_{45} = \frac{\gamma_1}{\alpha_2} - \frac{1}{2} \quad \dots(3.12)$$

It is important to note that the above expressions for the R-values are not dependent on the isotropic yield surface parameters c or k , as is reported by Karafillis and Boyce. This must be so as any isotropic yield surface can only produce R-values of one, implying that isotropic yield surface parameters *cannot* be coupled to the anisotropic R-values.

Equations (3.8), (3.9) and (3.12) are equations in α_1 , α_2 and γ_1 and can be solved thus:-

$$\alpha_1 = \frac{R_0 R_{90} + R_{90} 2R_0}{2R_{90}(R_0 + 1)} \quad \dots(3.13)$$

$$\alpha_2 = \frac{R_{90} + 1 - (R_{90} - 1)\alpha_1}{R_{90} + 1} \quad \dots(3.14)$$

$$\gamma_1 = (R_{45} + \frac{1}{2})\alpha_2 \quad \dots(3.15)$$

The values for γ_2 and γ_3 are not critical when describing orthotropic symmetry and are set equal to the corresponding isotropic values. The value of C for the mapping matrix has not been determined in the above procedure. This can only be achieved once the generic yield surface parameters k and c have been evaluated.

To this end the following procedure is suggested. If the average uniaxial yield strength Y is known, then the intercepts of the generic yield surface with the principal stress axes is also known. This is depicted in Figure 3.6 for the $\sigma_3 = 0$ plane in the first and fourth quadrants. Furthermore, if the average shear yield strength, S_y , is known then the stress vector associated with this yield strength, $(S_y - S_y \ 0)$, must lie somewhere on the pure shear line between the bounds, if this generic yield surface is to model the material under consideration.

Consequently the generic yield surface is fitted to the material data points by using the above pure shear stress vector to evaluate the effective stress for each k and c , sampled at small increments throughout their practical ranges. For yielding, the effective stress is obtained from Equation (3.3) as:-

$$\bar{\sigma} = \left[\frac{1}{2} \Phi(\underline{\tilde{s}}) \right]^{1/2k} \quad \dots(3.16)$$

The combination of k and c which produces an equivalent stress closest to the average uniaxial yield strength then gives the parameters to model the material in question.

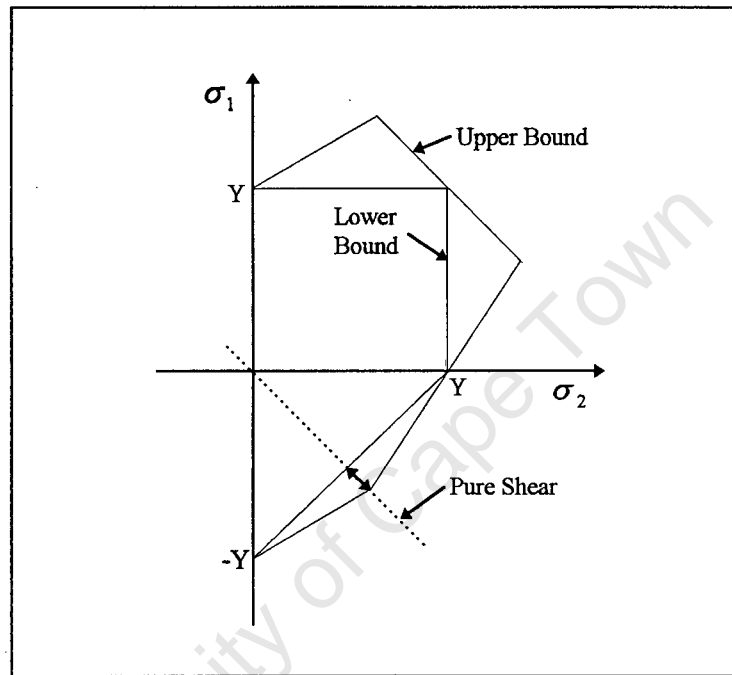


Figure 3.6. Shear and Uniaxial Yield Stresses on Generic Yield Surface

Having quantified the yield surface k and c values it is now possible to determine the mapping matrix C parameter. This is accomplished by requiring that the average experimentally determined uniaxial yield strength must equal the corresponding average effective stress determined by the generic yield function i.e.:-

$$\frac{\bar{\sigma}_0 + \bar{\sigma}_{45} + \bar{\sigma}_{90}}{3} = \frac{Y_0 + Y_{45} + Y_{90}}{3} \quad \dots(3.17)$$

where the Y 's are the yield strengths measured at the indicated directions and the $\bar{\sigma}$'s are the corresponding effective stresses defined by Equation (3.16).

Now let $\underline{L} = C\underline{\ell}$ where C is the coefficient to be determined. Inspection of Equation (3.3) shows that, for yielding, Equation (3.16) may be written :-

$$\bar{\sigma} = \left[\frac{1}{2} C^{2k} \Phi(\underline{\ell} \underline{\sigma}) \right]^{1/2k} = Y$$

$$\therefore C = \frac{Y}{\left[\frac{1}{2} \Phi(\underline{\underline{\sigma}}) \right]^{1/2k}}$$

So using Equation (3.17) C can now be written as:-

$$C = \frac{Y_0 + Y_{45} + Y_{90}}{\left(\frac{1}{2} \right)^{1/2k} \left[\Phi^{1/2k}(\underline{\underline{\sigma}}_0) + \Phi^{1/2k}(\underline{\underline{\sigma}}_{45}) + \Phi^{1/2k}(\underline{\underline{\sigma}}_{90}) \right]} \quad \dots(3.18)$$

where the $\underline{\underline{\sigma}}$'s are the stress *vectors* causing yielding in the indicated directions:-

$$\underline{\underline{\sigma}}_0 = Y_0 (1 \ 0 \ 0 \ 0 \ 0 \ 0)^T$$

$$\underline{\underline{\sigma}}_{45} = Y_{45} \left(\frac{1}{2} \ 1 \ 0 \ 1 \ 0 \ 0 \right)^T$$

and $\underline{\underline{\sigma}}_{90} = Y_{90} (0 \ 1 \ 0 \ 0 \ 0 \ 0)^T$

The above parameter evaluating procedure was coded as a FORTRAN 77 program and is listed in Appendix F. As input this program requires the R-values and uniaxial yield strengths measured at 0° , 45° and 90° as well as the average material shear yield strength. The output consists of the α and γ values and a table of k values running from 1 to 15, together with the corresponding c values giving the lowest error for the yield surface fitting. The errors and matrix C values are also reported for each k value. This program will be used to determine the material model parameters for a finite element deep drawing simulation of the alloy A3004-H19 which is discussed in Chapter Five.

The following chapter will discuss the implementation of the Karafillis-Boyce constitutive model in a general purpose finite element code.

CHAPTER FOUR

IMPLEMENTATION OF CONSTITUTIVE MODEL

Chapter Two introduced the incremental formulation necessary to implement a general, pressure independent yield function, with an associated flow rule, as a constitutive model in a finite element code using an implicit integration scheme. This chapter details the application of this formulation to the Karafillis-Boyce model.

Sections 4.1 to 4.3 deal with the formulation of the isotropic constitutive model, followed by Section 4.4 which details the mapping of the stress, plastic strain and tangent modulus between isotropic and anisotropic spaces. The resultant FORTRAN 77 code, as implemented in ABAQUS Version 5.4 [15], is listed in Appendix G.

4.1 Flow Vector and Flow Vector Derivative

It is evident from Section 2.2.2 that the first and second derivatives of the yield function with respect to the full Cauchy stress are necessary for the implementation of this constitutive model. In order to obtain these derivatives in a form which is computationally efficient it is necessary to:-

- perform a trigonometric substitution for the principal deviatoric stresses in the yield function such that it becomes a function of $J_2^{1/2}$ & $\theta = \theta(J_2, J_3)$
- determine the 1st and 2nd derivatives of this modified function with respect to these variables
- substitute these derivatives into expressions derived for the *flow tensor* $\left(\frac{\partial f}{\partial \sigma_{ij}}\right)$ and *flow tensor derivative* $\left(\frac{\partial^2 f}{\partial \sigma_{ij} \partial \sigma_{pq}}\right)$

- rearrange these tensors into the more efficient *flow vector* $\left(\frac{\partial f}{\partial \underline{\sigma}}\right)$ and *flow vector derivative* $\left(\frac{\partial^2 f}{\partial \underline{\sigma} \partial \underline{\sigma}^T}\right)$ forms.

4.1.1 Modified Yield Function and Derivatives

The isotropic yield function proposed by Karafillis and Boyce is a function of the principal deviatoric stresses and may be written in the form:-

$$f(\underline{s}(\underline{\sigma})) = (1 - c)\Phi_1(\underline{s}(\underline{\sigma})) + c \frac{3^{2k}}{2^{2k-1} + 1} \Phi_2(\underline{s}(\underline{\sigma})) - 2Y^{2k} \quad \dots(4.1)$$

with $\Phi_1(\underline{s}(\underline{\sigma})) = (S_1 - S_2)^{2k} + (S_2 - S_3)^{2k} + (S_3 - S_1)^{2k}$
 and $\Phi_2(\underline{s}(\underline{\sigma})) = S_1^{2k} + S_2^{2k} + S_3^{2k}$

where S_1, S_2 and S_3 are the principal deviatoric stresses.

An appropriate technique for extracting these principal deviatoric stresses from the stress tensor is presented by Owen and Hinton [7]. This method consists of the following trigonometric substitution:-

$$\begin{pmatrix} S_1 \\ S_2 \\ S_3 \end{pmatrix} = \frac{2J_2^{1/2}}{\sqrt{3}} \begin{pmatrix} \sin\left(\theta + \frac{2\pi}{3}\right) \\ \sin(\theta) \\ \sin\left(\theta + \frac{4\pi}{3}\right) \end{pmatrix} \quad \dots(4.2)$$

with $S_1 > S_2 > S_3$

$$\theta = -\frac{1}{3} \arcsin\left(\frac{3^{3/2} J_3}{2 J_2^{3/2}}\right) \quad \dots \quad -\frac{\pi}{6} \leq \theta \leq \frac{\pi}{6} \quad \dots(4.3)$$

& J_2, J_3 the second and third deviatoric stress invariants

The derivation of this substitution is reproduced in Appendix A.

Substitution of (4.2) into the yield function results in a yield criterion identical to (4.1), but which is now a function of $J_2^{1/2}$ and θ i.e.

$$f(J_2^{1/2}, \theta) = (1-c) \left[\left[\left(\frac{2J_2^{1/2}}{\sqrt{3}} \right) \left(\sin\left(\theta + \frac{2\pi}{3}\right) - \sin(\theta) \right) \right]^{2k} + \left[\left(\frac{2J_2^{1/2}}{\sqrt{3}} \right) \left(\sin(\theta) - \sin\left(\theta + \frac{4\pi}{3}\right) \right) \right]^{2k} \dots \right. \\ \left. + \left[\left(\frac{2J_2^{1/2}}{\sqrt{3}} \right) \left(\sin\left(\theta + \frac{4\pi}{3}\right) - \sin\left(\theta + \frac{2\pi}{3}\right) \right) \right]^{2k} \right] \\ + c \frac{3^{2k}}{2^{2k-1} + 1} \left[\left(\frac{2J_2^{1/2}}{\sqrt{3}} \sin\left(\theta + \frac{2\pi}{3}\right) \right)^{2k} + \left(\frac{2J_2^{1/2}}{\sqrt{3}} \sin(\theta) \right)^{2k} + \left(\frac{2J_2^{1/2}}{\sqrt{3}} \sin\left(\theta + \frac{4\pi}{3}\right) \right)^{2k} \right] - 2Y^{2k} \quad \dots(4.4)$$

A Mathcad 5 document [16] detailing this function with its first and second derivatives may be found in Appendix B. Note: For simplicity $J_2^{1/2}$ is represented by A in this appendix.

4.1.2 Derivation of Flow Tensor

For a general yield criterion f the flow tensor is defined by:-

$$a_{ij} = \frac{\partial f}{\partial \sigma_{ij}}$$

For a criterion of the form $f = f(J_2^{1/2}, \theta)$, the flow tensor may be expressed as:-

$$a_{ij} = \frac{\partial f}{\partial J_2^{1/2}} \cdot \frac{\partial J_2^{1/2}}{\partial \sigma_{ij}} + \frac{\partial f}{\partial \theta} \cdot \frac{\partial \theta}{\partial \sigma_{ij}} \quad \dots(4.5)$$

Now rearranging and differentiating (4.3), and noting that $\theta = \theta(\sigma_{ij})$,

$J_3 = J_3(\sigma_{ij})$ and $J_2^{1/2} = J_2^{1/2}(\sigma_{ij})$ gives :-

$$\frac{\partial \theta}{\partial \sigma_{ij}} = \frac{-\sqrt{3}}{2 \cos 3\theta} \left[\frac{1}{J_2^{3/2}} \frac{\partial J_3}{\partial \sigma_{ij}} - \frac{3J_3}{J_2^{1/2}} \frac{\partial J_2^{1/2}}{\partial \sigma_{ij}} \right] \quad \dots(4.6)$$

Substitute Equation (4.6) into (4.5) and simplify:-

$$\begin{aligned}
 a_{ij} &= \frac{\partial f}{\partial \sigma_{ij}} = \frac{\partial f}{\partial \theta} \frac{\sqrt{3}}{2 \cos 3\theta} \left[\frac{1}{J_2^{3/2}} \frac{\partial J_3}{\partial \sigma_{ij}} - \frac{3J_3}{J_2^2} \frac{\partial J_2^{1/2}}{\partial \sigma_{ij}} \right] \\
 &= \left[\frac{\partial f}{\partial J_2^{1/2}} + \frac{3\sqrt{3}}{2 \cos 3\theta} \frac{J_3}{J_2^2} \frac{\partial f}{\partial \theta} \right] a_{2ij} - \frac{\partial f}{\partial \theta} \frac{\sqrt{3}}{2 \cos 3\theta} \frac{1}{J_2^{3/2}} a_{3ij} \quad \dots(4.7)
 \end{aligned}$$

$$\text{with } a_{2ij} = \frac{\partial J_2^{1/2}}{\partial \sigma_{ij}} \quad \text{and} \quad a_{3ij} = \frac{\partial J_3}{\partial \sigma_{ij}}$$

Now rearrange (4.3) and substitute into (4.7):-

$$\frac{J_3}{J_2^2} = -\frac{1}{J_2^{1/2}} \frac{2 \sin 3\theta}{3\sqrt{3}}$$

$$\therefore a_{ij} = \left[\frac{\partial f}{\partial J_2^{1/2}} - \frac{\tan 3\theta}{J_2^{1/2}} \frac{\partial f}{\partial \theta} \right] a_{2ij} - \frac{\partial f}{\partial \theta} \frac{\sqrt{3}}{2 \cos 3\theta} \frac{1}{J_2^{3/2}} a_{3ij}$$

$$\text{Thus } a_{ij} = C_2 a_{2ij} + C_3 a_{3ij} \quad \dots(4.8)$$

$$\text{where } C_2 = \frac{\partial f}{\partial J_2^{1/2}} - \frac{\tan 3\theta}{J_2^{1/2}} \frac{\partial f}{\partial \theta} \quad \dots(4.9)$$

$$C_3 = -\frac{\sqrt{3}}{2 \cos 3\theta} \frac{1}{J_2^{3/2}} \frac{\partial f}{\partial \theta} \quad \dots(4.10)$$

$$a_{2ij} = \frac{\partial J_2^{1/2}}{\partial \sigma_{ij}} = \frac{1}{2J_2^{1/2}} \frac{\partial J_2}{\partial \sigma_{ij}} \quad \dots(4.11)$$

$$\text{and } a_{3ij} = \frac{\partial J_3}{\partial \sigma_{ij}} \quad \dots(4.12)$$

The 1st derivatives of the deviatoric stress invariants, which are derived in Appendix C, are :-

$$\frac{\partial J_2}{\partial \sigma_{ij}} = s_{ij}$$

and
$$\frac{\partial J_3}{\partial \sigma_{ij}} = s_{ik} s_{kj} - \frac{1}{3} \delta_{ij} s_{pk} s_{kp}$$

It will be noted that a_{ij} is a rank 2 tensor. Furthermore, it is apparent that C_2 and C_3 contain only yield function derivative information while a_{2ij} and a_{3ij} contain only stress information.

The following comments regarding the flow tensor in J_2 -plasticity are of interest:-

- $\frac{\partial f}{\partial \theta} = 0$ which leads to $a_{ij} = \frac{\partial f}{\partial J_2^{1/2}} a_{2ij}$

in the case of von Mises $f = \sqrt{3} J_2^{1/2} - \tilde{k}(\kappa) = 0$

so $a_{ij} = \sqrt{3} a_{2ij} = \frac{\sqrt{3} s_{ij}}{2 J_2^{1/2}}$

- By definition $a_{ij} = \frac{\partial f}{\partial \sigma_{ij}}$. However inspection of the derivation leading to

(4.8) shows that for J_2 - plasticity $\frac{\partial f}{\partial \sigma_{ij}} = \frac{\partial f}{\partial s_{ij}}$. This may lead one to

erroneously believe that $a_{ij} = \frac{\partial f}{\partial s_{ij}}$ for all yield criteria independent of the

hydrostatic stress.

4.1.3 Flow Tensor Derivative

The flow tensor derivative may be obtained by taking the derivative of Equation (4.8) with respect to the full Cauchy stress tensor:-

$$\text{i.e. } \frac{\partial a_{ij}}{\partial \sigma_{pq}} = b_{ijpq} = C_2 \frac{\partial a_{2ij}}{\partial \sigma_{pq}} + \frac{\partial C_2}{\partial \sigma_{pq}} a_{2ij} + C_3 \frac{\partial a_{3ij}}{\partial \sigma_{pq}} + \frac{\partial C_3}{\partial \sigma_{pq}} a_{3ij}$$

From which it follows that:-

$$\begin{aligned} b_{ijpq} = & C_2 \frac{\partial a_{2ij}}{\partial \sigma_{pq}} + C_3 \frac{\partial a_{3ij}}{\partial \sigma_{pq}} + \frac{\partial^2 f}{\partial \sigma_{pq} \partial J_2^{1/2}} a_{2ij} \dots \\ & - \frac{\partial}{\partial \sigma_{pq}} \left(\frac{\tan 3\theta}{J_2^{1/2}} \frac{\partial f}{\partial \theta} \right) a_{2ij} + \frac{\partial}{\partial \sigma_{pq}} \left(\frac{-\sqrt{3}}{2 \cos 3\theta} \frac{1}{J_2^{3/2}} \frac{\partial f}{\partial \theta} \right) a_{3ij} \end{aligned} \quad \dots(4.13)$$

Evaluation of (4.13) leads to an unwieldy expression for the flow tensor derivative, as Appendix D demonstrates. As shown by Crisfield [17], this expression can be rearranged and simplified resulting in a more elegant form for b_{ijpq} . This process, which is illustrated in Appendix E, results in the following expression for the flow tensor derivative:-

$$\begin{aligned} b_{ijpq} = & C_2 \tilde{b}_{1ijpq} + C_3 \tilde{b}_{2ijpq} + C_{22} a_{2ij} a_{2pq} + C_{23} a_{2ij} a_{3pq} + C_{32} a_{3ij} a_{2pq} \dots \\ & + C_{33} a_{3ij} a_{3pq} \end{aligned} \quad \dots(4.14)$$

with: C_2 and C_3 defined in (4.9) and (4.10)

$$\tilde{b}_{1ijpq} = \frac{\partial a_{2ij}}{\partial \sigma_{pq}} = \frac{1}{2} J_2^{-1/2} \frac{\partial^2 J_2}{\partial \sigma_{pq} \partial \sigma_{ij}} - \frac{1}{4} J_2^{-3/2} s_{ij} s_{pq} \quad \dots(4.15)$$

$$\frac{\partial^2 J_2}{\partial \sigma_{pq} \partial \sigma_{ij}} = \delta_{ip} \delta_{jq} - \frac{1}{3} \delta_{pq} \delta_{ij}$$

$$\tilde{b}_{2ijpq} = \frac{\partial a_{3ij}}{\partial \sigma_{pq}} = \delta_{ip} s_{jq} - \frac{2}{3} \delta_{pq} s_{ji} + \delta_{jq} s_{pi} - \frac{2}{3} \delta_{ij} s_{pq} \quad \dots(4.16)$$

a_{2ij} and a_{3ij} defined in (4.11) and (4.12)

$$\begin{aligned} C_{22} = & - \frac{\partial^2 f}{\partial \theta \partial J_2^{1/2}} \frac{\tan 3\theta}{J_2^{1/2}} + \frac{\partial^2 f}{\partial J_2^{1/2}} + \frac{3 \tan 3\theta}{J_2 \cos^2 3\theta} \frac{\partial f}{\partial \theta} \dots \\ & + \frac{\tan 3\theta}{J_2} \frac{\partial f}{\partial \theta} + \frac{\partial^2 f}{\partial \theta^2} \frac{\tan^2 3\theta}{J_2} - \frac{\tan 3\theta}{J_2^{1/2}} \frac{\partial^2 f}{\partial J_2^{1/2} \partial \theta} \end{aligned}$$

$$C_{33} = \frac{3 \left(3 \frac{\partial f}{\partial \theta} \tan 3\theta + \frac{\partial^2 f}{\partial \theta^2} \right)}{4 \cos^2 3\theta \cdot J_2^3}$$

$$C_{23} = \frac{\sqrt{3}}{2 \cos 3\theta \cdot J_2^{3/2}} \left(\frac{\partial^2 f}{\partial \theta^2} \frac{\tan 3\theta}{J_2^{1/2}} - \frac{\partial^2 f}{\partial \theta \partial J_2^{1/2}} \right) + \frac{3\sqrt{3}}{2 \cos^3 3\theta \cdot J_2^2} \frac{\partial f}{\partial \theta}$$

& $C_{32} = C_{23}$

Appendix C details the derivation of the deviatoric stress invariants.

4.1.4 Flow Tensor: Vector Form

Since the flow tensor is defined as $a_{ij} = \frac{\partial f}{\partial \sigma_{ij}}$ and the stress tensor is symmetric, it follows that a_{ij} is also symmetric. This is also confirmed by the definition of the plastic strain tensor, which must be symmetric, i.e.

$$\epsilon_{ij}^p = \lambda \frac{\partial f}{\partial \sigma_{ij}} \quad \dots(4.17)$$

This suggests that the flow tensor may be rewritten in the simpler vector form as:-

$$\underline{a} = (a_{11} \quad a_{22} \quad a_{33} \quad a_{12} \quad a_{13} \quad a_{23})^T$$

However, *engineering* strain is the preferred form for strain, therefore from (4.17) the appropriate form of the flow vector is:-

$$\underline{a} = (a_{11} \quad a_{22} \quad a_{33} \quad 2a_{12} \quad 2a_{13} \quad 2a_{23})^T \quad \dots(4.18)$$

It is evident from (4.8) that this form for the flow vector may be achieved by writing the tensors a_{2ij} and a_{3ij} in the vector form of (4.18). Furthermore, writing a general symmetric tensor t_{ij} in this form also ensures that the matrix form of the 4th order tensor $t_{ij}t_{pq}$ can conveniently be calculated as $\underline{t} \cdot \underline{t}^T$. This property will be useful in the following section where the flow tensor derivative is converted to matrix form.

4.1.5 Flow Tensor Derivative: Matrix Form

If all the 2nd order tensors of (4.14) are rewritten in the vector form of (4.18) and the 4th order tensors reduced to matrices by evaluating each tensor term and then, while noting symmetry of the tensor, regrouping them according to the "basis" of (4.18), the flow vector derivative may be written in the following matrix form:-

$$\underline{\underline{b}} = C_2 \underline{\underline{b}}_1 + C_3 \underline{\underline{b}}_2 + C_{22} \underline{\underline{a}}_2 \cdot \underline{\underline{a}}_2^T + C_{23} \underline{\underline{a}}_2 \cdot \underline{\underline{a}}_3^T + C_{32} \underline{\underline{a}}_3 \cdot \underline{\underline{a}}_2^T + C_{33} \underline{\underline{a}}_3 \cdot \underline{\underline{a}}_3^T \dots \quad \dots(4.19)$$

with $\underline{\underline{b}}_1 = \frac{1}{2} J_2^{-1/2} \cdot \frac{1}{3} \begin{bmatrix} 2 & -1 & -1 & 0 & 0 & 0 \\ -1 & 2 & -1 & 0 & 0 & 0 \\ -1 & -1 & 2 & 0 & 0 & 0 \\ 0 & 0 & 0 & 6 & 0 & 0 \\ 0 & 0 & 0 & 0 & 6 & 0 \\ 0 & 0 & 0 & 0 & 0 & 6 \end{bmatrix} - \frac{1}{4} J_2^{-3/2} \underline{\underline{s}} \cdot \underline{\underline{s}}^T \quad \dots(4.20)$

$$\underline{\underline{b}}_2 = \frac{2}{3} \begin{bmatrix} s_{11} & & & & & \\ s_{33} & s_{22} & & & & \\ & & \text{symmetric} & & & \\ s_{22} & s_{11} & s_{33} & & & \\ s_{12} & s_{12} & -2s_{12} & -3s_{33} & & \\ s_{13} & -2s_{13} & s_{13} & 3s_{23} & -3s_{22} & \\ -2s_{23} & s_{23} & s_{23} & 3s_{13} & 3s_{12} & -3s_{11} \end{bmatrix} \quad \dots(4.21)$$

and C_2, \dots, C_{33} as defined previously.

4.2 Equivalent Plasticity and Linear Hardening

This constitutive model will assume linear strain hardening for the material. It is therefore necessary to calculate the total equivalent plastic strain and uniaxial yield strength at each material point during the finite element solution process. For any increment n or iteration i during the solution process the current uniaxial yield stress at a material point is defined by:-

$$Y_n^{i+1} = Y^0 + H \bar{\epsilon}^p_i \quad \dots(4.22)$$

where Y_n^{i+1} is the uniaxial yield stress at the n 'th increment and $i+1$ 'th iteration
 Y^0 is the initial uniaxial yield stress
 $\bar{\epsilon}_n^i$ is the total equivalent plastic strain at the n 'th increment and i 'th iteration

and H is the material linear hardening parameter taken to be the slope of the *uniaxial yield stress /total equivalent plastic strain* curve

It is therefore necessary to evaluate the total equivalent plastic strain at each iteration in order to determine the uniaxial yield stress for the following iteration. The notion of equivalent plastic strain has its origin in the definition of the plastic work increment [1], i.e.:-

$$dW^P = \bar{\sigma} d\bar{\epsilon}^P = \underline{\sigma}^T \cdot d\underline{\epsilon}^P \quad \dots(4.23)$$

where dW^P is the plastic work increment
 $\bar{\sigma}$ is the effective stress
 $d\bar{\epsilon}^P$ is the Equivalent Plastic Strain increment
 $\underline{\sigma}$ is the stress vector causing the plastic work
 and $d\underline{\epsilon}^P$ is the plastic strain vector conjugate to the stress vector

Solving (4.23) for the equivalent plastic strain gives:-

$$d\bar{\epsilon}_p = \frac{\underline{\sigma}^T \cdot d\underline{\epsilon}_p}{\bar{\sigma}}$$

With reference to Figure 4.1 and noting that the Euler backward scheme is used for this formulation the equivalent plastic strain increment is expressed as:-

$$d\bar{\epsilon}_n^{i+1} = \frac{\underline{\sigma}^T \cdot d\underline{\epsilon}_n^p}{Y} \Big|_n^{i+1} = \frac{\underline{\sigma}^T \cdot d\underline{\epsilon}_n^p}{Y_n^i + H d\bar{\epsilon}_n^p} \Big|_n^{i+1}$$

This gives:-

$$H \left[d\bar{\epsilon}_n^{i+1} \right]^2 + Y_n^i \left[d\bar{\epsilon}_n^{i+1} \right] - \underline{\sigma}^T \cdot d\underline{\epsilon}_n^p \Big|_n^{i+1} = 0 \quad \dots(4.24)$$

Now solving for positive equivalent plastic strain gives:-

$$d\bar{\epsilon}_n^{i+1} = \frac{-Y_n^i + \sqrt{(Y_n^i)^2 + 4H \underline{\sigma}^T \cdot d\underline{\epsilon}_n^p \Big|_n^{i+1}}}{2H} \quad \dots(4.25)$$

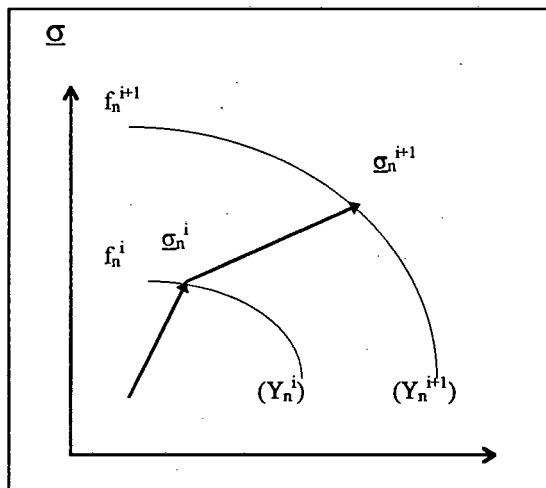


Figure 4.1 Stress Path for Strain Hardening Material

Thus the increment in equivalent plastic strain can be determined from the material linear hardening parameter, the uniaxial yield stress at the beginning of the increment and the stress and plastic strain increment vectors evaluated at the end of the increment.

Equations (4.25) and (4.22) are used during the solution process to track the equivalent plastic strain and uniaxial yield stress.

4.3 Reduced Order Yield Function

It was noted during initial testing of this constitutive model that the finite element global solution convergence rate was not as rapid as was anticipated. For example, with the yield function parameters set to $k = 1$ and $c = 0$ (the von Mises case) a quadratic convergence rate was expected, but not achieved. Furthermore it was noted that the stress return from the elastic predictor to the yield surface was achieved in many more steps than anticipated.

Investigation revealed that this was caused by the polynomial form of the yield function as presented by Karafillis and Boyce. As a remedy it was therefore decided to implement a reduced order form of the yield function. This meant that it was necessary to determine the derivatives of the reduced order function with respect to $J_2^{1/2}$ and θ . However, since the derivatives of the polynomial function were already known, it was expeditious to formulate the linear function derivatives in terms of these polynomial ones.

To this end the polynomial yield function may be written in the form:-

$$f = \Phi\left(\theta, J_2^{1/2}\right) - 2Y^{2k} = 0 \quad \dots(4.26)$$

From which it follows that:-

$$\begin{aligned} \frac{\partial f}{\partial \theta} &= \frac{\partial \Phi}{\partial \theta} & , & & \frac{\partial^2 f}{\partial \theta^2} &= \frac{\partial^2 \Phi}{\partial \theta^2} \\ \frac{\partial f}{\partial J_2^{1/2}} &= \frac{\partial \Phi}{\partial J_2^{1/2}} & \& & \frac{\partial^2 f}{\partial J_2^{1/2}{}^2} &= \frac{\partial^2 \Phi}{\partial J_2^{1/2}{}^2} \end{aligned} \quad \dots(4.27)$$

Now the reduced order form of the yield function may be expressed as:-

$$F = \left[\frac{1}{2} \Phi\left(\theta, J_2^{1/2}\right) \right]^{1/2k} - Y = 0 \quad \dots(4.28)$$

So differentiating Equation (4.28) with respect to θ and $J_2^{1/2}$ and making use of the equalities of (4.27) yields:-

$$\frac{\partial F}{\partial \theta} = 2^{-1/2k} \cdot \frac{1}{2k} \Phi^{\left(\frac{1}{2k}-1\right)} \frac{\partial f}{\partial \theta} \quad \dots(4.29)$$

$$\frac{\partial^2 F}{\partial \theta^2} = \left(\frac{1}{2^{1/2k} 2k} \right) \left[\left(\frac{1}{2k} - 1 \right) \Phi^{\left(\frac{1}{2k}-2\right)} \left(\frac{\partial f}{\partial \theta} \right)^2 + \Phi^{\left(\frac{1}{2k}-1\right)} \frac{\partial^2 f}{\partial \theta^2} \right] \quad \dots(4.30)$$

$$\frac{\partial F}{\partial J_2^{1/2}} = 2^{-1/2k} \cdot \frac{1}{2k} \Phi^{\left(\frac{1}{2k}-1\right)} \frac{\partial f}{\partial J_2^{1/2}} \quad \dots(4.31)$$

$$\frac{\partial^2 F}{\partial J_2^{1/2}{}^2} = \left(\frac{1}{2^{1/2k} 2k} \right) \left[\left(\frac{1}{2k} - 1 \right) \Phi^{\left(\frac{1}{2k}-2\right)} \left(\frac{\partial f}{\partial J_2^{1/2}} \right)^2 + \Phi^{\left(\frac{1}{2k}-1\right)} \frac{\partial^2 f}{\partial J_2^{1/2}{}^2} \right] \quad \dots(4.32)$$

and

$$\begin{aligned} \frac{\partial^2 F}{\partial \theta \partial J_2^{1/2}} &= \left(\frac{1}{2^{1/2k} 2k} \right) \left[\left(\frac{1}{2k} - 1 \right) \Phi^{\left(\frac{1}{2k}-2\right)} \frac{\partial f}{\partial \theta} \frac{\partial f}{\partial J_2^{1/2}} + \Phi^{\left(\frac{1}{2k}-1\right)} \frac{\partial^2 f}{\partial \theta \partial J_2^{1/2}} \right] \\ &\quad + \Phi^{\left(\frac{1}{2k}-1\right)} \frac{\partial^2 f}{\partial \theta \partial J_2^{1/2}} \end{aligned} \quad \dots(4.33)$$

Equations (4.29) to (4.33) therefore demonstrate that the linear yield function derivatives can be written in terms of the known polynomial yield function derivatives.

4.4 Mapping Between Anisotropic and Isotropic Spaces

An important part of this constitutive model is the mapping of the anisotropic stress to isotropic space, the isotropic plastic strain to anisotropic space and the isotropic tangent modulus to anisotropic space. Since it is more computationally efficient to work in vector and matrix forms it is desirable that these mappings take place in the relevant vector and matrix spaces and not the tensor spaces. The 4th order IPE mapping tensor L_{ijpq} , as introduced in Chapter Three, must therefore be rearranged into a form which allows this.

To this end it was shown in Chapter Three that for orthotropic symmetry L_{ijpq} may be reduced to the following matrix form:-

$$\underline{\underline{L}} = \underline{\underline{C}} \begin{bmatrix} 1 & \beta_1 & \beta_2 & 0 & 0 & 0 \\ \beta_1 & \alpha_1 & \beta_3 & 0 & 0 & 0 \\ \beta_2 & \beta_3 & \alpha_2 & 0 & 0 & 0 \\ 0 & 0 & 0 & \gamma_1 & 0 & 0 \\ 0 & 0 & 0 & 0 & \gamma_2 & 0 \\ 0 & 0 & 0 & 0 & 0 & \gamma_3 \end{bmatrix} \quad \dots(4.34)$$

with $\beta_1 = \frac{\alpha_2 - \alpha_1 - 1}{2}$

$$\beta_2 = \frac{\alpha_1 - \alpha_2 - 1}{2}$$

and $\beta_3 = \frac{1 - \alpha_1 - \alpha_2}{2}$

and that mapping between anisotropic and isotropic stress and strain spaces may be accomplished via:-

$$\underline{\underline{s}}_{iso} = \underline{\underline{L}} \underline{\underline{\sigma}}_{aniso} \quad \dots(4.35)$$

and $\underline{\underline{\epsilon}}_{aniso}^p = \underline{\underline{L}} \underline{\underline{e}}_{iso}^p \quad \dots(4.36)$

It is evident from Equation (4.35) that $\underline{\underline{L}}$ only maps from full stress space to deviatoric stress spaces. An inverse mapping from deviatoric to full stress space is not possible as $\underline{\underline{L}}$ is singular. Consequently it is proposed that a more convenient form for this mapping matrix be used i.e. one which allows two way mapping between isotropic and anisotropic spaces regardless of whether the vectors are deviatoric or not. Furthermore, this proposed form of $\underline{\underline{L}}$ which contains hydrostatic information is necessary for mapping the isotropic tangent modulus to anisotropic space as it would be erroneous to map it to deviatoric space.

The required modification to the mapping matrix involves simply adding the hydrostatic terms to the deviatoric vector i.e.:-

$$\underline{\underline{\sigma}}_{iso} = \underline{\underline{L}} \underline{\underline{\sigma}}_{aniso} + \frac{1}{3} \begin{bmatrix} 1 & 1 & 1 & 0 & 0 & 0 \\ 1 & 1 & 1 & 0 & 0 & 0 \\ 1 & 1 & 1 & 0 & 0 & 0 \\ 0 & 0 & 0 & 0 & 0 & 0 \\ 0 & 0 & 0 & 0 & 0 & 0 \\ 0 & 0 & 0 & 0 & 0 & 0 \end{bmatrix} \underline{\underline{\sigma}}_{aniso}$$

from which it is apparent that the non-singular mapping matrix is given by:-

$$\underline{\underline{L}}_v = \underline{\underline{L}} + \frac{1}{3} \begin{bmatrix} 1 & 1 & 1 & 0 & 0 & 0 \\ 1 & 1 & 1 & 0 & 0 & 0 \\ 1 & 1 & 1 & 0 & 0 & 0 \\ 0 & 0 & 0 & 0 & 0 & 0 \\ 0 & 0 & 0 & 0 & 0 & 0 \\ 0 & 0 & 0 & 0 & 0 & 0 \end{bmatrix} \quad \dots(4.37)$$

In order to map the isotropic tangent modulus to anisotropic space consider first the form of the equations, derived in Chapter Two, defining the tangent modulus:-

i.e.
$$\hat{\underline{\underline{D}}}_n = \underline{\underline{D}}_n^* - \frac{\underline{\underline{D}}_n^* \underline{\underline{a}}_n \underline{\underline{a}}_n^T \underline{\underline{D}}_n^*}{\underline{\underline{a}}_n^T \underline{\underline{D}}_n^* \underline{\underline{a}}_n + H_n}$$

with
$$\underline{\underline{D}}_n^* = \left(\underline{\underline{I}} + \lambda \underline{\underline{D}} \underline{\underline{b}}_n \right)^{-1} \underline{\underline{D}}$$

$$\underline{\underline{a}}_n = \left. \frac{\partial f}{\partial \underline{\underline{\sigma}}_n} \right|$$

and
$$\underline{\underline{b}}_n = \left. \frac{\partial \underline{\underline{a}}}{\partial \underline{\underline{\sigma}}_n} \right|$$

It is noted from these equations that for an isotropic elastic, anisotropic plastic material, such as the one under consideration, the only terms which *can* contain anisotropic information are the flow vector and its derivative as these must be derivatives of an *anisotropic* yield function. Consequently the anisotropic tangent modulus may be calculated by using anisotropic derivatives in the above equations.

However, the yield function under consideration is isotropic, therefore it is necessary to obtain expressions, via the mapping matrix $\underline{\underline{L}}$, for the required anisotropic derivatives. From Equation (4.36) it is clear that an appropriate expression for the anisotropic flow vector is :-

$$\underline{\underline{a}}_{\text{aniso}} = \underline{\underline{L}}_{\text{v}} \underline{\underline{a}}_{\text{iso}} \quad \dots(4.38)$$

For the anisotropic flow vector derivative:-

$$\begin{aligned} \frac{\partial \underline{\underline{a}}_{\text{aniso}}}{\partial \underline{\underline{\sigma}}_{\text{aniso}}} &= \underline{\underline{L}}_{\text{v}} \frac{\partial \underline{\underline{a}}_{\text{iso}}}{\partial \underline{\underline{\sigma}}_{\text{aniso}}} \quad \dots \text{from Equation (4.38)} \\ &= \underline{\underline{L}}_{\text{v}} \left(\frac{\partial \underline{\underline{\sigma}}_{\text{iso}}}{\partial \underline{\underline{\sigma}}_{\text{aniso}}} \right) \frac{\partial \underline{\underline{a}}_{\text{iso}}}{\partial \underline{\underline{\sigma}}_{\text{iso}}} \quad \dots(4.39) \end{aligned}$$

But:-

$$\begin{aligned} \partial \underline{\underline{\sigma}}_{\text{iso}} &= \underline{\underline{L}}_{\text{v}} \partial \underline{\underline{\sigma}}_{\text{aniso}} \\ \therefore \frac{\partial \underline{\underline{\sigma}}_{\text{iso}}}{\partial \underline{\underline{\sigma}}_{\text{aniso}}} &= \underline{\underline{L}}_{\text{v}} \quad \dots(4.40) \end{aligned}$$

Substituting Equation (4.40) into Equation (4.39) gives:-

$$\frac{\partial \underline{\underline{a}}_{\text{aniso}}}{\partial \underline{\underline{\sigma}}_{\text{aniso}}} = \underline{\underline{b}}_{\text{aniso}} = \underline{\underline{L}}_{\text{v}} \underline{\underline{L}}_{\text{v}} \underline{\underline{b}}_{\text{iso}} \quad \dots(4.41)$$

CHAPTER FIVE

USER-MATERIAL VERIFICATION

Verification of the FORTRAN 77 constitutive model coding, as listed in Appendix G, was effected in three parts:-

- 1) It was confirmed, for particular instances, that the generic yield surface is correctly positioned in isotropic stress space.
- 2) The performance of the code, with $k = 1$ and \underline{L} set for isotropic mapping, was identical to that of a standard von Mises model.
- 3) Iso-error plots of the plastic strain integration algorithm indicated that relatively small errors may be expected for reasonable elastic predictors.

5.1 Yield Surface Position in Stress Space

The positions of the lower bound ($k = 15, c = 0$), von Mises ($k = 15$), and upper bound ($k = 15, c = 1$) yield surfaces were determined in the $\sigma_1 = 0$, $\sigma_2 = 0$ and $\sigma_3 = 0$ principal stress planes. Figure 5.1 illustrates this for the $\sigma_3 = 0$ plane in the first and fourth quadrants. Here the positions of the stress points A.....J were determined by initialising the yield surface parameters k and c and then incrementally stepping along the stress paths defined by $\alpha = \sigma_2/\sigma_1$, for $\alpha = -1, +\frac{1}{2}, +1$ and $+2$, and recording the points at which plasticity first occurs in the $\sigma_3 = 0$ plane. This procedure was followed for both compressive and tensile stress quadrants. The following results were obtained for all three principal stress planes for a uniaxial yield strength of Y :-

Von Mises: A = (0.577, 1.155, 0)Y
 B = (1.155, 0.577, 0)Y
 C = (0.577, -0.577, 0)Y

Lower Bound E = (0.512, 1.023, 0)Y
 F = (1.024, 0.512, 0)Y
 G = (0.5117, -0.5117, 0)Y

Upper Bound $H = (0.6519, 1.303, 0)Y$
 $I = (1.303, 0.6519, 0)Y$
 $J = (0.6514, -0.6514, 0)Y$

and common to all surfaces:-

$$D = (Y, Y, 0)$$

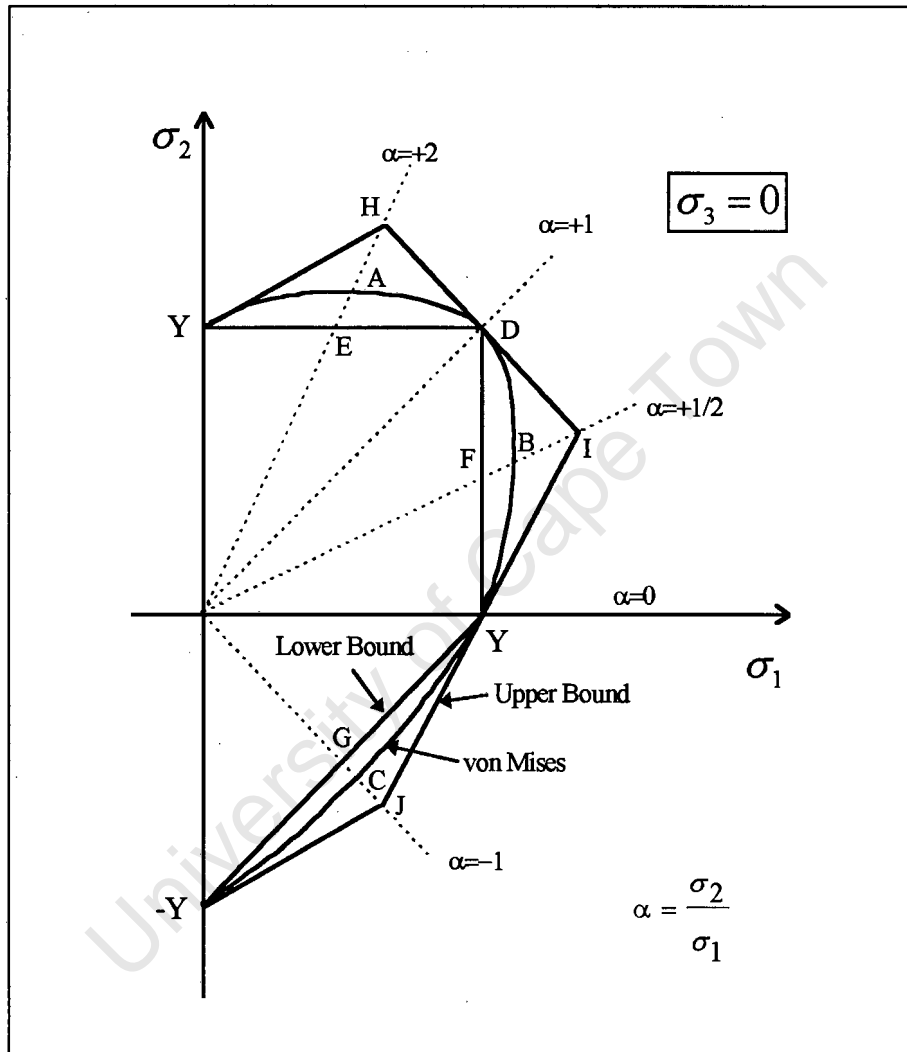


Figure 5.1. Generic Yield Surface Position in Principal Stress Space

The stress points associated with the von Mises yield surface agree with analytical values presented by Hosford and Caddell [1]. The lower bound (Tresca approximation) stress points closely approach the analytical ones which are:-

$$E = (0.500, 1.000, 0)Y$$

$$F = (1.000, 0.500, 0)Y$$

$$G = (0.500, -0.500, 0)Y$$

The discrepancy in the Tresca stresses is a result of limiting the yield surface parameter k to a maximum of 15.

No analytical stress points were determined for the upper bound yield surface for comparison purposes. However, the values obtained from the subroutine are reasonable when compared to those obtained for the previous yield surfaces and are therefore considered reliable.

5.2 von Mises Case

The Karafillis-Boyce constitutive model reduces to the isotropic von Mises case for $k = 1$ and $0 \leq c \leq 1$ with the mapping matrix $\underline{\underline{L}}$ parameters set to:-

$$C = \frac{2}{3} \quad \alpha_1 = \alpha_2 = 1 \quad \text{and} \quad \gamma_1 = \gamma_2 = \gamma_3 = \frac{3}{2}$$

With these parameter settings the calculated stress, plastic strain, equivalent plastic strain and consistent tangent modulus were compared to those obtained from a standard von Mises subroutine [15] for randomly selected strain increments. The two routines agreed on all accounts.

Furthermore, the performance of the subroutine was confirmed by comparing the results it produced for a typical finite element problem, against those produced for the standard von Mises routine. The problem consisted of a cantilever beam of unit length, breadth and depth which was subjected to various combinations of shear, tension and compression loads. The finite element model, which is illustrated in Figure 5.3, consisted of eight, 8-noded, 3-D, brick elements with the following material properties:-

$$E = 73 \text{ GPa} \quad \nu = 0.33 \quad Y = 293 \text{ MPa} \quad H = 5 \times 10^8 \text{ Pa}$$

Once again the solutions returned by the subroutines agreed, where it was noted that the solution convergence rates were quadratic for both cases when strains were kept within reasonable limits. Table 5.1 lists the residual force for an example problem which converged in one increment with four iterations. Here the free end of the beam was displaced by 2×10^{-2} in both the axial and lateral directions simultaneously.

Table 5.1. Force Residuals: von Mises Case

Iteration No.	1	2	3	4	
Residual Force	1329×10^8	1393×10^6	5.1272×10^4	-553	converged

5.3 Integration Algorithm Iso-Error Plots

An effective approach to quantify the error accumulated by an encoded constitutive model's stress return algorithm is presented by Peric *et al* [18]. A set of orthogonal axes, defined by a normal and a tangent, is defined at a selected stress point on the yield surface, point A as depicted in Figure 5.2. Each stress point in the plane defined by these axes is now used in the stress return algorithm as an elastic predictor. The returned stress is then determined via two paths:-

- 1) The stress return algorithm returns each stress to the yield surface directly.
- 2) The strain loading which causes each elastic predictor stress is divided into 1000 increments and the loading applied incrementally.

The stress calculated by method two is then considered the exact solution, $\underline{\sigma}_{\text{exact}}$, and the error associated with the standard return, $\underline{\sigma}_{\text{num}}$, is calculated as:-

$$\text{error} = \cos^{-1} \frac{\underline{\sigma}_{\text{exact}} \cdot \underline{\sigma}_{\text{num}}}{|\underline{\sigma}_{\text{exact}}| |\underline{\sigma}_{\text{num}}|} \quad \dots(5.1)$$

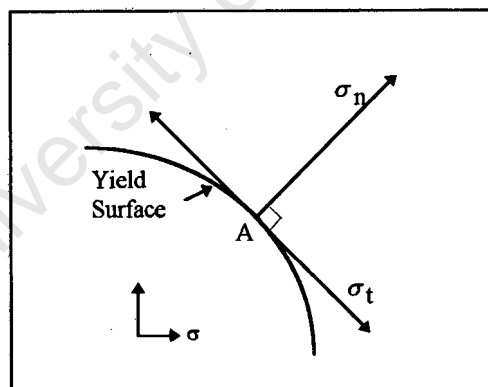


Figure 5.2. Iso-Error Axes on Yield Surface

Appendix H lists a FORTRAN 77 code which produces a matrix of errors that approximate the error distribution in the stress plane for a selected stress point on the yield surface. Since the yield surface under consideration is three dimensional this stress plane is appropriately chosen to fall in the π -plane. The range covered by the tangential stress axis is $-3Y$ to $+3Y$ and the normal stress axis from 0 to $6Y$, where Y is the material uniaxial yield strength.

Iso-error plots were produced for the lower and upper bound yield surfaces at the points $(Y, Y, 0)$, $(Y, 0, 0)$ and at the point of intersection of the yield surfaces with the

maximum shear line in $\sigma_3 = 0$ space. The material properties used were $E = 73 \text{ GPa}$, $\nu = 0.33$, $H = 10^8$ and $Y = 293 \text{ MPa}$. The iso-error plots, which were produced using Mathcad 5 [16], are presented in Figures 5.4 to 5.9.

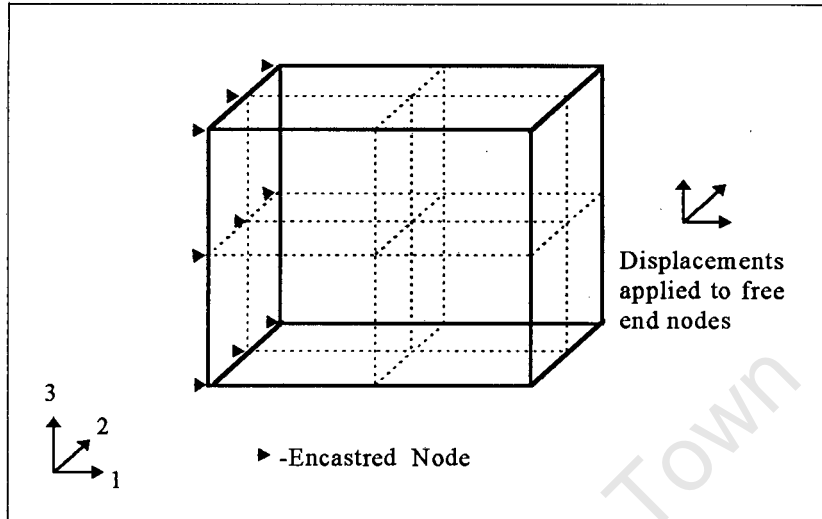


Figure 5.3. Cantilever Beam Mesh

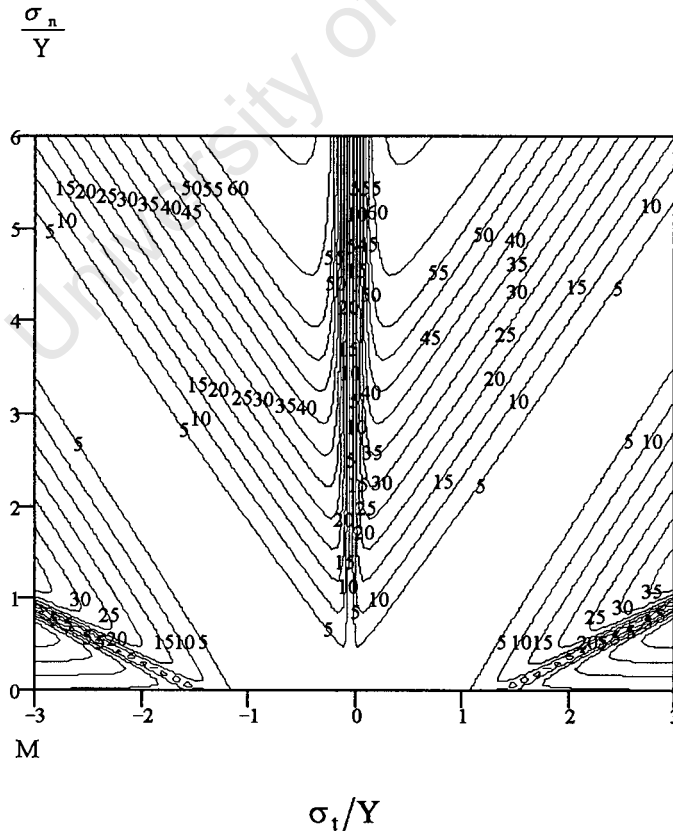
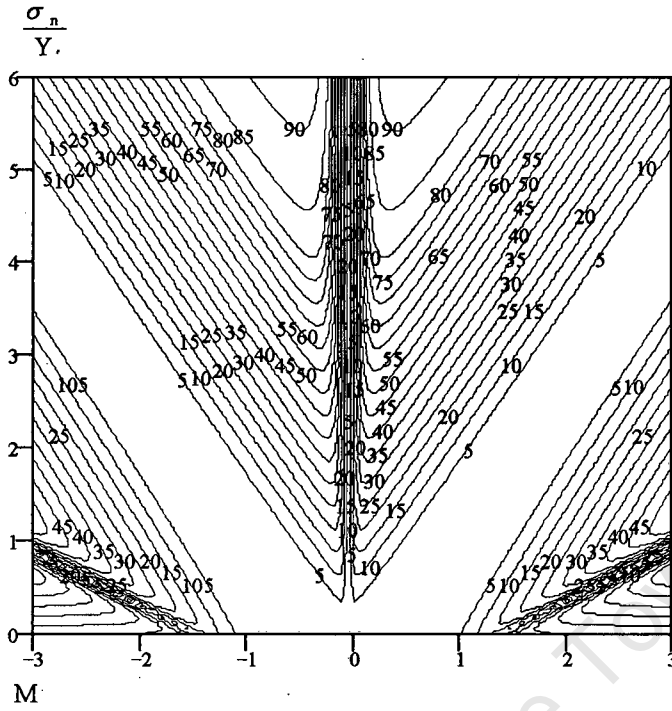
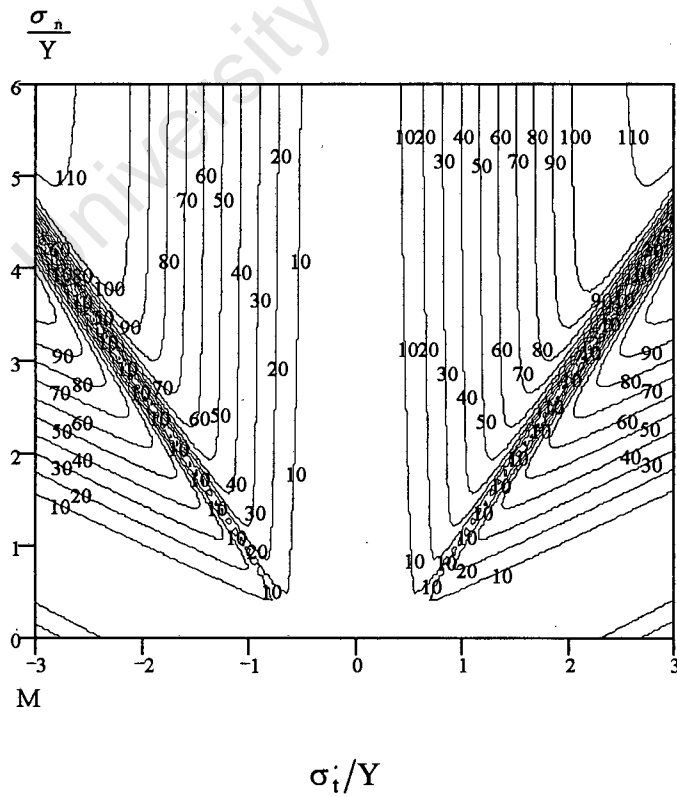


Figure 5.4. Iso-Error Plot: Lower Bound at $(Y, Y, 0)$



σ_t/Y
Figure 5.5. Iso-Error Plot: Lower Bound at (Y, 0, 0)



σ_t/Y
Figure 5.6. Iso-Error Plot: Lower Bound at (0.5117Y, -0.5117Y, 0)

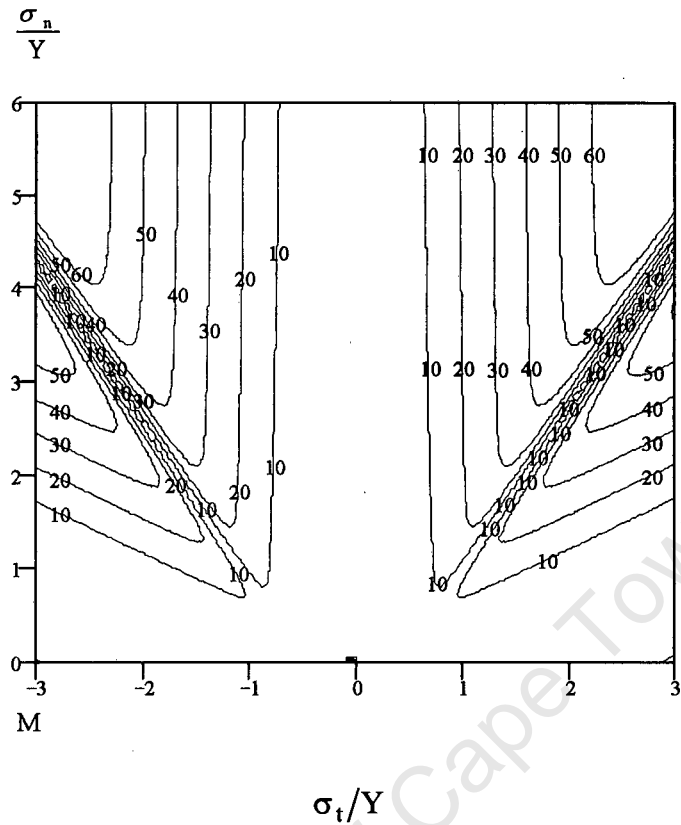


Figure 5.7. Iso-Error Plot: Upper Bound at (Y, Y, 0)

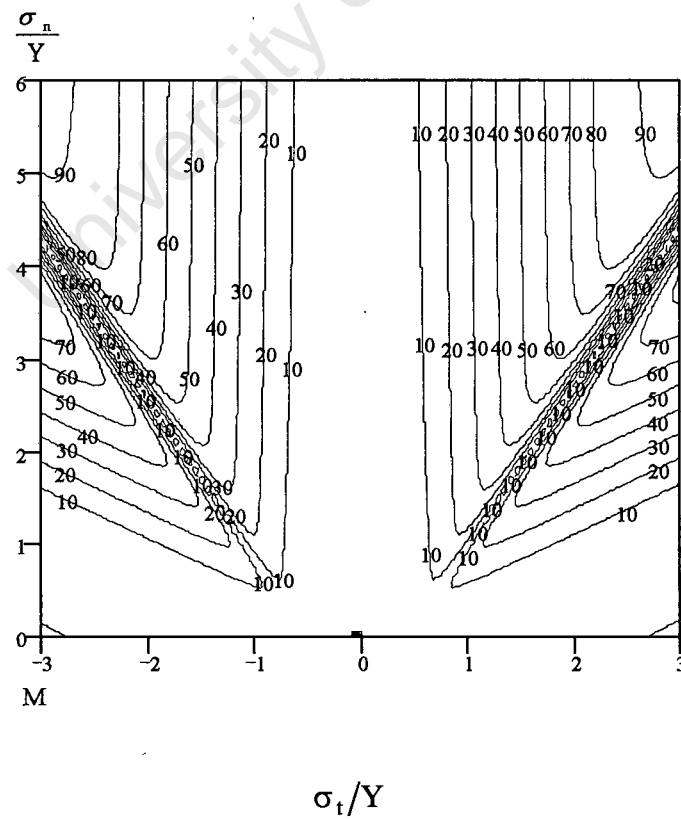


Figure 5.8. Iso-Error Plot: Upper Bound at (Y, 0, 0)

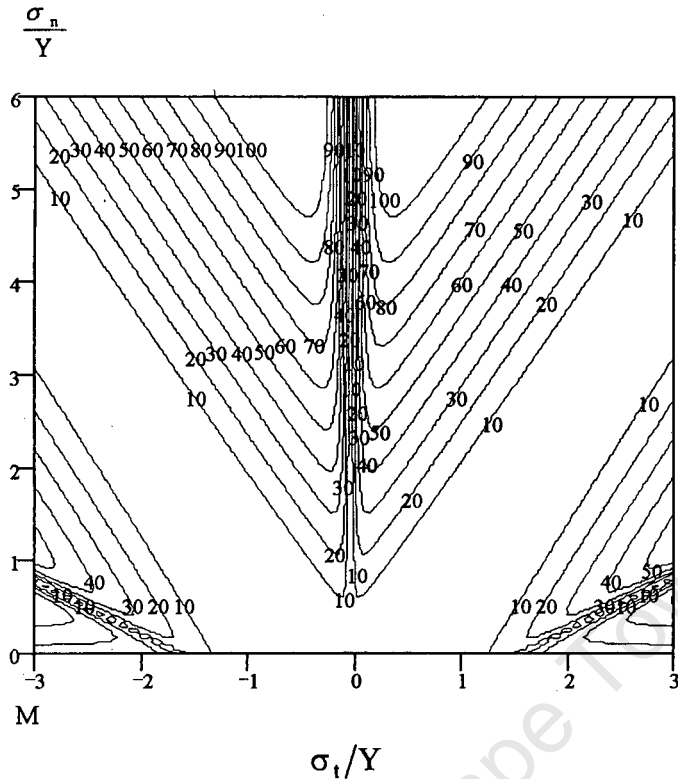


Figure 5.9. Iso-Error Plot: Upper Bound at $(0.6514Y, -0.6514Y, 0)$

These iso-error plots show zero error troughs radiating out from the yield surfaces, some of which are associated with extremely steep error gradients. Inspection of the upper and lower bound yield surfaces in the π -plane indicate that these regions of steep error gradient are associated with corners on the yield surfaces.

Similar iso-error plots for the von Mises case indicate zero error, as defined by Equation (5.1), for all points in stress space. Note that for von Mises the yield surface normal and radial from the hydrostatic line, coincide. It is therefore believed that the zero error troughs displayed in the above iso-error plots also indicate regions in stress space where the radial and the generic yield surface normal coincide.

The verification procedures discussed in this chapter for the FORTRAN 77 encoded Karafillis-Boyce constitutive model, while not exhaustive, are sufficient to invoke confidence in the implemented computer code. It is therefore believed that this subroutine may be used with confidence in a general purpose finite element code as a material constitutive model.

CHAPTER SIX

FINITE ELEMENT EARING SIMULATION

The implemented and tested anisotropic constitutive model subroutine, as presented in Chapters Four and Five, was used in the general purpose finite element code ABAQUS Version 5.4 to simulate earing in a deep drawing operation.

Four simulations were run using this constitutive model: two with the constitutive model parameters representing A3004-H19 can body stock material and two to investigate the effect of the choice of the isotropic yield surface on earing. For comparison purposes, a fifth case was run using the Hill (1948) material model which is an ABAQUS constitutive model option. These simulations are compared against experimentally determined results provided by Hulett Aluminium (Pty) Ltd

6.1 Deep Drawing Cupping Operation

The blank and tool geometries are taken from a standard industry cupping test and are illustrated in Figure 6.1. The mechanical properties of the A3004-H19 can body stock used in this study are:-

Table 6.1. A3004-H19 Material Properties

Elastic:	$E = 73 \text{ GPa}$	$\nu = 0.33$	$H = 5 \times 10^8 \text{ Pa}$
Plastic:	$Y_0 = 286 \text{ MPa}$	$Y_{45} = 290 \text{ MPa}$	$Y_{90} = 303 \text{ MPa}$
	$R_0 = 0.67$	$R_{45} = 0.93$	$R_{90} = 0.80$

$$\therefore \text{Average Yield Strength} = \bar{Y} = 293 \text{ MPa}$$

According to a suggestion by Hulett Aluminium (Pty) Ltd the average shear yield stress is estimated as:-

$$\text{Shear Yield Strength} = \bar{S}_y = 57\% \times \bar{Y} = 167 \text{ MPa}$$

For this material Equations (1.3), (1.1) and (1.5) give:-

$$\bar{R} = 0.8325 \quad \text{LDR} = 2.05 \text{ (with } \eta = 0.74\text{)}$$

and $\Delta R = -0.1950$

These figures show that the blank and tool geometries for the draw are within acceptable limits as the proposed draw ratio is only 1.68. Furthermore from Figure 1.10 and the ΔR value, it is clear that ears at 45° are anticipated. This is confirmed by experimental data obtained by Hulett Aluminium which reports 3.1% earing (Equation (1.6)) at 45° .

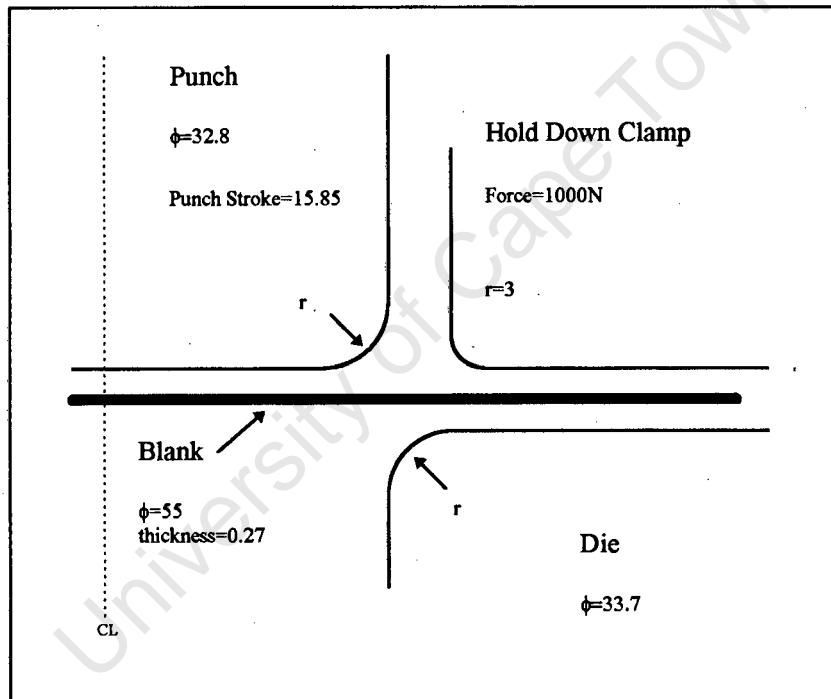


Figure 6.1. Blank and Tool Geometries

6.2 Material Model Parameters

The FORTRAN 77 code of Appendix F was used to fit the generic isotropic yield surface to the above material properties. The resultant values for the yield surface parameters, mapping matrix C value and the surface fitting errors are given in Table 6.2.

Table 6.2. Isotropic Yield Surface Parameters for A3004-H19 Alloy

k	c	% Error	C
1	0.0000	-1.279015	0.6498760385
2	0.0000	-1.279015	0.6498760385
3	0.3512	-0.000217	0.6496590997
4	0.5018	0.000482	0.6496563279
5	0.5947	-0.000402	0.6496535965
6	0.6695	0.000655	0.6496748894
7	0.7325	0.001006	0.6497268242
8	0.7855	-0.000567	0.6498040721
9	0.8294	-0.000628	0.6498966814
10	0.8653	-0.000734	0.6499960846
11	0.8943	-0.001707	0.6500955321
12	0.9174	-0.000165	0.6501898049
13	0.9357	0.000617	0.6502766366
14	0.9501	0.000446	0.6503546429
15	0.9614	-0.003212	0.6504236771

and the mapping matrix \underline{L} parameters:-

Table 6.3. IPE Mapping Matrix Parameters

$\alpha_1 = 1.00149700$	$\alpha_2 = 1.11127744$	
$\gamma_1 = 1.58912674$	$\gamma_2 = 1.50000000$	$\gamma_3 = 1.50000000$
$\beta_1 = -0.445109780$	$\beta_2 = -0.554890219$	$\beta_3 = -0.556387225$

Inspection of Table 6.2 shows that the lowest yield surface fitting errors occur for values of $k = 3$ and $k = 12$. These values and their respective c values are therefore selected for two deep drawing simulation cases.

Figures 6.2 and 6.3 illustrate the iso-error plots for the User-Material stress return algorithm using the selected material model parameters at the stress point $(\bar{Y}, \bar{Y}, 0)$. These plots show that integration errors of approximately 5% may be expected for elastic predictors within a radius \bar{Y} of the yield surface.

To investigate the effect of the choice of the yield surface shape on earing a case was run with the isotropic yield surface parameters determined for the material properties as above, but with the shear yield strength reduced to 53% of the average uniaxial yield strength. This shear strength requires a yield surface close to the lower bound. Such a yield surface produces a larger plastic strain than one tending towards the upper bound, for a given elastic predictor and should therefore produce a greater degree of earing. The constitutive model parameters determined by the FORTRAN 77 code of Appendix F are:-

Table 6.4. Alternative Yield Surface Parameters

k	c	% Error	C
6	0.0075	-0.000036	0.6475654063

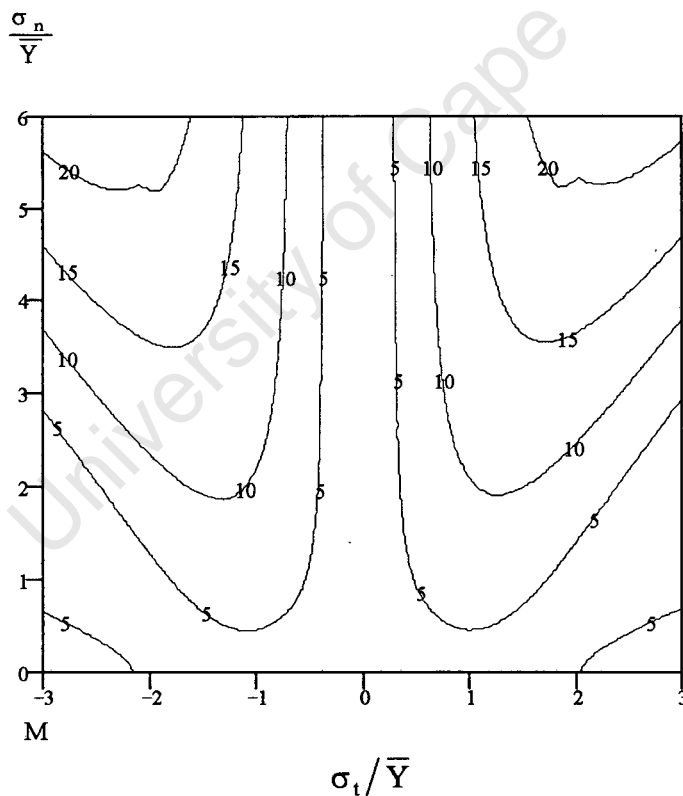
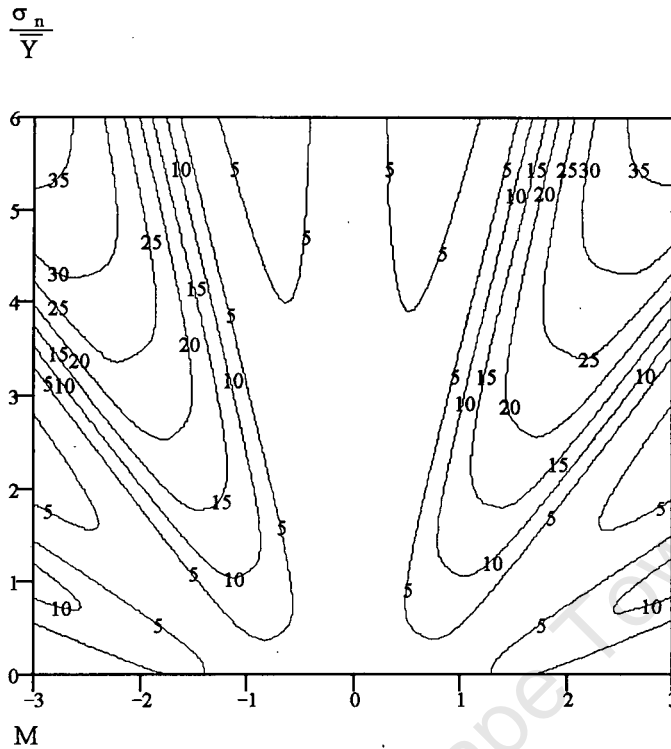


Figure 6.2. Iso-Error Plot: $k = 3$, $c = 0.3513$
 at $\underline{\sigma} = (\bar{Y}, \bar{Y}, 0)$



σ_t / \bar{Y}

Figure 6.3. Iso-Error Plot: $k = 12$, $c = 0.9174$
at $\underline{\sigma} = (\bar{Y}, \bar{Y}, 0)$

A fourth case study, with the yield surface parameters set for the von Mises case ($k = 1$) was considered necessary in order to gain further insight into the constitutive model's effect on earing. In this case the mapping matrix C parameter was found to be $C = 0.64987603$.

The material model parameters for the Hill (1948) case study were determined according to the procedure described in the ABAQUS Standard Users Manual [15] using the material R -values. These parameters are:-

$$\begin{array}{lll} \frac{\bar{\sigma}_{11}}{\sigma_0} = 1.00 & \frac{\bar{\sigma}_{22}}{\sigma_0} = 1.052520 & \frac{\bar{\sigma}_{33}}{\sigma_0} = 0.95333 \\ \frac{\bar{\tau}_{12}}{\tau_0} = 0.9764 & \frac{\bar{\tau}_{13}}{\tau_0} = 1.00 & \frac{\bar{\tau}_{23}}{\tau_0} = 1.00 \end{array}$$

where the $\bar{\sigma}$'s and $\bar{\tau}$'s are the material yield stresses in the indicated directions and σ_0 and τ_0 are the average uniaxial and shear yield stresses, respectively.

6.3 Finite Element Model

A finite element model of the blank and tools, as depicted in Figure 6.1, was implemented in ABAQUS Version 5.4. The punch, die and hold-down clamp were modelled as frictionless rigid surfaces and the blank was idealised by C3D8 brick elements (8 node full integration). The blank finite element mesh is illustrated in Figure 6.4. The ABAQUS input file, as Appendix I indicates, is standard in all respects, with the exception of the two options discussed below.

As a result of material anisotropy the tangent modulus produced by the encoded Karafillis-Boyce constitutive model is non-symmetric. Consequently the global stiffness matrix produced by ABAQUS is also non-symmetric. However, by default ABAQUS assumes symmetry of these matrices, therefore the UNSYMM option was used with the *HEADING and *USER MATERIAL keywords. These options require ABAQUS to use a full matrix solver routine, with the result that convergence is more likely, but more expensive in terms of CPU time.

Convergence of the finite element global solution is adversely effected by values of k and c which result in irregular shaped yield surfaces, such as the lower and upper bound yield surfaces. As a standard procedure for cases of slow convergence ABAQUS relaxes the residual solution tolerance from the standard $\frac{1}{2}\%$ to 2%. Since convergence was anticipated to be slow in some of the deep drawing simulations, it was deemed expeditious to pre-set the tolerance to 2% for all cases run with this constitutive model.

6.4 Results

Table 6.5 shows the CPU time and number of increments required for solution convergence for each of the five deep drawing cases:-

Table 6.5. CPU Time and Number of Increments

Case	Computer	CPU Time (hr)	No of Increments
$k = 3, c = 0.3513$	IBM RS6000 Model 560	21.64	63
$k = 12, c = 0.9174$	IBM RS6000 Model 390	26.19	110
$k = 6, c = 0.0075$	IBM RS6000 Model 390	102.76	429
$k = 1$	IBM RS6000 Model 560	15.84	53
Hill (1948)	IBM RS6000 Model 390	4.01	74

Table 6.6 summarises the pertinent geometric results for each case. The cases run with the Karafillis-Boyce constitutive all shared the same α and γ values in the IPE mapping matrix.

Table 6.6. Cup Geometry Results and Earing

Case	Δh	\bar{h}	% Earing
$k = 3, c = 0.3513$	-0.1292	15.1393	-0.8534
$k = 12, c = 0.9174$	-0.0977	15.0997	-0.6470
$k = 6, c = 0.0075$	-0.2161	15.2566	-1.416
$k = 1$	-0.0794	15.0730	-0.5268
Hill (1948)	-0.3331	15.0325	-2.216

In this table Δh , \bar{h} and the % earing are determined from Equation (1.6)

Figures 6.5-6.14 display the earing profiles and total equivalent plastic strain distributions for the five deep drawing cases. Figure 6.15 illustrates the punch force profiles for the Hill, von Mises, $k = 3$ and $k = 12$ cases.

6.5 Discussion of Results

Hulett Aluminium (Pty) Ltd report 3.1% earing at 45° to the rolling direction for the aluminium alloy A3004-H19. The results of Table 6.6 suggest, therefore, that in comparison to the Karafillis-Boyce criterion the Hill (1948) constitutive model is the more suitable one for ear prediction in this material.

Both constitutive models do, however, underpredict the degree of earing. This may partly be explained by the use of an increased die radius of 3 millimeters in the simulation to improve solution convergence. The die used in the laboratory drawn cups has a radius of 2 millimeters which causes significantly more plastic strain in the workpiece during the draw and therefore results in more earing. Ear prediction may be improved further by using a more realistic value for the linear hardening parameter H . The value of $H = 5 \times 10^8$ Pa, which may be unrealistically high, was chosen to prevent localised necking in the cup wall during the draw.

Inspection of the earing profiles for the five material cases shows that all the profiles are similar except for the $k = 6$ case which clearly has a greater average wall height. Furthermore, it is apparent that the earing profile for the Hill case is more gradual than for the Karafillis-Boyce cases which are characterised by sudden troughs at 0° and 90° . Comparison of the Hill and $k = 6$ cases demonstrate this phenomenon.

The predicted total equivalent plastic strain distribution for the five cases are also similar except, once again, for the $k = 6$ case which predicts a greater degree of plastic

strain. The increase in plastic strain and degree of earing for the $k = 6$ case confirms the anticipated behaviour of a material with a yield surface contracted in stress space. It should be noted that Figure 6.14, which shows the total equivalent plastic strain distribution for this case, has a different colour legend to the other plots.

Comparison of Figures 6.10 and 6.12 shows that the total equivalent plastic strain distributions are very similar for the $k = 3$ and $k = 12$ cases. This is expected as these cases have similarly shaped yield surfaces in stress space and should therefore produce similar plastic strains.

It is clear from the earing profile and total equivalent plastic strain figures that the results for the von Mises case are not significantly differently from the $k = 3$ and $k = 12$ cases. This may be explained by the relative positions of these yield surfaces in stress space. The position of the generic isotropic yield surface is determined from the average uniaxial yield strength \bar{Y} and the average shear yield strength \bar{S}_y . $\bar{Y} = 293\text{MPa}$ for all cases; $\bar{S}_y = 57\% \times \bar{Y}$ for A3004-H19 and by definition $\bar{S}_y = \frac{1}{\sqrt{3}} \times \bar{Y} \approx 57.7\% \times \bar{Y}$ for the von Mises criterion. Clearly in this case the best fit Karafillis-Boyce yield surfaces closely approximate the von Mises yield surface and will therefore produce similar results.

The punch force profiles for the Hill, von Mises, $k = 3$ and $k = 12$ cases, illustrated in Figure 6.15, indicate discrepancies between the material model cases over the region where the punch forces are the greatest. Significantly the punch forces for the $k = 3$ and $k = 12$ cases do not agree in this region, suggesting that either small differences in plastic behaviour have a marked affect on the punch force in this region, or that plasticity considerations alone are not sufficient to describe punch force behaviour during this part of the draw. Punch forces are in close agreement for all cases outside this region.

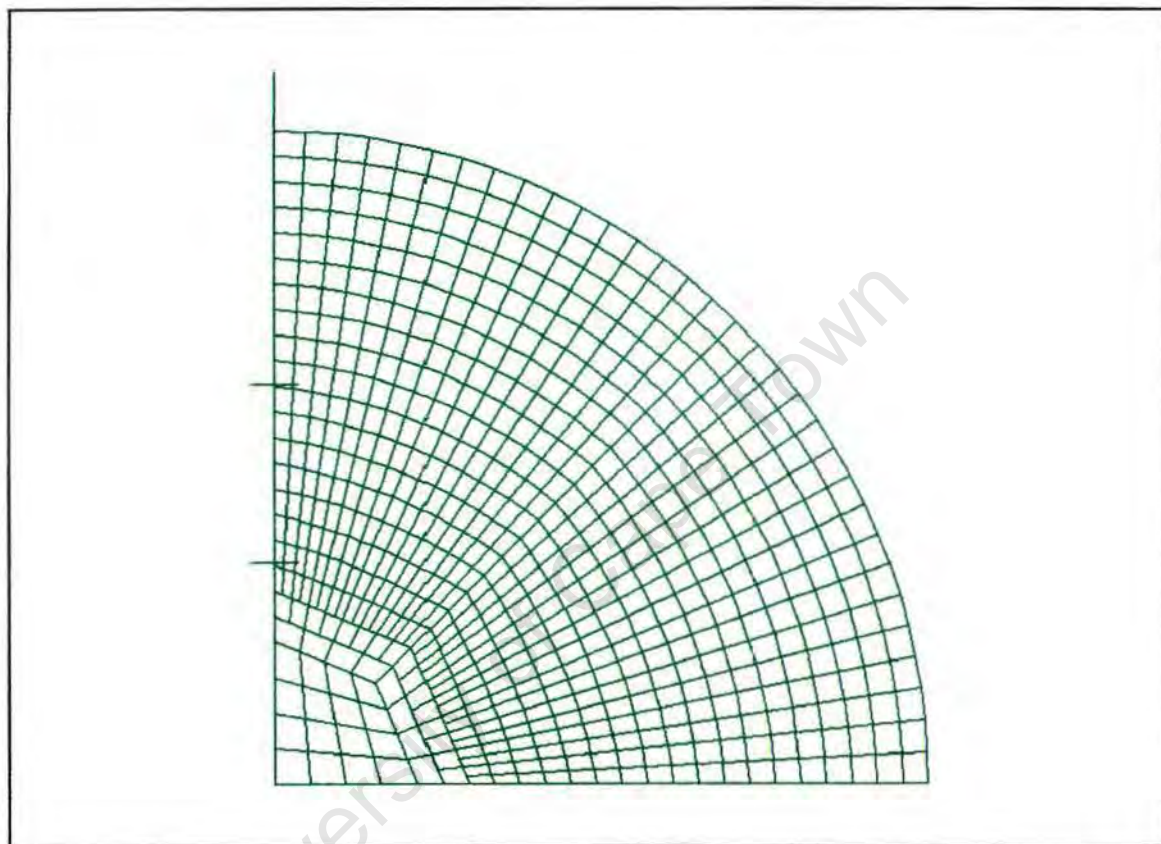


Figure 6.4. Blank Mesh: Eight Noded (C3D8) Brick Elements

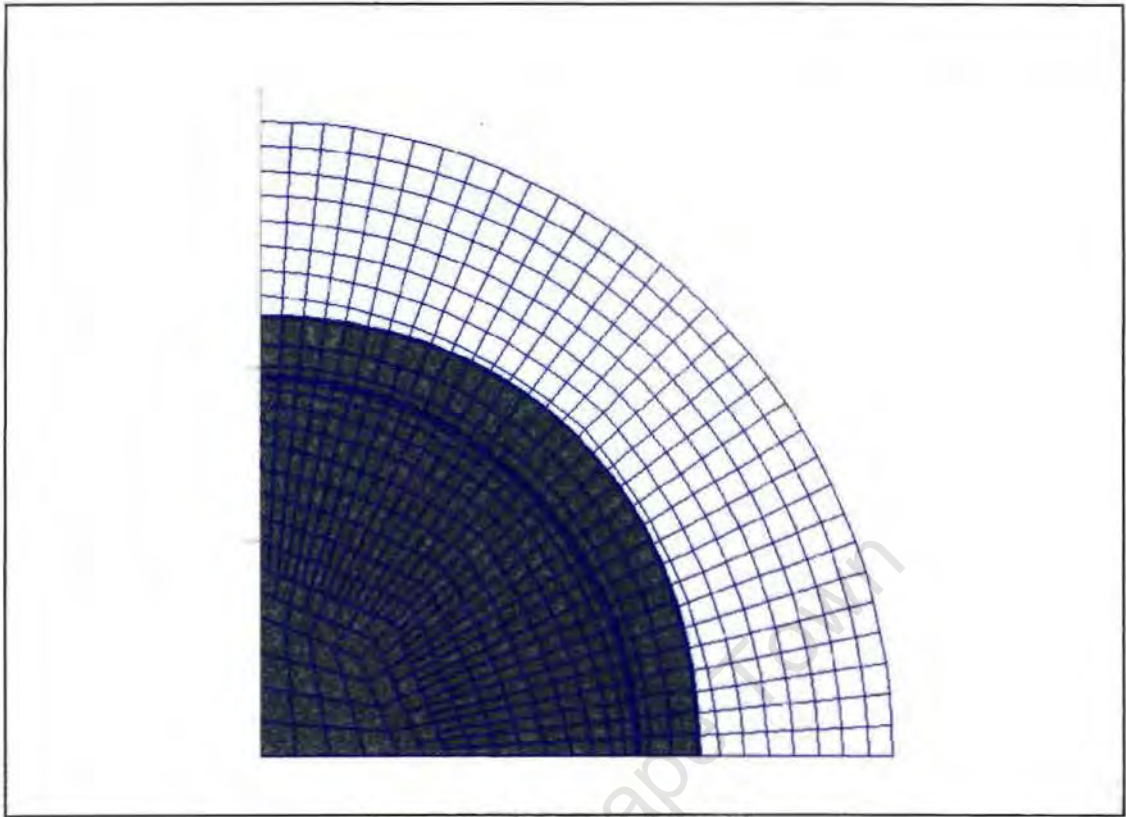


Figure 6.5. Earing Profile: Hill

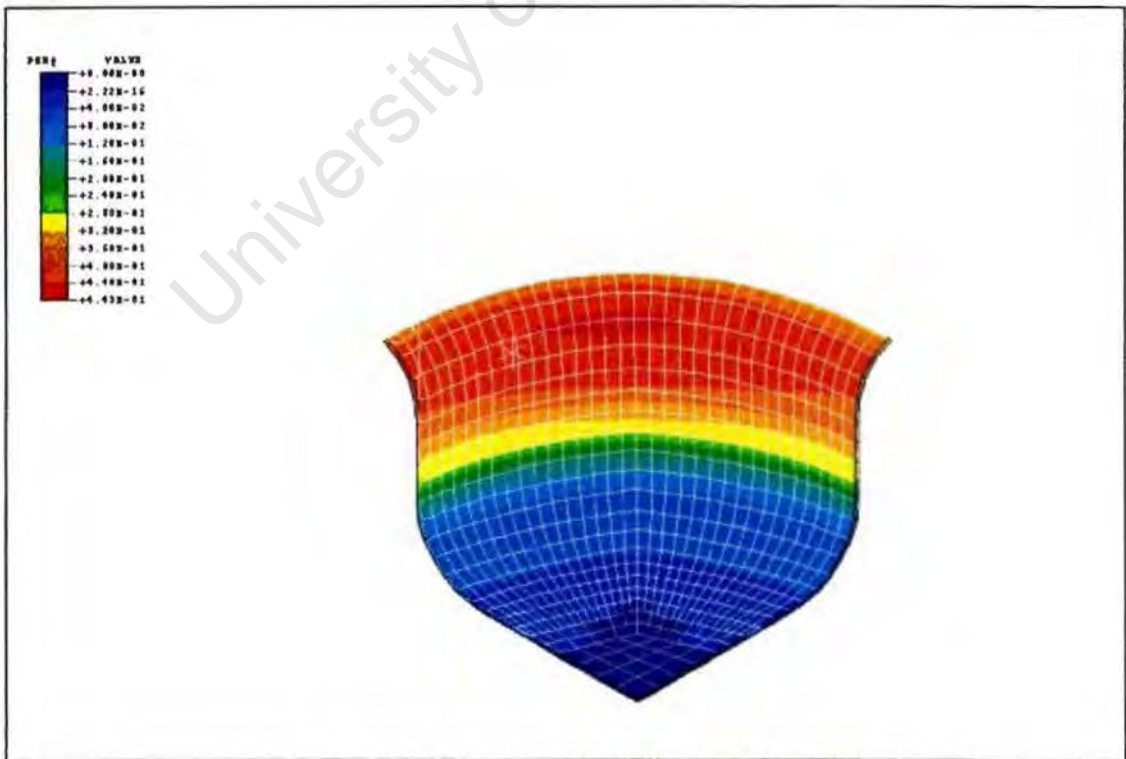


Figure 6.6. Total Equivalent Plasticity: Hill

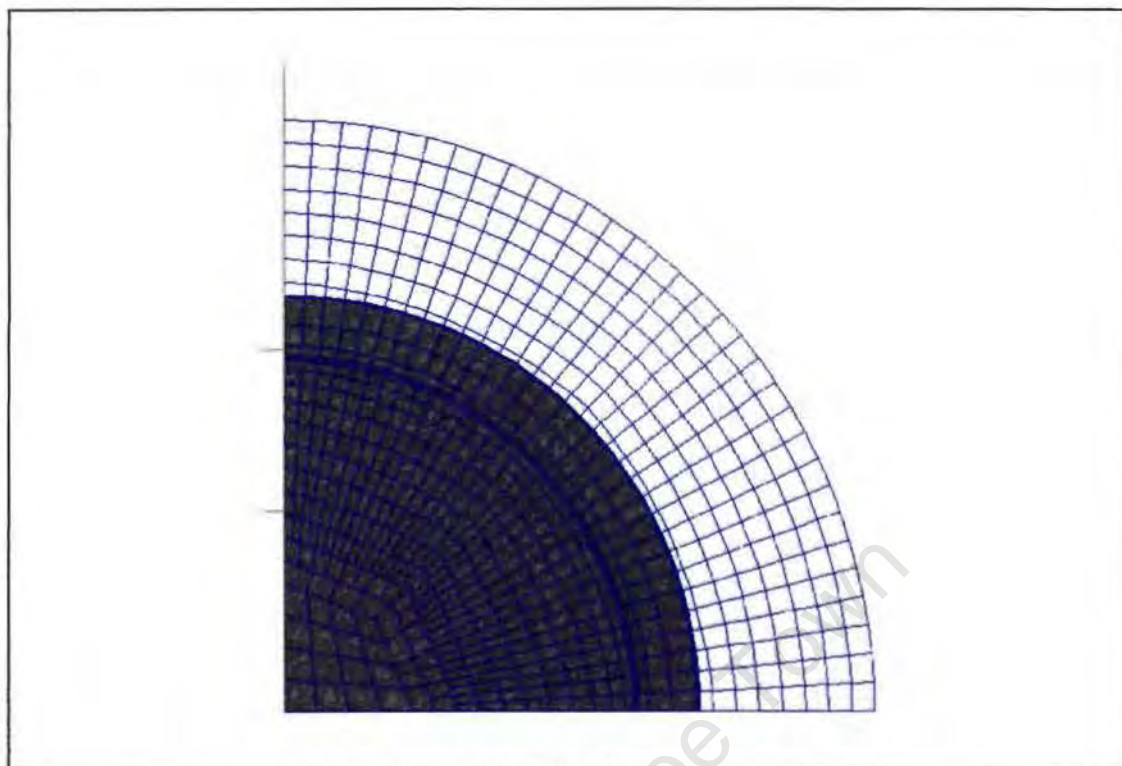


Figure 6.7. Earing Profile: $k = 1$, $c = 0$

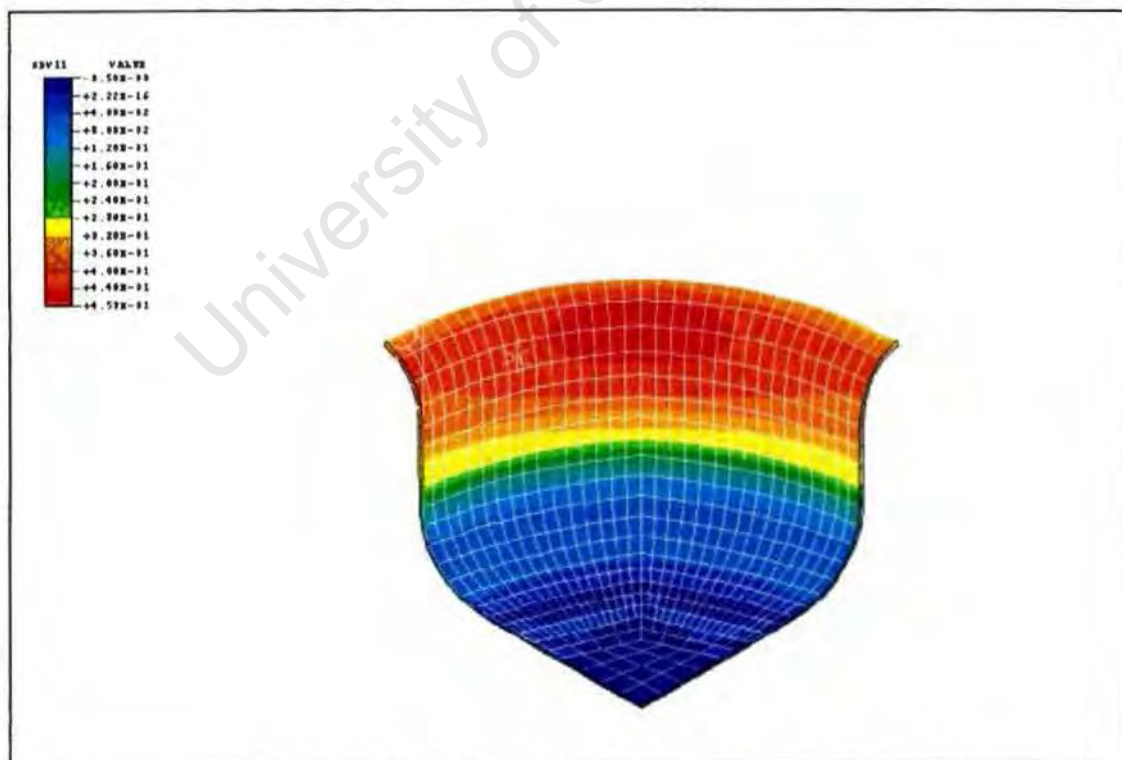


Figure 6.8. Total Equivalent Plasticity: $k = 1$, $c = 0$

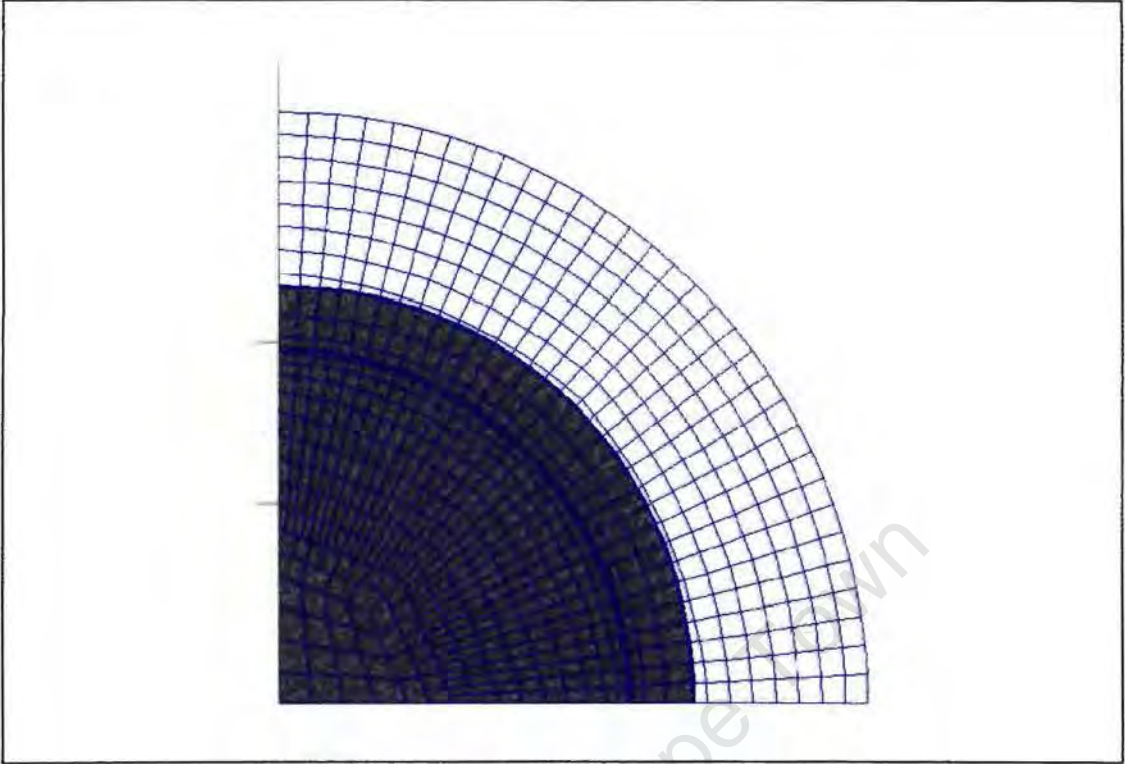


Figure 6.9. Earing Profile: $k = 3$, $c = 0.3513$

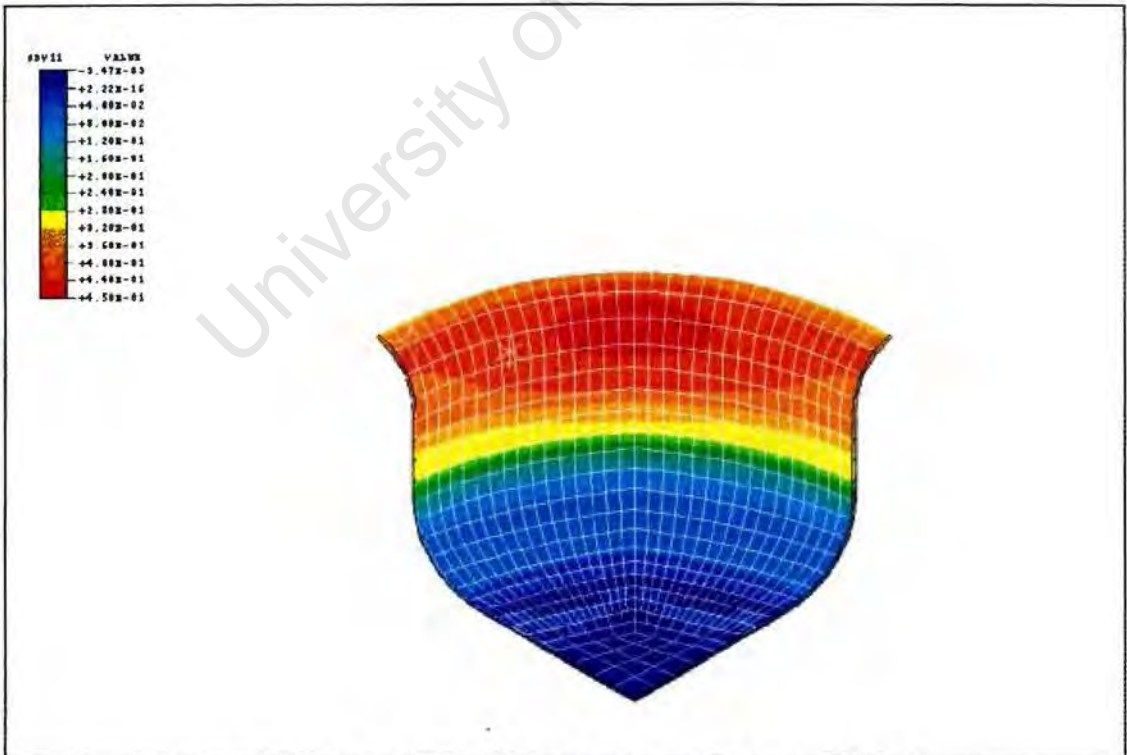


Figure 6.10. Total Equivalent Plasticity: $k = 3$, $c = 0.3513$

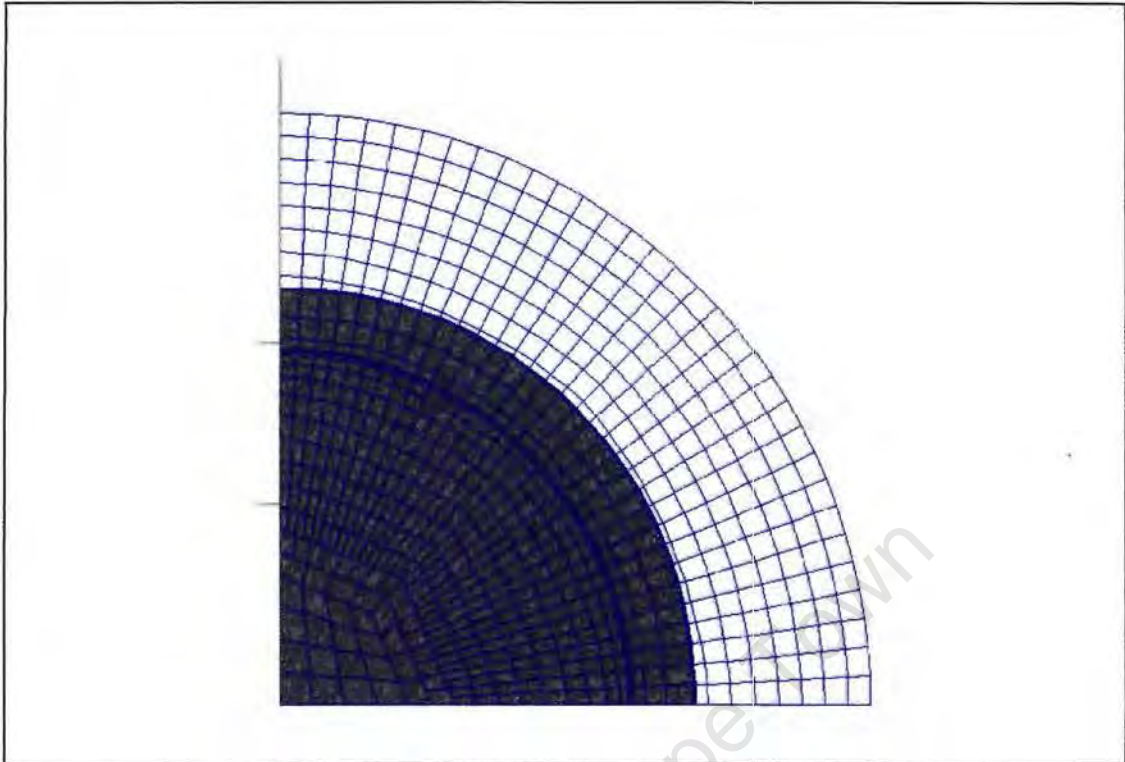


Figure 6.11. Earing Profile: $k = 12$, $c = 0.9174$

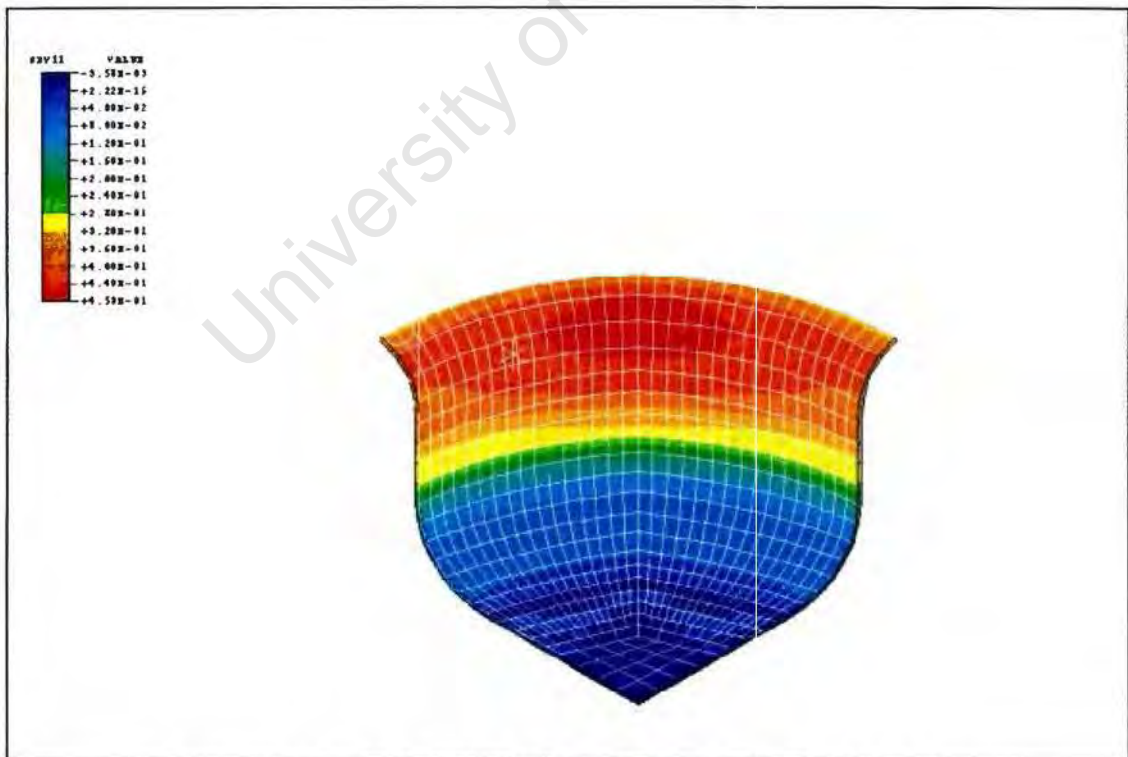


Figure 6.12. Total Equivalent Plasticity: $k = 12$, $c = 0.9174$

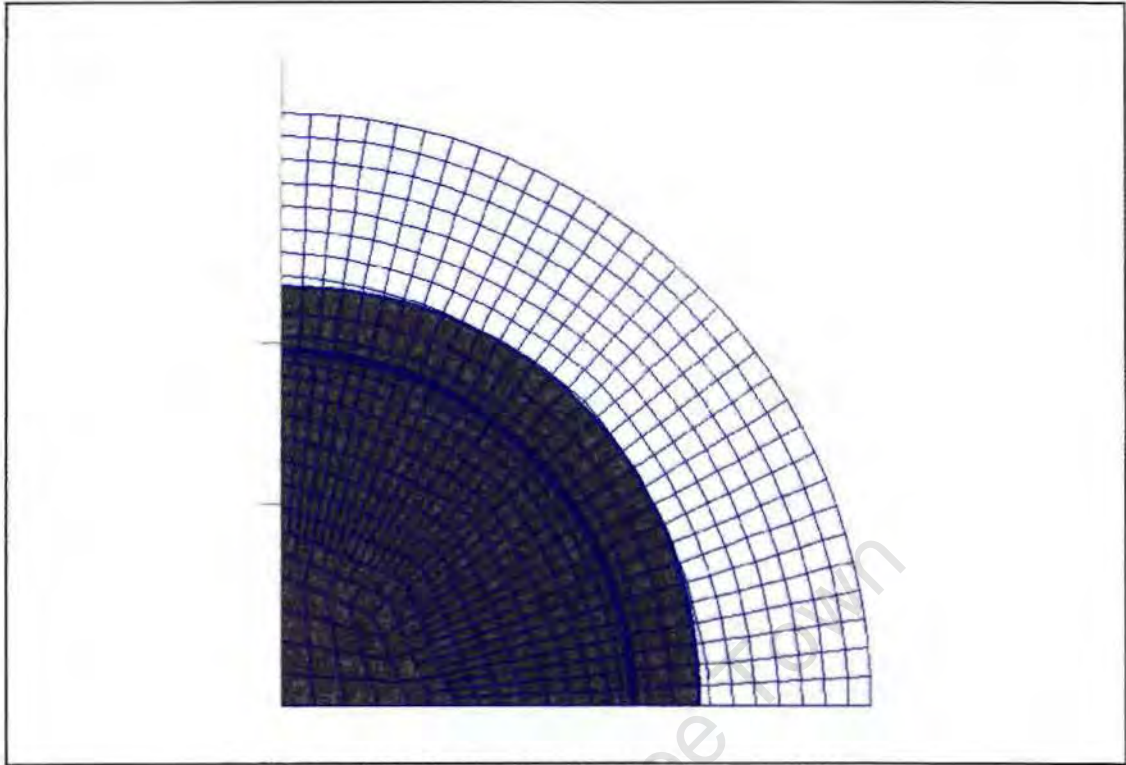


Figure 6.13. Earing Profile: $k = 6$, $c = 0.0075$

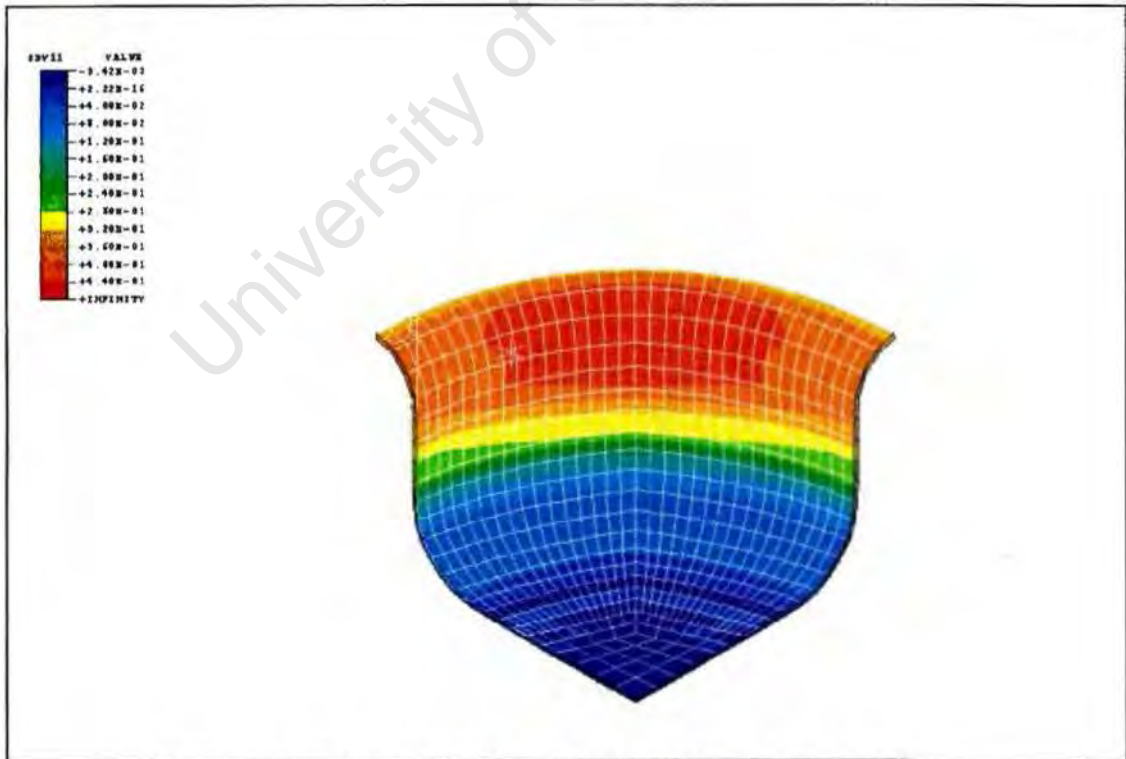


Figure 6.14. Total Equivalent Plasticity: $k = 6$, $c = 0.0075$

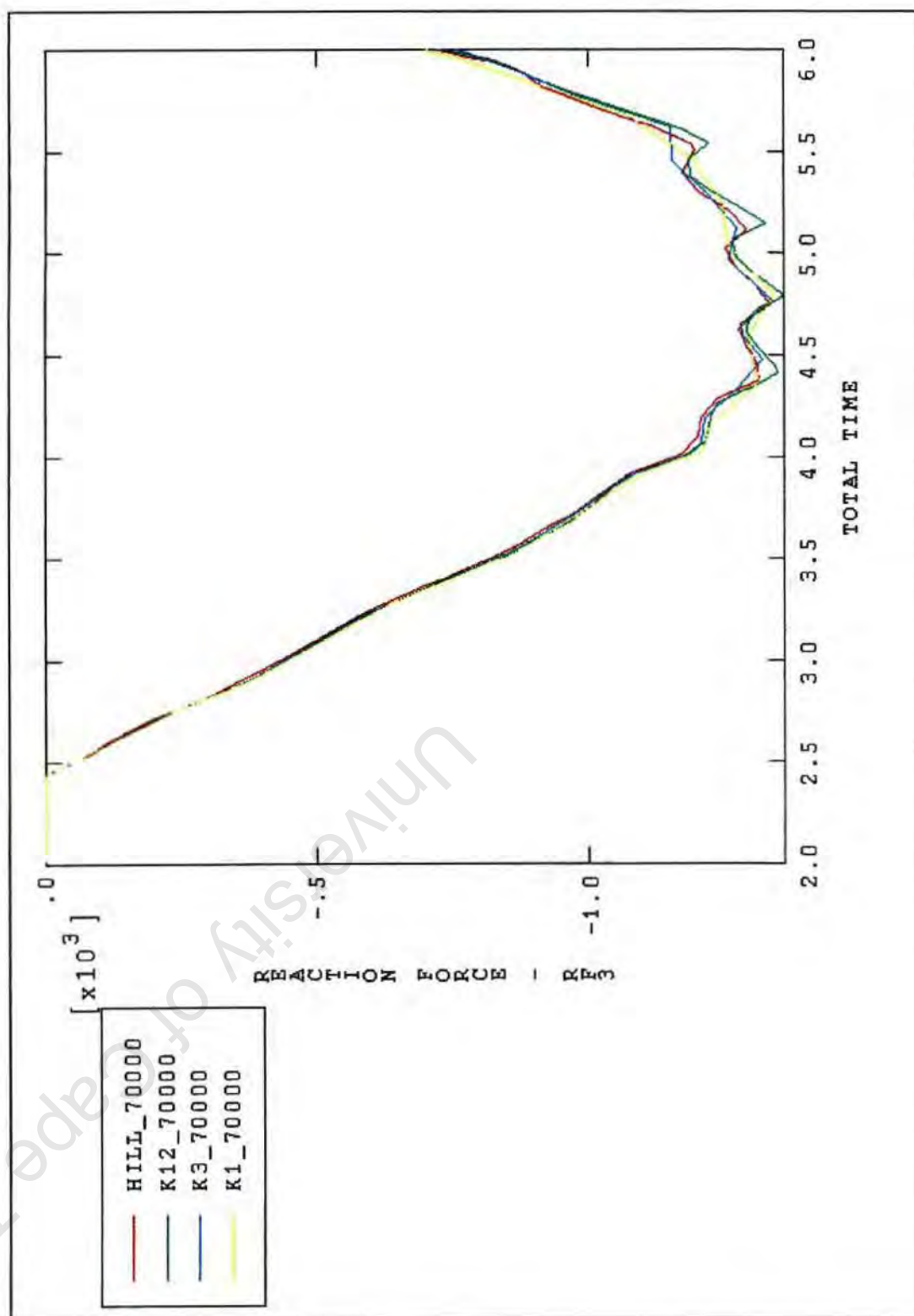


Figure 6.15. Punch Force/Time Profile

CHAPTER SEVEN

CONCLUSION AND RECOMMENDATIONS

7.1 Conclusion

An anisotropic constitutive model proposed by Karafillis and Boyce was implemented in the general purpose finite element code ABAQUS Version 5.4 as a User-Material Subroutine in order to simulate *earing* in the deep drawing of an aluminium axisymmetric cup. Finite element simulation of this cupping operation with this constitutive model and Hill's 1948 one suggests that the Hill model is more suitable for simulating the anisotropic behaviour of A3004-H19 can body stock.

Both material models under predict the degree of earing for this material. This may be improved by decreasing the finite element model die radius from 3 millimetres to 2 millimetres so that it corresponds to the laboratory tooling geometry and by using a more realistic linear hardening parameter H .

The earing profile for the Hill model is characterised by a gradual change in cup wall height, while that for the Karafillis-Boyce model shows broader ears associated with steeper troughs. These profiles have not been compared to experimental ones.

Punch force profiles for the Hill model and for different cases of the Karafillis-Boyce model are in close agreement except in the region where the punch force is the greatest. The reason for this has not been investigated.

7.2 Recommendations

This thesis has presented a limited investigation into the suitability of the Karafillis-Boyce constitutive model for simulating the earing phenomena in aluminium sheet. The following steps are recommended to further establish its ability to model anisotropy in sheet metal:-

- 1) Compare ear profile prediction to experimentally determined ones for various *face centred cubic* and *body centred cubic* materials with different degrees of anisotropy. In particular, establish the performance of the model for materials with average plastic strain ratios greater and less than one.

- 2) Confirm that the degree of earing will increase with a reduced die radius of 2 millimetres.
- 3) Confirm that the degree of earing will increase for a more realistic linear hardening parameter H . This may best be achieved by implementing piece-wise linear material hardening in the User-Material subroutine. Furthermore, some materials exhibit significant material strain rate dependence in deep drawing applications. It is therefore recommended that a suitable routine be implemented in the User-Material subroutine.
- 4) Establish the reason or reasons for the divergence of the punch force profiles over the region where the punch force is the greatest for the different material cases.

University of Cape Town

REFERENCES

1. Hosford W. F., Caddell R. M., *Metal Forming Mechanics and Metallurgy*, Prentice-Hall, Inc., Englewood Cliffs, N.J. 07632, 1983.
2. Ward J.D.B., *The Numerical Modelling of Transformation Induced Plasticity in the Deep Drawing of Stainless Steel*, MSc thesis, Department of Mechanical Engineering, University of Cape Town, Cape Town, 1993.
3. Naoyuki K., Yasuhisa T., Toshio O., *Calculations from Texture of Earing in Deep Drawing for FCC Metal Sheet*, Int. J. Mech. Sci., Vol. 25, No. 5, pp 337-345, 1983.
4. Malin A. S., Chen B. K., *Six-Fold Symmetry in Deep Drawn Cups*, Aluminum Alloys for Packaging, The Minerals, Metals & Materials Society, Australia, 1993.
5. Becker R., Smelser R. E., Panchanadeeswarin S., *Simulations of Earing in Aluminium Single Crystals and Polycrystal*, Modelling Simul. Mater. Sci. Eng., pp 1203-224, 1993.
6. Smelser R. E., Becker R., *Earing in a Cup Drawing of a (100) Single Crystal*, ABAQUS Users Conf. Proc., pp 457-471, Sept 11-13, 1991.
7. Owen D. R. J., Hinton E., *Finite Elements In Plasticity: Theory and Practice*, Pineridge Press Ltd ,1986.
8. Lubliner J., *Plasticity Theory*, Macmillan Publishing Company, 1990.
9. Mitchell G. P., *Topics in the Numerical Analysis of Inelastic Solids*, PhD thesis, Department of Civil Engineering, University of Wales, Swansea, 1990.
10. Hibbitt, Karlsson & Sorensen, Inc., *ABAQUS Theory Manual, Version 5.4*, 1994.
11. Hosford W. F., *The Mechanics of Crystals and Textured Polycrystals*, Oxford University Press, 1993.
12. Hill R., *A User-Friendly Theory of Orthotropic Plasticity in Sheet Metals*, Int. J. Mech. Sci., Vol 35, No.1, pp 19-25, 1993.
13. Karafillis A. P., Boyce M. C., *A General Anisotropic Yield Criterion Using Bounds And A Transformation Weighting Tensor*, J. Mech. Phys. Solids, Vol 41, No 12, pp 1859-1886, 1993.

14. Mendelson S., *Plasticity: Theory and Application*, Macmillan, New York, 1968.
15. Hibbitt, Karlsson & Sorensen, Inc., *ABAQUS / Standard User's Manual, Version 5.4*, 1994.
16. Math Soft Inc, *Mathcad 5.0 for Windows User's Guide*, 1994.
17. Crisfield M. A., *Consistent Schemes for Plasticity Computation with the Newton-Raphson Method*, Proc. Int. Conf. Computational Plasticity: Models, Software and Applications, Barcelona, Pineridge Press, pp133-159, 1987 .
18. Peric D., Dutko M., Owen D. R. J., *Universal Anisotropic Yield Criterion Based on Superquadric Functional Representation: Computational Issues with Applications*. Proc. 3rd Int. Conf. on Computational Plasticity III: Fundamentals and Applications, Barcelona, Pineridge Press, pp77-102, 1992.
19. Simo J. C., Ortiz M., *An Analysis of a New Class of Integration Algorithms for Elasto-Plastic Constitutive Relations*, Int. J. Num. Mech. Eng., v23, pp353-366, 1986.

APPENDIX A

PRINCIPAL DEVIATORIC STRESSES

Following the method of Owen and Hinton [7] the principal deviatoric stresses S_1 , S_2 and S_3 are given as the roots of the cubic equation:-

$$S^3 - J_2 S - J_3 = 0 \quad \dots(A.1)$$

let $S = r \sin \theta$, substitute into (A 1) and rearrange:-

$$\sin^3 \theta - \frac{J_2}{r^2} \sin \theta - \frac{J_3}{r^3} = 0 \quad \dots(A.2)$$

now comparing (A 2) to the trigonometric identity:-

$$\sin^3 \theta - \frac{3}{4} \sin \theta + \frac{1}{4} \sin 3\theta = 0$$

it is apparent that:-

$$\frac{3}{4} = \frac{J_2}{r^2} \quad \text{and} \quad -\frac{J_3}{r^3} = \frac{1}{4} \sin 3\theta$$

which leads to :-

$$\sin 3\theta = -\frac{3^{3/2}}{2} \frac{J_3}{J_2^{3/2}} \quad \dots(A.3)$$

and thus solving for the principal deviatoric stresses in terms of θ and $J_2^{1/2}$:-

$$\begin{pmatrix} S_1 \\ S_2 \\ S_3 \end{pmatrix} = \frac{2J_2^{1/2}}{\sqrt{3}} \begin{pmatrix} \sin\left(\theta + \frac{2\pi}{3}\right) \\ \sin(\theta) \\ \sin\left(\theta + \frac{4\pi}{3}\right) \end{pmatrix} \quad \dots(\text{A.4})$$

$$\text{with } S_1 \geq S_2 \geq S_3 \quad \text{and} \quad -\frac{\pi}{6} \leq \theta \leq \frac{\pi}{6}$$

University of Cape Town

APPENDIX B

MATHCAD DOCUMENT: YIELD FUNCTION DERIVATIVES

Note: The square root of J_2 is represented by A.

f(θ,A)

$$(1 - c) \cdot \left[\left[\left(\frac{2 \cdot A}{\sqrt{3}} \cdot \left(\sin\left(\theta + \frac{2 \cdot \pi}{3}\right) - \sin(\theta) \right) \right)^{2 \cdot k} + \left[\left(\frac{2 \cdot A}{\sqrt{3}} \cdot \left(\sin(\theta) - \sin\left(\theta + \frac{4 \cdot \pi}{3}\right) \right) \right)^{2 \cdot k} \right] \dots \right. \right. \\ \left. \left. + \left[\left(\frac{2 \cdot A}{\sqrt{3}} \cdot \left(\sin\left(\theta + \frac{4 \cdot \pi}{3}\right) - \sin\left(\theta + \frac{2 \cdot \pi}{3}\right) \right) \right)^{2 \cdot k} \right] \right] \right. \\ \left. + c \cdot \frac{3^{2 \cdot k}}{2^{2 \cdot k - 1} + 1} \left[\left(\frac{2 \cdot A}{\sqrt{3}} \cdot \sin\left(\theta + \frac{2 \cdot \pi}{3}\right) \right)^{2 \cdot k} + \left(\frac{2 \cdot A}{\sqrt{3}} \cdot \sin(\theta) \right)^{2 \cdot k} + \left(\frac{2 \cdot A}{\sqrt{3}} \cdot \sin\left(\theta + \frac{4 \cdot \pi}{3}\right) \right)^{2 \cdot k} \right] - 2 \cdot Y^{2 \cdot k} \right.$$

df/dA

$$(1 - c) \cdot \left[2 \cdot \left[\frac{2 \cdot A \cdot \sqrt{3}}{3} \cdot \left(\cos\left(\theta + \frac{1}{6} \cdot \pi\right) - \sin(\theta) \right) \right]^{(2 \cdot k)} \cdot \frac{k}{A} + 2 \cdot \left[\frac{2 \cdot A \cdot \sqrt{3}}{3} \cdot \left(\sin(\theta) + \sin\left(\theta + \frac{1}{3} \cdot \pi\right) \right) \right]^{(2 \cdot k)} \cdot \frac{k}{A} \dots \right. \\ \left. + 2 \cdot \left[\frac{2 \cdot A \cdot \sqrt{3}}{3} \cdot \left(-\sin\left(\theta + \frac{1}{3} \cdot \pi\right) - \cos\left(\theta + \frac{1}{6} \cdot \pi\right) \right) \right]^{(2 \cdot k)} \cdot \frac{k}{A} \right] \dots \\ + c \cdot \frac{3^{(2 \cdot k)}}{[2^{(2 \cdot k - 1)} + 1]} \left[2 \cdot \left[\frac{2 \cdot A \cdot \sqrt{3}}{3} \cdot \cos\left(\theta + \frac{1}{6} \cdot \pi\right) \right]^{(2 \cdot k)} \cdot \frac{k}{A} + 2 \cdot \left[\frac{2 \cdot A \cdot \sqrt{3}}{3} \cdot \sin(\theta) \right]^{(2 \cdot k)} \cdot \frac{k}{A} \dots \right. \\ \left. + 2 \cdot \left[\frac{-2 \cdot A \cdot \sqrt{3}}{3} \cdot \sin\left(\theta + \frac{1}{3} \cdot \pi\right) \right]^{(2 \cdot k)} \cdot \frac{k}{A} \right]$$

d^2f/dA^2

$$\begin{aligned}
 (1-c) & \left[4 \left[\frac{2}{3} \cdot A \cdot \sqrt{3} \cdot \left(\cos\left(\theta + \frac{1}{6}\pi\right) - \sin(\theta) \right) \right]^{(2\cdot k)} \cdot \frac{k^2}{A^2} - 2 \left[\frac{2}{3} \cdot A \cdot \sqrt{3} \cdot \left(\cos\left(\theta + \frac{1}{6}\pi\right) - \sin(\theta) \right) \right]^{(2\cdot k)} \cdot \frac{k}{A^2} \dots \right. \\
 & + 4 \left[\frac{2}{3} \cdot A \cdot \sqrt{3} \cdot \left(\sin(\theta) + \sin\left(\theta + \frac{1}{3}\pi\right) \right) \right]^{(2\cdot k)} \cdot \frac{k^2}{A^2} - 2 \left[\frac{2}{3} \cdot A \cdot \sqrt{3} \cdot \left(\sin(\theta) + \sin\left(\theta + \frac{1}{3}\pi\right) \right) \right]^{(2\cdot k)} \cdot \frac{k}{A^2} \dots \\
 & \left. + 4 \left[\frac{2}{3} \cdot A \cdot \sqrt{3} \cdot \left(-\sin\left(\theta + \frac{1}{3}\pi\right) - \cos\left(\theta + \frac{1}{6}\pi\right) \right) \right]^{(2\cdot k)} \cdot \frac{k^2}{A^2} - 2 \left[\frac{2}{3} \cdot A \cdot \sqrt{3} \cdot \left(-\sin\left(\theta + \frac{1}{3}\pi\right) - \cos\left(\theta + \frac{1}{6}\pi\right) \right) \right]^{(2\cdot k)} \cdot \frac{k}{A^2} \right] \\
 + c & \left[\frac{3^{(2\cdot k)}}{2^{(2\cdot k-1)} + 1} \left[4 \left(\frac{2}{3} \cdot A \cdot \sqrt{3} \cdot \cos\left(\theta + \frac{1}{6}\pi\right) \right)^{(2\cdot k)} \cdot \frac{k^2}{A^2} - 2 \left(\frac{2}{3} \cdot A \cdot \sqrt{3} \cdot \cos\left(\theta + \frac{1}{6}\pi\right) \right)^{(2\cdot k)} \cdot \frac{k}{A^2} \dots \right. \right. \\
 & + 4 \left(\frac{2}{3} \cdot A \cdot \sqrt{3} \cdot \sin(\theta) \right)^{(2\cdot k)} \cdot \frac{k^2}{A^2} - 2 \left(\frac{2}{3} \cdot A \cdot \sqrt{3} \cdot \sin(\theta) \right)^{(2\cdot k)} \cdot \frac{k}{A^2} \dots \\
 & \left. + 4 \left(\frac{-2}{3} \cdot A \cdot \sqrt{3} \cdot \sin\left(\theta + \frac{1}{3}\pi\right) \right)^{(2\cdot k)} \cdot \frac{k^2}{A^2} - 2 \left(\frac{-2}{3} \cdot A \cdot \sqrt{3} \cdot \sin\left(\theta + \frac{1}{3}\pi\right) \right)^{(2\cdot k)} \cdot \frac{k}{A^2} \right]
 \end{aligned}$$

$d^2f/d\theta dA$

$$\begin{aligned}
 (1-c) & \left[4 \left[\frac{2}{3} \cdot A \cdot \sqrt{3} \cdot \left(\cos\left(\theta + \frac{1}{6}\pi\right) - \sin(\theta) \right) \right]^{(2\cdot k)} \cdot k^2 \cdot \frac{\left(-\sin\left(\theta + \frac{1}{6}\pi\right) - \cos(\theta) \right)}{\left[\left(\cos\left(\theta + \frac{1}{6}\pi\right) - \sin(\theta) \right) \cdot A \right]} \dots \right. \\
 & + 4 \left[\frac{2}{3} \cdot A \cdot \sqrt{3} \cdot \left(\sin(\theta) + \sin\left(\theta + \frac{1}{3}\pi\right) \right) \right]^{(2\cdot k)} \cdot k^2 \cdot \frac{\left(\cos(\theta) + \cos\left(\theta + \frac{1}{3}\pi\right) \right)}{\left[\left(\sin(\theta) + \sin\left(\theta + \frac{1}{3}\pi\right) \right) \cdot A \right]} \dots \\
 & \left. + 4 \left[\frac{2}{3} \cdot A \cdot \sqrt{3} \cdot \left(-\sin\left(\theta + \frac{1}{3}\pi\right) - \cos\left(\theta + \frac{1}{6}\pi\right) \right) \right]^{(2\cdot k)} \cdot k^2 \cdot \frac{\left(-\cos\left(\theta + \frac{1}{3}\pi\right) + \sin\left(\theta + \frac{1}{6}\pi\right) \right)}{\left[\left(-\sin\left(\theta + \frac{1}{3}\pi\right) - \cos\left(\theta + \frac{1}{6}\pi\right) \right) \cdot A \right]} \right] \\
 + c & \left[\frac{3^{(2\cdot k)}}{2^{(2\cdot k-1)} + 1} \left[-4 \left(\frac{2}{3} \cdot A \cdot \sqrt{3} \cdot \cos\left(\theta + \frac{1}{6}\pi\right) \right)^{(2\cdot k)} \cdot k^2 \cdot \frac{\sin\left(\theta + \frac{1}{6}\pi\right)}{\left(\cos\left(\theta + \frac{1}{6}\pi\right) \cdot A \right)} + 4 \left(\frac{2}{3} \cdot A \cdot \sqrt{3} \cdot \sin(\theta) \right)^{(2\cdot k)} \cdot k^2 \cdot \frac{\cos(\theta)}{\left(\sin(\theta) \cdot A \right)} \dots \right. \right. \\
 & \left. + 4 \left(\frac{-2}{3} \cdot A \cdot \sqrt{3} \cdot \sin\left(\theta + \frac{1}{3}\pi\right) \right)^{(2\cdot k)} \cdot k^2 \cdot \frac{\cos\left(\theta + \frac{1}{3}\pi\right)}{\left(\sin\left(\theta + \frac{1}{3}\pi\right) \cdot A \right)} \right]
 \end{aligned}$$

$df/d\theta$

$$\begin{aligned}
 & (1-c) \cdot 2 \cdot \left[\frac{2}{3} \cdot A \cdot \sqrt{3} \cdot \left(\cos\left(\theta + \frac{1}{6} \cdot \pi\right) - \sin(\theta) \right) \right]^{(2 \cdot k)} \cdot k \cdot \frac{\left(-\sin\left(\theta + \frac{1}{6} \cdot \pi\right) - \cos(\theta) \right)}{\left(\cos\left(\theta + \frac{1}{6} \cdot \pi\right) - \sin(\theta) \right)} \dots \\
 & + 2 \cdot \left[\frac{2}{3} \cdot A \cdot \sqrt{3} \cdot \left(\sin(\theta) + \sin\left(\theta + \frac{1}{3} \cdot \pi\right) \right) \right]^{(2 \cdot k)} \cdot k \cdot \frac{\left(\cos(\theta) + \cos\left(\theta + \frac{1}{3} \cdot \pi\right) \right)}{\left(\sin(\theta) + \sin\left(\theta + \frac{1}{3} \cdot \pi\right) \right)} \dots \\
 & + 2 \cdot \left[\frac{2}{3} \cdot A \cdot \sqrt{3} \cdot \left(-\sin\left(\theta + \frac{1}{3} \cdot \pi\right) - \cos\left(\theta + \frac{1}{6} \cdot \pi\right) \right) \right]^{(2 \cdot k)} \cdot k \cdot \frac{\left(-\cos\left(\theta + \frac{1}{3} \cdot \pi\right) + \sin\left(\theta + \frac{1}{6} \cdot \pi\right) \right)}{\left(-\sin\left(\theta + \frac{1}{3} \cdot \pi\right) - \cos\left(\theta + \frac{1}{6} \cdot \pi\right) \right)} \dots \\
 & + c \cdot \frac{3^{(2 \cdot k)}}{\left[2^{(2 \cdot k - 1)} + 1 \right]} \cdot \left[-2 \cdot \left(\frac{2}{3} \cdot A \cdot \sqrt{3} \cdot \cos\left(\theta + \frac{1}{6} \cdot \pi\right) \right)^{(2 \cdot k)} \cdot k \cdot \frac{\sin\left(\theta + \frac{1}{6} \cdot \pi\right)}{\cos\left(\theta + \frac{1}{6} \cdot \pi\right)} + 2 \cdot \left(\frac{2}{3} \cdot A \cdot \sqrt{3} \cdot \sin(\theta) \right)^{(2 \cdot k)} \cdot k \cdot \frac{\cos(\theta)}{\sin(\theta)} \dots \right. \\
 & \left. + 2 \cdot \left(\frac{-2}{3} \cdot A \cdot \sqrt{3} \cdot \sin\left(\theta + \frac{1}{3} \cdot \pi\right) \right)^{(2 \cdot k)} \cdot k \cdot \frac{\cos\left(\theta + \frac{1}{3} \cdot \pi\right)}{\sin\left(\theta + \frac{1}{3} \cdot \pi\right)} \right]
 \end{aligned}$$

University of Cape Town

$$\begin{aligned}
& + 2 \cdot \left(\frac{2}{3} \cdot A \cdot \sqrt{3} \cdot \cos\left(\theta + \frac{1}{6} \cdot \pi\right) \right)^{(2 \cdot k)} \cdot k \cdot \frac{\sin\left(\theta + \frac{1}{6} \cdot \pi\right)}{\cos\left(\theta + \frac{1}{6} \cdot \pi\right)^2} + 4 \cdot \left(\frac{2}{3} \cdot A \cdot \sqrt{3} \cdot \sin(\theta) \right)^{(2 \cdot k)} \cdot k^2 \cdot \frac{\cos(\theta)^2}{\sin(\theta)^2} \dots \\
& + 2 \cdot \left(\frac{2}{3} \cdot A \cdot \sqrt{3} \cdot \sin(\theta) \right)^{(2 \cdot k)} \cdot k - 2 \cdot \left(\frac{2}{3} \cdot A \cdot \sqrt{3} \cdot \sin(\theta) \right)^{(2 \cdot k)} \cdot k \cdot \frac{\cos(\theta)^2}{\sin(\theta)^2} \dots \\
& + 4 \cdot \left(\frac{-2}{3} \cdot A \cdot \sqrt{3} \cdot \sin\left(\theta + \frac{1}{3} \cdot \pi\right) \right)^{(2 \cdot k)} \cdot k^2 \cdot \frac{\cos\left(\theta + \frac{1}{3} \cdot \pi\right)^2}{\sin\left(\theta + \frac{1}{3} \cdot \pi\right)^2} - 2 \cdot \left(\frac{-2}{3} \cdot A \cdot \sqrt{3} \cdot \sin\left(\theta + \frac{1}{3} \cdot \pi\right) \right)^{(2 \cdot k)} \cdot k \dots \\
& + 2 \cdot \left(\frac{-2}{3} \cdot A \cdot \sqrt{3} \cdot \sin\left(\theta + \frac{1}{3} \cdot \pi\right) \right)^{(2 \cdot k)} \cdot k \cdot \frac{\cos\left(\theta + \frac{1}{3} \cdot \pi\right)^2}{\sin\left(\theta + \frac{1}{3} \cdot \pi\right)^2}
\end{aligned}$$

d²f/dA d θ

$$\begin{aligned}
(1 - c) \cdot & \left[4 \cdot \left[\frac{2}{3} \cdot A \cdot \sqrt{3} \cdot \left(\cos\left(\theta + \frac{1}{6} \cdot \pi\right) - \sin(\theta) \right) \right]^{(2 \cdot k)} \cdot \frac{k^2 \cdot \left(-\sin\left(\theta + \frac{1}{6} \cdot \pi\right) - \cos(\theta) \right)}{A \cdot \left(\cos\left(\theta + \frac{1}{6} \cdot \pi\right) - \sin(\theta) \right)} \dots \right. \\
& + 4 \cdot \left[\frac{2}{3} \cdot A \cdot \sqrt{3} \cdot \left(\sin(\theta) + \sin\left(\theta + \frac{1}{3} \cdot \pi\right) \right) \right]^{(2 \cdot k)} \cdot \frac{k^2 \cdot \left(\cos(\theta) + \cos\left(\theta + \frac{1}{3} \cdot \pi\right) \right)}{A \cdot \left(\sin(\theta) + \sin\left(\theta + \frac{1}{3} \cdot \pi\right) \right)} \dots \\
& \left. + 4 \cdot \left[\frac{2}{3} \cdot A \cdot \sqrt{3} \cdot \left(-\sin\left(\theta + \frac{1}{3} \cdot \pi\right) - \cos\left(\theta + \frac{1}{6} \cdot \pi\right) \right) \right]^{(2 \cdot k)} \cdot \frac{k^2 \cdot \left(-\cos\left(\theta + \frac{1}{3} \cdot \pi\right) + \sin\left(\theta + \frac{1}{6} \cdot \pi\right) \right)}{A \cdot \left(-\sin\left(\theta + \frac{1}{3} \cdot \pi\right) - \cos\left(\theta + \frac{1}{6} \cdot \pi\right) \right)} \right] \\
+ c \cdot & \frac{3^{(2 \cdot k)}}{2^{(2 \cdot k - 1)} + 1} \cdot \left[4 \cdot \left(\frac{2}{3} \cdot A \cdot \sqrt{3} \cdot \cos\left(\theta + \frac{1}{6} \cdot \pi\right) \right)^{(2 \cdot k)} \cdot \frac{k^2 \cdot \sin\left(\theta + \frac{1}{6} \cdot \pi\right)}{A \cdot \cos\left(\theta + \frac{1}{6} \cdot \pi\right)} + 4 \cdot \left(\frac{2}{3} \cdot A \cdot \sqrt{3} \cdot \sin(\theta) \right)^{(2 \cdot k)} \cdot \frac{k^2 \cdot \cos(\theta)}{A \cdot \sin(\theta)} \dots \right. \\
& \left. + 4 \cdot \left(\frac{-2}{3} \cdot A \cdot \sqrt{3} \cdot \sin\left(\theta + \frac{1}{3} \cdot \pi\right) \right)^{(2 \cdot k)} \cdot \frac{k^2 \cdot \cos\left(\theta + \frac{1}{3} \cdot \pi\right)}{A \cdot \sin\left(\theta + \frac{1}{3} \cdot \pi\right)} \right]
\end{aligned}$$

APPENDIX C

DEVIATORIC STRESS INVARIANT DERIVATIVES

$$\frac{\partial J_2}{\partial \sigma_{ij}}$$

$$J_2 = \frac{1}{2} S_{ij} S_{ij}$$

$$\begin{aligned} \therefore \frac{\partial J_2}{\partial S_{pq}} &= \frac{1}{2} \left[\frac{\partial S_{ij}}{\partial S_{pq}} S_{ij} + S_{ij} \frac{\partial S_{ij}}{\partial S_{pq}} \right] \\ &= \frac{1}{2} \left[\delta_{ip} \delta_{jq} S_{ij} + S_{ij} \delta_{ip} \delta_{jq} \right] \\ &= \frac{1}{2} \left[S_{pq} + S_{pq} \right] \\ &= S_{pq} \end{aligned} \quad \dots(C.1)$$

$$\begin{aligned} \frac{\partial S_{ij}}{\partial \sigma_{pq}} &= \frac{\partial \sigma_{ij}}{\partial \sigma_{pq}} - \frac{1}{3} \frac{\partial \sigma_{kk}}{\partial \sigma_{pq}} \delta_{ij} \\ &= \delta_{ip} \delta_{jq} - \frac{1}{3} \delta_{kp} \delta_{kq} \delta_{ij} \\ &= \delta_{ip} \delta_{jq} - \frac{1}{3} \delta_{pq} \delta_{ij} \end{aligned} \quad \dots(C.2)$$

$$\begin{aligned} \text{so } \frac{\partial J_2}{\partial \sigma_{pq}} &= \frac{\partial J_2}{\partial S_{mn}} \frac{\partial S_{mn}}{\partial \sigma_{pq}} = S_{mn} \left[\delta_{mp} \delta_{nq} - \frac{1}{3} \delta_{pq} \delta_{mn} \right] \\ &= S_{pq} - \frac{1}{3} S_{mn} \delta_{pq} \end{aligned}$$

$$\text{but } S_{mm} = 0$$

$$\therefore \frac{\partial J_2}{\partial \sigma_{pq}} = S_{pq} \quad \dots(C.3)$$

$$\frac{\partial^2 J_2}{\partial \sigma_{pq} \partial \sigma_{ij}}$$

$$\frac{\partial^2 J_2}{\partial \sigma_{pq} \partial \sigma_{ij}} = \frac{\partial S_{ij}}{\partial \sigma_{pq}}$$

$$\therefore \frac{\partial^2 J_2}{\partial \sigma_{pq} \partial \sigma_{ij}} = \delta_{ip} \delta_{jq} - \frac{1}{3} \delta_{pq} \delta_{ij} \quad \dots(C.4)$$

$$\frac{\partial J_3}{\partial \sigma_{ij}}$$

$$J_3 = \frac{1}{3} S_{ij} S_{jk} S_{ki}$$

$$\therefore \frac{\partial J_3}{\partial S_{pq}} = \frac{1}{3} \left[\frac{\partial S_{ij}}{\partial S_{pq}} S_{jk} S_{ki} + S_{ij} \frac{\partial S_{jk}}{\partial S_{pq}} S_{ki} + S_{ij} S_{jk} \frac{\partial S_{ki}}{\partial S_{pq}} \right]$$

$$= \frac{1}{3} \left[\delta_{ip} \delta_{jq} S_{jk} S_{ki} + S_{ij} S_{ki} \delta_{jp} \delta_{kq} + S_{ij} S_{jk} \delta_{kp} \delta_{iq} \right]$$

$$= \frac{1}{3} \left[S_{qk} S_{kp} + S_{ip} S_{qi} + S_{qj} S_{jp} \right]$$

$$= S_{pk} S_{kq} \quad \dots(C.5)$$

$$\frac{\partial J_3}{\partial \sigma_{ij}} = \frac{\partial J_3}{\partial S_{pq}} \frac{\partial S_{pq}}{\partial \sigma_{ij}} = S_{pk} S_{kq} \left[\delta_{pi} \delta_{qj} - \frac{1}{3} \delta_{ij} \delta_{pq} \right]$$

$$\therefore \frac{\partial J_3}{\partial \sigma_{ij}} = S_{ik} S_{kj} - \frac{1}{3} \delta_{ij} S_{pk} S_{kp} \quad \dots(C.6)$$

$$\frac{\partial^2 J_3}{\partial \sigma_{ij} \partial \sigma_{pq}}$$

$$\begin{aligned} \frac{\partial^2 J_3}{\partial S_{ij} \partial S_{pq}} &= \frac{\partial (S_{pk} S_{kq})}{\partial S_{ij}} \\ &= \frac{\partial S_{pk}}{\partial S_{ij}} S_{kq} + S_{pk} \frac{\partial S_{kq}}{\partial S_{ij}} \\ &= \delta_{pi} \delta_{kj} S_{kq} + S_{pk} \delta_{ki} \delta_{qj} \\ &= \delta_{pi} S_{jq} + \delta_{qj} S_{pi} \end{aligned} \quad \dots (C.7)$$

Now

$$\begin{aligned} \frac{\partial^2 J_3}{\partial \sigma_{ij} \partial \sigma_{pq}} &= \frac{\partial}{\partial \sigma_{ij}} \left[\frac{\partial J_3}{\partial \sigma_{pq}} \right] \\ &= \frac{\partial}{\partial \sigma_{ij}} \left[\frac{\partial J_3}{\partial S_{kl}} \frac{\partial S_{kl}}{\partial \sigma_{pq}} \right] \\ &= \frac{\partial}{\partial S_{mn}} \left[\frac{\partial J_3}{\partial S_{kl}} \frac{\partial S_{kl}}{\partial \sigma_{pq}} \right] \frac{\partial S_{mn}}{\partial \sigma_{ij}} \end{aligned}$$

$$\begin{aligned} &= \frac{\partial}{\partial S_{mn}} \left[S_{ko} S_{ol} \left(\delta_{kp} \delta_{lq} - \frac{1}{3} \delta_{pq} \delta_{kl} \right) \right] \left(\delta_{mi} \delta_{nj} - \frac{1}{3} \delta_{ij} \delta_{mn} \right) \\ &= (\delta_{km} \delta_{on} S_{ol} + \delta_{om} \delta_{ln} S_{ko}) (\uparrow) (\uparrow) \\ &= (\delta_{km} S_{nl} + \delta_{ln} S_{km}) \left(\delta_{kp} \delta_{lq} - \frac{1}{3} \delta_{pq} \delta_{kl} \right) (\uparrow) \\ &= \left(\delta_{km} \delta_{kp} \delta_{lq} S_{nl} - \frac{1}{3} \delta_{km} \delta_{pq} \delta_{kl} S_{nl} + \delta_{ln} \delta_{kp} \delta_{lq} S_{km} \dots \right. \\ &\quad \left. - \frac{1}{3} \delta_{ln} \delta_{pq} \delta_{kl} S_{km} \right) (\uparrow) \\ &= \left(\delta_{mp} S_{nq} - \frac{1}{3} \delta_{km} \delta_{pq} S_{nk} + \delta_{nq} S_{pm} - \frac{1}{3} \delta_{ln} \delta_{pq} S_{lm} \right) (\uparrow) \\ &= \left(\delta_{mp} S_{nq} - \frac{1}{3} \delta_{pq} S_{nm} + \delta_{nq} S_{pm} - \frac{1}{3} \delta_{pq} S_{nm} \right) \dots \\ &\quad \times \left(\delta_{mi} \delta_{nj} - \frac{1}{3} \delta_{ij} \delta_{mn} \right) \\ &= \delta_{mi} \delta_{nj} \delta_{mp} S_{nq} - \frac{2}{3} \delta_{mi} \delta_{nj} \delta_{pq} S_{nm} + \delta_{mi} \delta_{nj} \delta_{nq} S_{pm} \dots \end{aligned}$$

$$\begin{aligned}
 & -\frac{1}{3}\delta_{ij}\delta_{mn}\delta_{mp}S_{nq} + \frac{2}{9}\delta_{ij}\delta_{mn}\delta_{pq}S_{nm} - \frac{1}{3}\delta_{ij}\delta_{mn}\delta_{nq}S_{pm} \\
 & = \delta_{ip}S_{jq} - \frac{2}{3}\delta_{pq}S_{ji} + \delta_{jq}S_{pi} - \frac{1}{3}\delta_{ij}S_{pq} \dots \\
 & \quad + \frac{2}{9}\delta_{ij}\delta_{pq}S_{mn} - \frac{1}{3}\delta_{ij}S_{pq}
 \end{aligned}$$

$$\therefore \frac{\partial^2 J_3}{\partial \sigma_{ij} \partial \sigma_{pq}} = \delta_{ip}S_{jq} - \frac{2}{3}\delta_{pq}S_{ji} + \delta_{jq}S_{pi} - \frac{2}{3}\delta_{ij}S_{pq} \quad \dots(C.8)$$

University of Cape Town

APPENDIX D

DERIVATION OF FLOW TENSOR DERIVATIVE

As per Equation (4.8) the flow tensor for a yield function independent of the hydrostatic stress is defined by:-

$$a_{ij} = C_2 a_{2ij} + C_3 a_{3ij}$$

$$\therefore \frac{\partial a_{ij}}{\partial \sigma_{pq}} = C_2 \frac{\partial a_{2ij}}{\partial \sigma_{pq}} + \frac{\partial C_2}{\partial \sigma_{pq}} + C_3 \frac{\partial a_{3ij}}{\partial \sigma_{pq}} + \frac{\partial C_3}{\partial \sigma_{pq}} a_{3ij} \quad \dots(D.1)$$

Substitute equations (4.9) and (4.10) into (D.1):-

$$\begin{aligned} \frac{\partial a_{ij}}{\partial \sigma_{pq}} &= C_2 \frac{\partial a_{2ij}}{\partial \sigma_{pq}} + C_3 \frac{\partial a_{3ij}}{\partial \sigma_{pq}} + \frac{\partial}{\partial \sigma_{pq}} \left(\frac{\partial f}{\partial J_2^{1/2}} - \frac{\tan 3\theta}{J_2^{1/2}} \frac{\partial f}{\partial \theta} \right) a_{2ij} \dots \\ &\quad + \frac{\partial}{\partial \sigma_{pq}} \left(\frac{-\sqrt{3}}{2 \cos 3\theta} \frac{1}{J_2^{3/2}} \frac{\partial f}{\partial \theta} \right) a_{3ij} \\ &= C_2 \frac{\partial a_{2ij}}{\partial \sigma_{pq}} + C_3 \frac{\partial a_{3ij}}{\partial \sigma_{pq}} + \frac{\partial^2 f}{\partial \sigma_{pq} \partial J_2^{1/2}} a_{2ij} \dots \\ &\quad - \frac{\partial}{\partial \sigma_{pq}} \left(\frac{\tan 3\theta}{J_2^{1/2}} \frac{\partial f}{\partial \theta} \right) a_{2ij} + \frac{\partial}{\partial \sigma_{pq}} \left(\frac{-\sqrt{3}}{2 \cos 3\theta} \frac{1}{J_2^{3/2}} \frac{\partial f}{\partial \theta} \right) a_{3ij} \quad \dots(D.2) \end{aligned}$$

Now evaluate each term of (D.2), noting that C_2 and C_3 are defined in Equations (4.9) and (4.10) and the deviatoric stress invariant derivatives are defined in Appendix C.

$$\frac{\partial a_{2ij}}{\partial \sigma_{pq}}$$

$$a_{2ij} = \frac{1}{2J_2^{1/2}} \frac{\partial J_2}{\partial \sigma_{ij}}$$

$$\therefore \frac{\partial a_{2ij}}{\partial \sigma_{pq}} = \frac{1}{2} \left(-\frac{1}{2} J_2^{-3/2} \frac{\partial J_2}{\partial \sigma_{ij}} \frac{\partial J_2}{\partial \sigma_{pq}} + J_2^{-1/2} \frac{\partial^2 J_2}{\partial \sigma_{pq} \partial \sigma_{ij}} \right)$$

so

$$\frac{\partial a_{2ij}}{\partial \sigma_{pq}} = \frac{1}{2} J_2^{-1/2} \frac{\partial^2 J_2}{\partial \sigma_{pq} \partial \sigma_{ij}} - \frac{1}{4} J_2^{-3/2} \frac{\partial J_2}{\partial \sigma_{ij}} \frac{\partial J_2}{\partial \sigma_{pq}} \quad \dots(D.3)$$

$$\frac{\partial a_{3ij}}{\partial \sigma_{pq}}$$

$$a_{3ij} = \frac{\partial J_3}{\partial \sigma_{ij}}$$

$$\therefore \frac{\partial a_{3ij}}{\partial \sigma_{pq}} = \frac{\partial^2 J_3}{\partial \sigma_{pq} \partial \sigma_{ij}} \quad \dots(D.4)$$

$$\frac{\partial^2 f}{\partial \sigma_{pq} \partial J_2^{1/2}}$$

We are considering a yield function of the form $f = f(J_2^{1/2}, \theta)$

thus

$$\frac{\partial f}{\partial J_2^{1/2}} = \frac{\partial f}{\partial J_2^{1/2}} \left(J_2^{1/2}(\sigma_{ij}), \theta(\sigma_{ij}) \right)$$

Using the chain rule:-

$$\frac{\partial^2 f}{\partial \sigma_{pq} \partial J_2^{1/2}} = \frac{\partial^2 f}{\partial \theta \partial J_2^{1/2}} \frac{\partial \theta}{\partial \sigma_{pq}} + \frac{\partial^2 f}{\partial J_2^{1/2}} \frac{\partial J_2^{1/2}}{\partial \sigma_{pq}} \quad \dots(D.5)$$

Now from the definitions of a_{2ij} and a_{3ij} and using equation (4.6) we can write:-

$$\frac{\partial^2 f}{\partial \sigma_{pq} \partial J_2^{1/2}} a_{2ij} = -\frac{\partial^2 f}{\partial \theta \partial J_2^{1/2}} \frac{\sqrt{3}}{2 \cos 3\theta} \left[\frac{1}{J_2^{3/2}} a_{3pq} - 3 \frac{J_3}{J_2^2} a_{2pq} \right] a_{2ij} \dots$$

$$+ \frac{\partial^2 f}{\partial J_2^{1/2}} a_{2ij} a_{2pq}$$

$$\therefore \frac{\partial^2 f}{\partial \sigma_{pq} \partial J_2^{1/2}} = -\frac{\partial^2 f}{\partial \theta \partial J_2^{1/2}} \frac{\sqrt{3}}{2 \cos 3\theta} \frac{1}{J_2^{3/2}} a_{2ij} a_{3pq} \dots$$

$$+ \left[\frac{\partial^2 f}{\partial \theta \partial J_2^{1/2}} \frac{3\sqrt{3}}{2 \cos 3\theta} \frac{J_3}{J_2^2} + \frac{\partial^2 f}{\partial J_2^{1/2}} \right] a_{2ij} a_{2pq} \dots \quad \dots (D.6)$$

$$\frac{\partial}{\partial \sigma_{pq}} \left(\frac{\tan 3\theta}{J_2^{1/2}} \frac{\partial f}{\partial \theta} \right) a_{2ij}$$

$$= \frac{\partial \left(\tan 3\theta \cdot J_2^{-1/2} \right)}{\partial \sigma_{pq}} \frac{\partial f}{\partial \theta} a_{2ij} + \frac{\tan 3\theta}{J_2^{1/2}} \frac{\partial^2 f}{\partial \sigma_{pq} \partial \theta} a_{2ij}$$

$$= \left[\tan 3\theta \frac{\partial J_2^{-1/2}}{\partial \sigma_{pq}} + J_2^{-1/2} \frac{\partial \tan 3\theta}{\partial \sigma_{pq}} \right] \frac{\partial f}{\partial \theta} a_{2ij} + \frac{\tan 3\theta}{J_2^{1/2}} \frac{\partial^2 f}{\partial \sigma_{pq} \partial \theta} a_{2ij}$$

$$= \left[-\frac{\tan 3\theta}{2} J_2^{-3/2} \frac{\partial J_2}{\partial \sigma_{pq}} + J_2^{1/2} \frac{\partial \tan 3\theta}{\partial \theta} \frac{\partial \theta}{\partial \sigma_{pq}} \right] \frac{\partial f}{\partial \theta} a_{2ij} \dots$$

$$+ \frac{\tan 3\theta}{J_2^{1/2}} \left[\frac{\partial^2 f}{\partial \theta^2} \frac{\partial \theta}{\partial \sigma_{pq}} + \frac{\partial^2 f}{\partial J_2^{1/2} \partial \theta} \frac{\partial J_2^{1/2}}{\partial \sigma_{pq}} \right] a_{2ij}$$

$$= \left[J_2^{-1/2} 3 \sec^2 3\theta \frac{\partial \theta}{\partial \sigma_{pq}} - \frac{\tan 3\theta}{J_2} a_{2pq} \right] \frac{\partial f}{\partial \theta} a_{2ij} + \frac{\tan 3\theta}{J_2^{1/2}} \left[\uparrow \right] a_{2ij}$$

Which on substitution of Equation (4.6) and rearranging becomes:-

$$\begin{aligned} \frac{\partial}{\partial \sigma_{pq}} \left(\frac{\tan 3\theta}{J_2^{1/2}} \frac{\partial f}{\partial \theta} \right) a_{2ij} &= \left(\frac{3^{5/2} \sec^3 3\theta \cdot J_3}{2J_2^{5/2}} \frac{\partial f}{\partial \theta} - \frac{\tan 3\theta}{J_2} \frac{\partial f}{\partial \theta} \dots \right. \\ &+ \left. \frac{\partial^2 f}{\partial \theta^2} \frac{\tan 3\theta}{J_2^{1/2}} \frac{3\sqrt{3}}{2 \cos 3\theta} \frac{J_3}{J_2^2} + \frac{\tan 3\theta}{J_2^{1/2}} \frac{\partial^2 f}{\partial J_2^{1/2} \partial \theta} \right) a_{2ij} a_{2pq} \dots \\ &- \left(\frac{3^{3/2} \sec^3 3\theta}{J_2^2} \frac{\partial f}{\partial \theta} + \frac{\partial^2 f}{\partial \theta^2} \frac{\tan 3\theta}{J_2^{1/2}} \frac{\sqrt{3}}{2 \cos 3\theta} \frac{1}{J_2^{3/2}} \right) a_{2ij} a_{3pq} \dots \end{aligned} \quad \dots(D.7)$$

$$\begin{aligned} \frac{\partial}{\partial \sigma_{pq}} \left(-\frac{\sqrt{3}}{2 \cos 3\theta} \frac{1}{J_2^{3/2}} \frac{\partial f}{\partial \theta} \right) a_{3ij} &= \frac{\partial}{\partial \sigma_{pq}} \left(\frac{\sqrt{3}}{2 \cos 3\theta} \right) \frac{1}{J_2^{3/2}} \frac{\partial f}{\partial \theta} a_{3ij} - \frac{\sqrt{3}}{3 \cos 3\theta} \frac{\partial}{\partial \sigma_{pq}} \left(\frac{1}{J_2^{3/2}} \frac{\partial f}{\partial \theta} \right) a_{3ij} \\ &= -\frac{\sqrt{3}}{2} \frac{\partial \sec 3\theta}{\partial \theta} \frac{\partial \theta}{\partial \sigma_{pq}} \frac{1}{J_2^{3/2}} \frac{\partial f}{\partial \theta} a_{3ij} + \frac{\sqrt{3}}{2 \cos 3\theta} \frac{\partial f}{\partial \theta} \frac{3}{2} J_2^{-5/2} \frac{\partial J_2}{\partial \sigma_{pq}} a_{3ij} \dots \\ &\quad - \frac{\sqrt{3}}{2 \cos 3\theta} \frac{1}{J_2^{3/2}} \frac{\partial^2 f}{\partial \sigma_{pq} \partial \theta} a_{3ij} \end{aligned}$$

Which on substitution of Equation (4.6) and rearranging becomes:-

$$\begin{aligned} \frac{\partial}{\partial \sigma_{pq}} \left(-\frac{\sqrt{3}}{2 \cos 3\theta} \frac{1}{J_2^{3/2}} \frac{\partial f}{\partial \theta} \right) a_{3ij} \dots &= \frac{9 \sec^2 3\theta \cdot \tan 3\theta}{2J_2^{3/2}} \frac{\partial f}{\partial \theta} \left(\frac{1}{J_2^{3/2}} a_{3ij} a_{3pq} - 3 \frac{J_3}{J_2^2} a_{3ij} a_{2pq} \right) \dots \end{aligned}$$

$$\begin{aligned}
 & + \frac{3^{3/2}}{2 \cos 3\theta} \frac{1}{J_2^2} \frac{\partial f}{\partial \theta} a_{3ij} a_{2pq} \dots \\
 & - \frac{\sqrt{3}}{2 \cos 3\theta \cdot J_2^{3/2}} \left[\frac{\partial^2 f}{\partial \theta^2} \frac{\sqrt{3}}{2 \cos 3\theta \cdot J_2^{3/2}} a_{3ij} a_{3pq} \dots \right. \\
 & \left. + \left(\frac{\partial^2 f}{\partial J_2^{1/2} \partial \theta} + \frac{3\sqrt{3}}{2 \cos 3\theta} \frac{\partial^2 f}{\partial \theta^2} \frac{J_3}{J_2^2} \right) a_{3ij} a_{2pq} \right] \dots \text{(D.8)}
 \end{aligned}$$

University of Cape Town

APPENDIX E

REORDERING OF FLOW TENSOR DERIVATIVE

Appendix D demonstrates that the flow tensor derivative may be written in the form:-

$$\frac{\partial^2 f}{\partial \sigma_{ij} \partial \sigma_{pq}} = b_{ijpq} = C_2 \tilde{b}_{1ijpq} + C_3 \tilde{b}_{2ijpq} + \tilde{b}_{3ijpq} - \tilde{b}_{4ijpq} + \tilde{b}_{5ijpq} \quad \dots(E.1)$$

with

$$\begin{aligned} \tilde{b}_{1ijpq} &= \frac{\partial a_{2ij}}{\partial \sigma_{pq}} \\ \tilde{b}_{2ijpq} &= \frac{\partial a_{3ij}}{\partial \sigma_{pq}} \\ \tilde{b}_{3ijpq} &= B_1 a_{2ij} a_{3pq} + B_2 a_{2ij} a_{2pq} \\ \tilde{b}_{4ijpq} &= B_3 a_{2ij} a_{2pq} + B_4 a_{2ij} a_{3pq} \\ \tilde{b}_{5ijpq} &= B_5 a_{3ij} a_{3pq} + B_6 a_{3ij} a_{2pq} \end{aligned}$$

and with the B_i 's scalar constants dependent on the yield function.

We require the flow tensor in the form:-

$$\begin{aligned} b_{ijpq} = C_2 \tilde{b}_{1ijpq} + C_3 \tilde{b}_{2ijpq} + C_{22} a_{2ij} a_{2pq} + C_{23} a_{2ij} a_{3pq} + C_{32} a_{3ij} a_{2pq} \dots \\ + C_{33} a_{3ij} a_{3pq} \quad \dots(E.2) \end{aligned}$$

Therefore :-

$$\begin{aligned} C_{22} &= B_2 - B_3 \\ C_{23} &= B_1 - B_4 \\ C_{32} &= B_6 \\ C_{33} &= B_5 \end{aligned}$$

Now evaluate these constants in terms of the derived terms of Equation (D.2).

C₂₂

$$C_{22} = \frac{\partial^2 f}{\partial \theta \partial J_2^{1/2}} \frac{3\sqrt{3}}{2 \cos 3\theta} \frac{J_3}{J_2^2} + \frac{\partial^2 f}{\partial J_2^{1/2 \ 2}} - \frac{9\sqrt{3}}{2 \cos^3 3\theta} \frac{J_3}{J_2^{5/2}} \frac{\partial f}{\partial \theta} \dots$$

$$+ \frac{\tan 3\theta}{J_2} \frac{\partial f}{\partial \theta} - \frac{\partial^2 f}{\partial \theta^2} \frac{\tan 3\theta}{J_2^{1/2}} \frac{3\sqrt{3}}{2 \cos 3\theta} \frac{J_3}{J_2^2} - \frac{\tan 3\theta}{J_2^{1/2}} \frac{\partial^2 f}{\partial J_2^{1/2} \partial \theta}$$

Now $\frac{J_3}{J_2^2} = -\frac{1}{J_2^{1/2}} \frac{2 \sin 3\theta}{3\sqrt{3}}$

$$\therefore C_{22} = \frac{\partial^2 f}{\partial \theta \partial J_2^{1/2}} \frac{3\sqrt{3}}{2 \cos 3\theta} \left(-\frac{1}{J_2^{1/2}} \frac{2 \sin 3\theta}{3\sqrt{3}} \right) + \frac{\partial^2 f}{\partial J_2^{1/2 \ 2}} \dots$$

$$- \frac{3}{J_2^{1/2} \cos^2 3\theta} \frac{3\sqrt{3}}{2 \cos 3\theta} \left(-\frac{1}{J_2^{1/2}} \frac{2 \sin 3\theta}{3\sqrt{3}} \right) \frac{\partial f}{\partial \theta} + \frac{\tan 3\theta}{J_2} \frac{\partial f}{\partial \theta} \dots$$

$$- \frac{\partial^2 f}{\partial \theta^2} \frac{\tan 3\theta}{J_2^{1/2}} \frac{3\sqrt{3}}{2 \cos 3\theta} \left(-\frac{1}{J_2^{1/2}} \frac{2 \sin 3\theta}{3\sqrt{3}} \right) - \frac{\tan 3\theta}{J_2^{1/2}} \frac{\partial^2 f}{\partial J_2^{1/2} \partial \theta}$$

Thus $C_{22} = -\frac{\partial^2 f}{\partial \theta \partial J_2^{1/2}} \frac{\tan 3\theta}{J_2^{1/2}} + \frac{\partial^2 f}{\partial J_2^{1/2 \ 2}} + \frac{3 \tan 3\theta}{J_2 \cos^2 3\theta} \frac{\partial f}{\partial \theta} \dots$

$$+ \frac{\tan 3\theta}{J_2} \frac{\partial f}{\partial \theta} + \frac{\partial^2 f}{\partial \theta^2} \frac{\tan^2 3\theta}{J_2} - \frac{\tan 3\theta}{J_2^{1/2}} \frac{\partial^2 f}{\partial J_2^{1/2} \partial \theta} \dots \quad \dots(E.3)$$

C₃₃

$$C_{33} = \frac{9 \tan 3\theta}{4 \cos^2 3\theta} \frac{1}{J_2^3} \frac{\partial f}{\partial \theta} + \frac{3}{4 \cos^2 3\theta} \frac{\partial^2 f}{J_2^3 \partial \theta^2}$$

$$= \frac{3 \left(3 \frac{\partial f}{\partial \theta} \tan 3\theta + \frac{\partial^2 f}{\partial \theta^2} \right)}{4 \cos^2 3\theta J_2^3} \quad \dots(E.4)$$

C₂₃

$$C_{23} = -\frac{\partial^2 f}{\partial \theta \partial J_2^{1/2}} \frac{\sqrt{3}}{2 \cos 3\theta} \frac{1}{J_2^{3/2}} + \frac{\partial^2 f \tan 3\theta}{\partial \theta^2} \frac{\sqrt{3}}{J_2^{1/2} 2 \cos 3\theta \cdot J_2^{3/2}} \dots$$

$$+ \frac{3\sqrt{3} \sec^3 3\theta}{2J_2^2} \frac{\partial f}{\partial \theta}$$

$$\therefore C_{23} = \frac{\sqrt{3}}{2 \cos 3\theta \cdot J_2^{3/2}} \left(\frac{\partial^2 f \tan 3\theta}{\partial \theta^2} \frac{1}{J_2^{1/2}} - \frac{\partial^2 f}{\partial \theta \partial J_2^{1/2}} \right) + \frac{3\sqrt{3}}{2 \cos^3 3\theta \cdot J_2^2} \frac{\partial f}{\partial \theta} \quad \dots(E.5)$$

C₃₂

Similarly, following substitution and simplification, it can be shown that:-

$$\underline{C_{32} = C_{23}}$$

APPENDIX F

FORTRAN 77 LISTING: MATERIAL MODEL PARAMETERS

```
C.....
C   Routine to determine components of mapping matrix [L] and
C   KARAFILLIS/BOYCE isotropic yield surface parameters k and c
C   from experimentally determined material parameters
C
C   * Input   Material R values at 0, 45 & 90 degrees
C             Material uniaxial yield stresses at the same angles
C             Material shear yield stress
C   * Output  File TABLE.OUT with matrix [L] components and k & c
C
C   * Subroutines called:-
C
C       -PHI Returns the LHS of the Boyce polynomial yield function
C         for a given deviatoric stress vector {stress} and material
C         constants.
C
C       -MATMUL Matrix multiplication
C
C                                           G.D.Thomas   27 May 1996
C.....

implicit none

real*8  r0,r90,r45,alpha,alpha2,gamma1,y0,y45,y90,c,cc,
&       phi0,phi45,phi90,l(6,6),beta1,beta2,beta3,yst0(6),
&       yst45(6),yst90(6),s0(6),s45(6),s90(6),gamma2,gamma3,
&       error2,const1,error,y,flag,
&       yshear,yshr(6),phis,efstress,error1

integer k,i,j,n

C           USER INPUT
C.....
C   Enter R values and Yield Strength values:-
C   r0= 0.670D0
C   r45=0.930D0
C   r90=0.80D0
C   y0= 286.0D6
C   y45=290.0D6
C   y90=303.0D6
C   yshear=155.29D6
C.....

y=(y0+y45+y90)/3.0D0

flag=1.0D0
open (unit=10,file='table.out',status='unknown',
&     access='sequential')

C.... [L] matrix parameters:-
alpha1=(r0*r90+r90+2.0D0*r0)/2.0D0/r90/(r0+1.0D0)
alpha2=(r90+1.0D0-(r90-1.0D0)*alpha1)/(r90+1)
gamma1=(r45+0.5D0)*alpha2
gamma2=3.0D0/2.0D0
gamma3=3.0D0/2.0D0
beta1=(alpha2-alpha1-1.0D0)/2.0D0
beta2=(alpha1-alpha2-1.0D0)/2.0D0
beta3=(1.0D0-alpha1-alpha2)/2.0D0

C ... Load [1] i.e. [L] with C=1.0
do 10 i=1,6
  do 10 j=1,6
```

```

                l(i,j)=0.0D0
10 continue
  l(1,1)=1.0D0
  l(1,2)=beta1
  l(1,3)=beta2
  l(2,1)=l(1,2)
  l(2,2)=alpha1
  l(2,3)=beta3
  l(3,1)=l(1,3)
  l(3,2)=l(2,3)
  l(3,3)=alpha2
  l(4,4)=gamma1
  l(5,5)=gamma2
  l(6,6)=gamma3

c ... load stress vectors which cause yielding at 0, 45 & 90 degrees
c and stress vector which causes yielding in pure shear:-
  do 20 i=1,6
    yst0(i)= 0.0D0
    yst45(i)=0.0D0
    yst90(i)=0.0D0
    yshr(i)= 0.0D0
20 continue
  yst0(1)=y0
  yst90(2)=y90
  yst45(1)=0.5D0*y45
  yst45(2)=yst45(1)
  yst45(4)=yst45(1)
  yshr(1)=yshear
  yshr(2)=-yshear

c ... Map above yield stress vectors via [1] to deviatoric space:-
  call MATMUL(1,yst0,s0,6,6,1)
  call MATMUL(1,yst45,s45,6,6,1)
  call MATMUL(1,yst90,s90,6,6,1)

  write(10,*) 'R0=',r0
  write(10,*) 'R45=',r45
  write(10,*) 'R90=',r90
  write(10,*) 'Y0=',Y0
  write(10,*) 'Y45=',y45
  write(10,*) 'Y90=',y90
  write(10,*)
  write(10,*) 'alpha1=',alpha1
  write(10,*) 'alpha2=',alpha2
  write(10,*) 'gamma1=',gamma1
  write(10,*) 'gamma2=',gamma2
  write(10,*) 'gamma3=',gamma3
  write(10,*) 'beta1=',beta1
  write(10,*) 'beta2=',beta2
  write(10,*) 'beta3=',beta3
  write(10,*)
  write(10,*) 'Average yield strength',y
  write(10,*)
  write(10,*) 'Shear yield strength',yshear
  write(10,*)

c ... Confirm yshear/yuni is within yield surface bounds. If not give
c closest bound k and c parameters:-
  if (yshear/y .lt. 0.51168D0) then
    write(10,*) 'WARNING: Lower Bound Approximation'
    write(10,*)
    write(10,*) 'k=15   c=0.0'
    k=15
    c=0.0D0
    goto 100
  end if
  if (yshear/y .gt. 0.6514D0) then
    write(10,*) 'WARNING: Upper Bound Approximation'
    write(10,*)
    write(10,*) 'k=15   c=1.0'
    k=15
    c=1.0D0
    goto 100
  end if

  write(10,*) '   k           c           %error           C'
  write(10,*) '=====          =====          =====          ====='

```

```

flag=-1.0D0
error1=1.0D6

do 30 k=1,15
  do 50 n=0,10000
    c=n/10000.0D0

    call PHI(yshr,k,c,phis)
    efstress=(phis/2.0D0)**(0.5D0/k)
    error2=(efstress-y)/y*100.0D0

    if (dabs(error2) .lt. dabs(error1)) then
      error1=error2
      error=error2
      const1=c
    end if

50    continue

    call PHI(s0,k,const1,phi0)
    call PHI(s45,k,const1,phi45)
    call PHI(s90,k,const1,phi90)
    cc=(y0+y45+y90)/0.5D0**(0.5D0/k)
    & / (phi0**(0.5D0/k)+phi45**(0.5D0/k)+phi90**(0.5D0/k))

    write(10,900) k,const1,error,cc
    error1=1.0D6

30 continue

c ... Calculate C iff shear stress is out of bounds
100 if (flag .gt. 0.0D0) then
  call PHI(s0,k,c,phi0)
  call PHI(s45,k,c,phi45)
  call PHI(s90,k,c,phi90)
  cc=(y0+y45+y90)/0.5D0**(0.5D0/k)
  & / (phi0**(0.5D0/k)+phi45**(0.5D0/k)+phi90**(0.5D0/k))
  write(10,*)
  write(10,*) 'C=',cc
end if

close (unit=10)

900 format(i2, 8x,f8.4, 8x,f10.6,8x,f12.10,3x,d12.5,3x,d12.5,f12.5)
910 format(6(d12.5,1x))

stop
end

C.....
c Subroutine PHI returns the LHS of the Boyce polynomial yield
c function for a given deviatoric stress vector {stress} and
c material constants
c
c in {stress} - deviatoric stress vector
c k - INTEGER material constant
c c - REAL material constant
c out phi - LHS of Boyce yield function
C.....
subroutine PHI (stress,k,c,phi0)

implicit none

real*8 stress(6),c,j2,j3,o,sij(6,6),s1,s2,s3,const1,
& pi,phil,phi2,angle,phi0

integer i,j,l,k

c ... set up deviatoric stress tensor
sij(1,1)=stress(1)
sij(2,2)=stress(2)
sij(3,3)=stress(3)
sij(1,2)=stress(4)
sij(1,3)=stress(5)
sij(2,1)=stress(4)
sij(2,3)=stress(6)
sij(3,1)=stress(5)
sij(3,2)=stress(6)

```

```

c ... deviatoric invariants
  j2=0.0D0
  j3=0.0D0
  do 10 i=1,3
    do 10 j=1,3
      j2=j2+sij(i,j)*sij(i,j)/2.0D0
10 continue
  do 20 i=1,3
    do 20 j=1,3
      do 20 l=1,3
        j3=j3+sij(i,j)*sij(j,l)*sij(l,i)/3.0D0
20 continue

c ... stress angle theta
  angle=(-3.0D0**1.5D0/2.0D0*j3/j2**1.5D0)
  if (dabs(angle) .ge. 1.0D0) then
    angle=dsign(0.999999999999999D0,angle)
  end if
  o=dasin(angle)/3.0D0
  if (o .eq. 0.0D0) then
    o=1.0D-15
  end if

c ... principal deviatoric stresses
  const1=2.0D0/dsqrt(3.0D0)*dsqrt(j2)
  pi=2.0D0*dasin(1.0D0)
  s1=const1*dsin(o+2.0D0/3.0D0*pi)
  s2=const1*dsin(o)
  s3=const1*dsin(o+4.0D0/3.0D0*pi)

c ... calculate phi
  phi1=(s1-s2)**(2*k)+(s2-s3)**(2*k)+(s3-s1)**(2*k)
  phi2=s1**(2*k)+s2**(2*k)+s3**(2*k)
  phi0=(1.0D0-c)*phi1+c*3.0D0**(2*k)
  & /((2.0D0**(2*k-1))+1.0D0)*phi2

  return
end

```

APPENDIX G

FORTRAN 77 LISTING: ABAQUS USER-MATERIAL

```
.....
c
c Subroutine UMAT: ABAQUS User-Material
c =====
c
c -----
c Implementation of a General Anisotropic Yield Criterion Using
c Bounds and a Transformation Weighting Tensor, as proposed by
c A.P. Karafillis and M.C. Boyce 1993
c -----
c
c * Anisotropic (Orthotropic Symmetry)
c Linear Hardening, Pressure Independent Plasticity
c Strain Rate Independent
c
c * All arguments parsed to and from this UMAT subroutine as per
c ABAQUS Users Manual.
c
c * Material Properties and Print Control:-
c   e      : Young's Modulus      [Pa]           props(1)
c   poisson : Poissons Ratio      props(2)
c   h      : Plastic Linear Hardening Parameter [Pa] props(3)
c   y0     : Material Uniaxial Yield Stress [Pa]  props(4)
c   k      : INTEGER yield function constant     props(5)
c   c      : REAL yield function constant        props(6)
c   lun    : Logical Unit Number=16 to print UMAT props(7)
c           output to file msg.msg after each call
c
c * IPE Transformation Tensor parameters:-
c   C      : props(8)
c   alpha1 : props(9)
c   alpha2 : props(10)
c   gamma1 : props(11)
c   gamma2 : props(12)
c   gamma3 : props(13)
c
c * Solution Dependent State Variables (*DEPVAR=11)
c   statev(1...6) -> : Total Plastic Strain Vector
c   statev(7)     -> : von Mises Equivalent Stress
c   statev(8)     -> : von Mises Equivalent Plastic Strain
c   statev(9)     -> : Boyce Effective Stress
c   statev(10)    -> : Boyce Equivalent Plastic Strain (aniso)
c   statev(11)    -> : Boyce Equivalent Plastic Strain (iso)
c
c * Subroutines called:-
c
c - PLASTIC:- For a given stress with f>0.0 and for given material
c constants, this subroutine calculates the returned stress, the
c plastic strain increment and the increment isotropic
c equivalent plasticity. Linear hardening is included.
c
c - YF. Returns the yield function value, stress angle
c (theta) and deviatoric invariants for a given stress
c vector {stress} and material constants.
c
c - DERIVS Evaluates the yield function derivatives with respect
c to theta and A (A=square root of J2).
c
c - FVECTOR Returns yield surface flow-vector.
c
c - FV_DER Returns flow-vector derivative.
```



```

cc=props(8)
alpha=props(9)
alpha2=props(10)
gamma1=props(11)
gamma2=props(12)
gamma3=props(13)

c ... Solution Dependent State Variables (*DEPVAR=11)
c Values at beginning of increment:-
c statev(1...6) -> pstrain : Total Plastic Strain
c statev(7) -> : von Mises Equivalent Stress
c statev(8) -> : von Mises Equivalent Plastic Strain
c statev(9) -> : Boyce Effective Stress
c statev(10) -> : Boyce Equivalent Plastic Strain (aniso)
c statev(11) -> : Boyce Equivalent Plastic Strain (iso)

do 10 i=1,6
  pstrain(i)=statev(i)
  dplas(i)=0.0D0
10 continue

teps=statev(11)

c ... Define IPE TRANSFORMATION TENSOR [L] (deviatoric mapping)
do 20 i=1,6
  do 20 j=1,6
    l(i,j)=0.0D0
20 continue
l(1,1)=cc
l(2,2)=cc*alpha1
l(3,3)=cc*alpha2
l(4,4)=cc*gamma1
l(5,5)=cc*gamma2
l(6,6)=cc*gamma3
l(1,2)=cc*(alpha2-alpha1-1.0D0)/2.0D0
l(1,3)=cc*(alpha1-alpha2-1.0D0)/2.0D0
l(2,3)=cc*(1.0D0-alpha1-alpha2)/2.0D0
l(2,1)=l(1,2)
l(3,1)=l(1,3)
l(3,2)=l(2,3)

c ... Define TRANSFORMATION TENSOR [lv] (non-deviatoric mapping)
do 30 i=1,6
  do 30 j=1,6
    lv(i,j)=l(i,j)
30 continue
do 40 i=1,3
  do 40 j=1,3
    lv(i,j)=l(i,j)+1.0D0/3.0D0
40 continue

c ... Determine [inlv] INVERSE of[lv]:-
call MATINV(lv,inlv)

c ... Define ELASTIC CONSTITUTIVE MATRIX :-
do 50 i=1,6
  dummy(i)=0.0D0
50 continue
call ELASTIC(d,dummy,dummy,e,poisson)

c ... Calculate Increment Initial Yield Strength
y=y0+h*teps

c ... Calculate current increment TOTAL STRAIN:-
do 60 i=1,6
  strain(i)=stran(i)+dstran(i)
60 continue

c ... Calculate VOLUMETRIC STRAIN & HYDROSTATIC STRESS
volstran=strain(1)+strain(2)+strain(3)
volstrs=kk*volstran

```

```

c ....Evaluate ELASTIC PREDICTOR
  call MATMUL(d,dstran,ep1,6,6,1)
  do 70 i=1,6
    epredict(i)=stress(i)+ep1(i)
  70 continue

c ... If Elastic Predictor=(0) in deviatoric space (ie. J2 & J3=0.0)
c   then go ELASTIC:-
  do 80 i=1,3
    epredict1(i)=epredict(i)-volstrs
    epredict1(i+3)=epredict(i+3)
  80 continue
  call MATMUL(epredict1,epredict1,scratch,1,6,1)
  if (scratch(1) .lt. 1.0D-3) then
    call ELASTIC(ddsde,dstran,stress,e,poisson)
    f0=-1.0D0
    j2=0.0D0
    fwork=-y
    ywork=y
    goto 500
  end if

c ... MAP anisotropic Elastic Predictor to isotropic stress space:-
  call MATMUL(lv,epredict,ep,6,6,1)

c -----
c   . Determine if Elastic Predictor stress is in plastic range .
c   . and call relevent subroutine
c -----

c ... calculate yield function value
  call YF(ep,k,c,y,f0,j2,j3,o)

c ... ELASTIC
c -----
  if (f0 .le. 0.0D0) then
    call ELASTIC(ddsde,dstran,stress,e,poisson)
    fwork=f0
    ywork=y
    goto 500
  endif

c ... PLASTIC
c -----

c ... set stress vector {stress1}=Elastic Predictor
  do 90 i=1,6
    stress1(i)=ep(i)
  90 continue
  call PLASTIC(stress1,d,k,c,y0,h,teps,dplastic,lambda,ywork,dep)
  spd=dep*(y0+h*teps + ywork)*2.0D0

c ... MAP plastic strain increment and isotropic stress to anisotropic space:-
  call MATMUL(1,dplastic,dplas,6,6,1)
  call MATMUL(invlv,stress1,stressa,6,6,1)

c -----
c   . CONSISTENT TANGENT MODULUS .
c -----

c ... Evaluate the isotropic flow vector {a} at new stress:-
  call YF(stress1,k,c,ywork,fwork,j2,j3,o)
  call DERIVS(o,dsqrt(j2),k,c,dfda,d2fd2a,d2fdoda,dfdo,
&          d2fd2o,d2fdado)
  call FVECTOR(stress1,j2,dfda,dfdo,o,a,a2,a3,c2,c3)

c ... Evaluate the anisotropic flow vector {aa}:-
  call MATMUL(lv,a,aa,6,6,1)

c ... Evaluate the isotropic flow vector derivative [b]
  call FV_DER(stress1,j2,d2fd2a,d2fdoda,dfdo,d2fd2o,d2fdado,o,
&          c2,c3,a2,a3,b)

c ... Evaluate the anisotropic flow vector derivative [bb]:-
  call MATMUL(lv,b,bbl,6,6,6)
  call MATMUL(lv,bbl,bb,6,6,6)

c ... Evaluate TANGENT MODULUS [ddsde]

```

```

call TANMOD(lambda,e,poisson,h,aa,bb,ddsdde)

c -----
c . REPORT TO ABAQUS .
c -----

c ... STRESS VECTOR
do 100 i=1,6
    stress(i)=stressa(i)
100 continue

c ... TOTAL PLASTIC STRAIN
do 110 i=1,6
    pstrain(i)=pstrain(i)+dplas(i)
    statev(i)=pstrain(i)
110 continue

c ... EFFECTIVE STRESS
c ... von Mises Effective Stress
500 statev(7)=dsqrt(3.0D0*j2)

c ... Boyce Effective Stress
statev(9)=(fwork+ywork)

c ... TOTAL EQUIVALENT PLASTIC STRAIN
if ( f0 .gt. 0.0D0) then
c ... von Mises Total Equivalent Plastic Strain:-
c calculate e(i,j)e(i,j): {dplas} is engineering strain
c vector, therefore shear terms are modified in order to obtain
c correct tensor multiplication.
    scratch(1)=dplas(1)**2+dplas(2)**2+dplas(3)**2
&             +dplas(4)**2/2.0D0
&             +dplas(5)**2/2.0D0
&             +dplas(6)**2/2.0D0

    dmises=dsqrt(2.0D0/3.0D0*scratch(1))
    statev(8)=statev(8)+dmises

c ... Boyce Total Equivalent Plastic Strain (anisotropic)
do 120 i=1,3
    s(i)=stress(i)-volstrs
    s(i+3)=stress(i+3)
120 continue
call MATMUL(s,dplas,scratch,1,6,1)
if (scratch(1).le. 0.0D0) then
    write(6,*) 'The total incremental plastic work is'
&             ,scratch(1)
    statev(10)=statev(10)+dmises
else
    if (h .lt. 1.0D0) then
        statev(10)=statev(10)+scratch(1)/y
    else
        statev(10)=statev(10)+
&             (-y+dsqrt(y**2+4.0D0*h*scratch(1)))/(2.0D0*h)
    end if
end if

c ... Boyce Total Equivalent Plastic Strain (isotropic)
statev(11)=statev(11)+dep
endif

c ... Print UMAT output to file msg.msg if required by user:-
if (lun .ne.16) then
    return
end if

open (unit=lun,file='msg.msg',
& status='unknown',access='sequential')
write(lun,*) '      E          Poisson          H          Y
&field'
write(lun,*) ' =====          =====          =====          ==
&====='
write(lun,900) e,poisson,h,y0
write(lun,*)
write(lun,*)

```

```

write(lun,*) '      k          c          D          p
&      dtime '
write(lun,*) ' ====='
&=====
write(lun,930) k,c
write(lun,*)
write(lun,*)
write(lun,*) '      C          alpha1          alpha2          gammal
& gamma2          gamma3'
write(lun,*) ' ====='
&=====
write(lun,910) cc,alpha1,alpha2,gammal,gamma2,gamma3
write(lun,*)
write(lun,*)
write(lun,*) 'Total Strain(in) Plastic Strain(in) Updated Stress
& Plastic Strain (out)'
write(lun,*) '=====
&=====
write(lun,920) (strain(i),pstrain(i)-dplas(i),stress(i),
&statev(i),i=1,6)
write(lun,*)
write(lun,*)
write(lun,*) 'Effective Stress'
write(lun,*) '=====
write(lun,*) ' Boyce          von Mises'
write(lun,*) ' -----
write(lun,900) statev(9),statev(7)
write(lun,*)
write(lun,*)
write(lun,*) 'Total Equivalent Plastic Strains'
write(lun,*) '=====
write(lun,*) 'Boyce (aniso) Boyce (iso) von Mises'
write(lun,*) '-----
write(lun,900) statev(10),statev(11),statev(8)
write(lun,*)
write(lun,*)
write(lun,*) '[DDSDDE]'
write(lun,*) '=====
write(lun,910) ((dssdde(i,j),j=1,6),i=1,6)

close (unit=lun)

900 format (4(d12.5,4x))
910 format (6(d12.5,1x))
920 format (4(d12.5,7x))
930 format (3x,i2,7x,d12.5,5x,d12.5,5x,d12.5,5x,d12.5)

return
end

C.....
C Subroutine PLASTIC. For a given stress with f>0.0 and for given
C material constants, this subroutine calculates the returned
C stress, the plastic strain increment and the increment isotropic
C equivalent plasticity. Linear hardening is included
C
C
C in {stress} - incoming stress vector (f>0.0; iso)
C d - elastic constitutive matrix
C k - INTEGER material constant
C c - REAL material constant
C y0 - initial yield strength
C h - material linear hardening parameter
C teps - total equivalent plastic strain (iso)
C out {stress} - updated stress vector (iso)
C {dplastic} - increment plastic strain vector (iso)
C lambda - plastic multiplier
C y2 - yield strength at end of increment
C dep - inc. isotropic equivalent plasticity
C.....
subroutine PLASTIC (stress,d,k,c,y0,h,teps,dplastic,lambda,y2,dep)

implicit none

real*8 stress(6),dplastic(6),c,h,lambda,f1,f2,tol,j2,j3,
& dfda,d2fd2a,d2fdoda,dfdo,d2fd2o,d2fdado,a(6),a2(6),a3(6),
& c2,c3,d(6,6),da(6),ada(1),dlambda,stest(6),ep,teps,

```

```

&      volstrs,s2(6),scratch(1,1),y0,y2,dptest(6),dep,o,y1

      integer k,i

c ... Initialise parameters...
      volstrs=(stress(1)+stress(2)+stress(3))/3.0D0
      do 10 i=1,6
        dplastic(i)=0.0D0
10    continue
      dep=0.0D0
      y1=y0+h*teps

c ... Initialise convergence parameters:-
c      f1 -> yield function value at beginning of iteration
c      f2 -> " " " " end " "
c      tol -> maximum allowable value of f2 for acceptable
c            convergence to yield surface

      tol=1.0D-1
      f2=1.0D300
      lambda=0.0D0

c ... stress return
2000 if ( dabs(f2) .gt. tol) then
c ...      Evaluate yield function, J2, J3 and theta
      call YF(stress,k,c,y1,f1,j2,j3,o)

c ...      Evaluate derivatives of yield function wrt sqrt(J2) & theta
      call DERIVS(o,dsqrt(j2),k,c,dfda,d2fd2a,d2fdoda,dfdo,
&              d2fd2o,d2fdado)

c ...      Evaluate flow vector {a}
      call FVECTOR(stress,j2,dfda,dfdo,o,a,a2,a3,c2,c3)

c ...      Evaluate plastic multiplier
      call MATMUL(d,a,da,6,6,1)
      call MATMUL(a,da,ada,1,6,1)
      dlambda=f1/(ada(1)+h)

c ...      Calculate anticipated stress vector and increment in plastic strain
c      vector for iteration:-
1000  do 20 i=1,6
        stest(i)=stress(i)-dlambda*da(i)
        dptest(i)=dlambda*a(i)
20    continue

c ...      anticipated deviatoric stress:-
      do 30 i=1,3
        s2(i)=stest(i)-volstrs
        s2(i+3)=stest(i+3)
30    continue

c ...      anticipated increment in equiv. plastic strain:-
      call MATMUL(s2,dptest,scratch,1,6,1)
      if (h .lt. 1.0D0) then
        ep=scratch(1,1)/y1
      else
        ep=(-y1+dsqrt(y1**2+4.0D0*h*scratch(1,1)))/(2.0D0*h)
      end if

      if (scratch(1,1) .le. 0.0D0) then
        write(6,*) 'The subincremental plastic work is'
&      ,scratch(1,1)
        ep=1.0D-20
      end if

c ...      update uniaxial yield strength at end of iteration:-
      y2=y1+h*ep

c ...      Confirm f2>0 at anticipated stress, if not revise magnitude of
c      plastic multiplier:-
      call YF(stest,k,c,y2,f2,j2,j3,o)
      if (dabs(f2).lt. tol) then
        goto 3000
      end if
      if (f2 .lt. 0.0D0) then
        dlambda =dlambda*0.995D0
        goto 1000

```

```

        end if

c ...   Update LAMBDA, STRESS & PLASTIC, STRAIN INCREMENT:-
3000   do 40 i=1,6
        stress(i)=stress(i)-dlambda*da(i)
        dplastic(i)=dplastic(i)+dlambda*a(i)
40     continue
        lambda=lambda+dlambda
        dep=dep+ep
        y1=y2

        goto 2000
    end if

910 format (6(d12.5,1x))
    return
end

C.....
c      Subroutine YF returns the yield function value, stress angle
c      (theta) and deviatoric invariants for a given stress
c      vector {stress} and material constants.
c
c      in {stress} - full stress vector
c                k - INTEGER material constant
c                c - REAL material constant
c                y - material uniaxial yield stress
c      out        f - yield function value
c                j2 - second deviatoric invariant
c                j3 - third deviatoric invariant
c                o - theta
C.....
      subroutine YF (stress,k,c,y,f,j2,j3,o)

      implicit none

      real*8 stress(6),c,y,f,j2,j3,o,sij(6,6),s1,s2,s3,const1,
&          pi,phil,phi2,angle,volstrs,scale

      integer i,j,l,k

      scale=1.0D-6

c ... set up deviatoric stress tensor
      volstrs=(stress(1)+stress(2)+stress(3))/3.0D0
      sij(1,1)=stress(1)-volstrs
      sij(2,2)=stress(2)-volstrs
      sij(3,3)=stress(3)-volstrs
      sij(1,2)=stress(4)
      sij(1,3)=stress(5)
      sij(2,1)=stress(4)
      sij(2,3)=stress(6)
      sij(3,1)=stress(5)
      sij(3,2)=stress(6)

c ... deviatoric invariants
      j2=0.0D0
      j3=0.0D0
      do 10 i=1,3
        do 10 j=1,3
          j2=j2+sij(i,j)*sij(i,j)/2.0D0
10     continue
      do 20 i=1,3
        do 20 j=1,3
          do 20 l=1,3
            j3=j3+sij(i,j)*sij(j,l)*sij(l,i)/3.0D0
20     continue

c ... stress angle theta
      angle=(-3.0D0**1.5D0/2.0D0*j3/j2**1.5D0)
      if (dabs(angle) .ge. 1.0D0) then
        angle=dsign(0.999999999999999D0,angle)
      end if
      o=dasin(angle)/3.0D0
      if (o .eq. 0.0D0) then
        o=1.0D-15

```

```

end if

c ... principal deviatoric stresses (multiplied by scaling factor to
c prevent overflow error)
const1=2.0D0/dsqrt(3.0D0)*dsqrt(j2)
pi=2.0D0*dasin(1.0D0)
s1=const1*dsin(o+2.0D0/3.0D0*pi)*scale
s2=const1*dsin(o)*scale
s3=const1*dsin(o+4.0D0/3.0D0*pi)*scale

c ... linearise yield function
phi1=(s1-s2)**(2*k)+(s2-s3)**(2*k)+(s3-s1)**(2*k)
phi2=s1**(2*k)+s2**(2*k)+s3**(2*k)
f=(0.5D0*((1.0D0-c)*phi1+c*3.0D0**(2*k)
& / (2.0D0**(2*k-1)+1.0D0)*phi2))**(1.0D0/(2.0D0*k))/scale
& -y

return
end

C.....
c Subroutine DERIVS to evaluate yield function derivatives
c with respect to theta and A (A=square root of J2)
c
c in f - yield function value
c y - uniaxial yield stress
c o - theta
c a - square root of J2
c k - INTEGER material constant
c c - REAL material constant
c out dfda-d2fdado - yield function derivatives
C.....

subroutine DERIVS (o,a,k,c,dfda,d2fd2a,d2fdoda,dfdo,
& d2fd2o,d2fdado)

implicit none

real*8 o,a,c,dfda,d2fd2a,d2fdoda,dfdo,d2fd2o,d2fdado,pi,al,a2,
& f1,f2,f3,f4,f5,f6,f7,f8,f9,f10,f11,f12,phi,aa,
& const1,const2,dgda,d2gd2a,d2gdoda,dgdo,d2gd2o

integer k

c ... yield function derivatives (polynomial)

c Define working constants
aa=a
a=1.0D0
pi=2.0D0*dasin(1.0D0)
al=2.0D0/3.0D0*a*dsqrt(3.0D0)
a2=c*3.0D0**(2*k)/(2.0D0**(2*k-1)+1.0D0)
f1=(al*(dcos(o+pi/6.0D0)-dsin(o))**(2*k)
f2=(-dsin(o+pi/6.0D0)-dcos(o))/(dcos(o+pi/6.0D0)-dsin(o))
f3=(al*(dsin(o)+dsin(o+pi/3.0D0))**(2*k)
f4=(dcos(o)+dcos(o+pi/3.0D0))/(dsin(o)+dsin(o+pi/3.0D0))
f5=(al*(-dsin(o+pi/3.0D0)-dcos(o+pi/6.0D0))**(2*k)
f6=(-dcos(o+pi/3.0D0)+dsin(o+pi/6.0D0))
& /(-dsin(o+pi/3.0D0)-dcos(o+pi/6.0D0))
f7=(al*dcos(o+pi/6.0D0))**(2*k)
f8=dtan(o+pi/6.0D0)
f9=(al*dsin(o))**(2*k)/dtan(o)
f10=(-al*dsin(o+pi/3.0D0))**(2*k)/dtan(o+pi/3.0D0)
f11=(al*dsin(o))**(2*k)/(dtan(o))**2
f12=(-al*dsin(o+pi/3.0D0))**(2*k)/(dtan(o+pi/3.0D0))**2

c dfda
c ----
dfda=(1.0D0-c)*(2.0D0*f1*k/a+2.0D0*f3*k/a
& +2.0D0*f5*k/a)
& +a2
& *(2.0D0*f7*k/a+2.0D0*(al*dsin(o))**(2*k)*k/a
& +2.0D0*((-al)*dsin(o+pi/3.0D0))**(2*k)*k/a)

c d2fd2a

```

```

c
c -----
d2fd2a=(1.0D0-c)
&   *(4.0D0*f1*(k/a)**2-2.0D0*f1*k/(a**2)
&     +4.0D0*f3*(k/a)**2-2.0D0*f3*k/(a**2)
&     +4.0D0*f5*(k/a)**2-2.0D0*f5*k/a**2)
&   +a2
&   *(4.0D0*f7*(k/a)**2-2.0D0*f7*k/a**2
&     +4.0D0*(a1*dsin(o))** (2*k)*(k/a)**2
&     -2.0D0*(a1*dsin(o))** (2*k)*k/a**2
&     +4.0D0*((-a1)*dsin(o+pi/3.0D0))** (2*k)*(k/a)**2
&     -2.0D0*((-a1)*dsin(o+pi/3.0D0))** (2*k)*k/a**2)

c   d2fdoda
c -----

d2fdoda=(1.0D0-c)
&   *(4.0D0*f1*k**2/a*f2
&     +4.0D0*f3*k**2/a*f4
&     +4.0D0*f5*k**2/a*f6)
&   +a2
&   *(-4.0D0*f7*k**2/a*f8
&     +4.0D0*f9*k**2/a
&     +4.0D0*f10*k**2/a)

c   d2fdado
c -----
d2fdado=d2fdoda

c   dfdo
c -----
dfdo=(1.0D0-c)
&   *(2.0D0*f1*k*f2
&     +2.0D0*f3*k*f4
&     +2.0D0*f5*k*f6)
&   +a2
&   *(-2.0D0*f7*k*f8
&     +2.0D0*f9*k
&     +2.0D0*f10*k)

c   d2fd2o
c -----
d2fd2o=(1.0D0-c)
&   *(4.0D0*f1*k**2*f2**2
&     -2.0D0*f1*k
&     -2.0D0*f1*k*f2**2
&     +4.0D0*f3*k**2*f4**2
&     -2.0D0*f3*k
&     -2.0D0*f3*k*f4**2
&     +4.0D0*f5*k**2*f6**2
&     -2.0D0*f5*k
&     -2.0D0*f5*k*f6**2)
&   +a2
&   *(4.0D0*f7*k**2*f8**2-2.0D0*f7*k
&     -2.0D0*f7*k*f8**2+4.0D0*f11*k**2
&     -2.0D0*(a1*dsin(o))** (2*k)*k-2.0D0*f11*k
&     +4.0D0*f12*k**2-2.0D0*(-a1*dsin(o+pi/3.0D0))** (2*k)*k
&     -2.0D0*f12*k)

c ... yield function derivatives (linearised)
const1=1.0D0/(2.0D0** (1.0D0/(2.0D0*k)+1.0D0)*k)
const2=1.0D0/(2.0D0*k)-1.0D0
phi= (2.0D0*a/dsqrt(3.0D0))** (2*k)
&   *((1.0D0-c)
&     *((dsin(o+2.0D0*pi/3.0D0)-dsin(o))** (2*k)
&       +(dsin(o)-dsin(o+4.0D0*pi/3.0D0))** (2*k)
&       +(dsin(o+4.0D0*pi/3.0D0)-dsin(o+2.0D0*pi/3.0D0))** (2*k)))
&   +a2
&   *((dsin(o+2.0D0*pi/3.0D0))** (2*k)
&     +(dsin(o))** (2*k)
&     +(dsin(o+4.0D0*pi/3.0D0))** (2*k)))
dgdo=const1*phi**const2*dfdo
d2gd2o=const1*(const2*phi** (const2-1.0D0)*dfdo**2
&   +phi**const2*d2fd2o)
dgda=const1*phi**const2*dfda
d2gd2a=const1*(const2*phi** (const2-1.0D0)*dfda**2

```

```

&      +phi**const2*d2fd2a)
d2gdoda=const1*(const2*phi**(const2-1.0D0)*dfda*dfdo
&      +phi**const2*d2fdoda)

dfdo=dgdo*aa
d2fd2o=d2gd2o*aa
d2fdoda=d2gdoda
d2fdado=d2gdoda
dfda=dgda
d2fd2a=d2gd2a/aa

return
end
C.....
c      Subroutine FVECTOR returns yield surface flow-vector wrt
c      full Cauchy stress tensor
c
c      in {stress}      - full stress vector
c      j2              - second deviatoric stress invariant
c      dfda,dfdo      - yield surface derivatives wrt A (sqrt(j2))
c                    - and theta
c      o              - theta
c      out {a}        - yield surface flow vector wrt full stress
c      {a2},{a3}      - flow vector sub-vectors
c      c2,c3          - flow vector sub-coefficients
C.....
      subroutine FVECTOR (stress,j2,dfda,dfdo,o,a,a2,a3,c2,c3)

      implicit none

      real*8  stress(6),s(6),j2,dfda,dfdo,o,a(6),
&           a2(6),a3(6),c2,c3,s11,s22,s33,s12,s13,s23,volstrs

      integer i

      volstrs=(stress(1)+stress(2)+stress(3))/3.0D0
      do 10 i=1,3
        s(i)=stress(i)-volstrs
        s(i+3)=stress(i+3)
10 continue
      s11=s(1)
      s22=s(2)
      s33=s(3)
      s12=s(4)
      s13=s(5)
      s23=s(6)

c ... Flow Vector {a}
c -----
      do 20 i=1,3
        a2(i)=s(i)/(2.0D0*dsqrt(j2))
        a2(i+3)=s(i+3)/(2.0D0*dsqrt(j2))*2.0D0
20 continue

      a3(1)=s22*s33-s23**2+j2/3.0D0
      a3(2)=s11*s33-s13**2+j2/3.0D0
      a3(3)=s11*s22-s12**2+j2/3.0D0
      a3(4)=(s23*s13-s33*s12)*2.0D0
      a3(5)=(s12*s23-s22*s13)*2.0D0
      a3(6)=(s13*s12-s11*s23)*2.0D0

      c2=dfda-dtan(3.0D0*o)*dfdo/dsqrt(j2)
      c3=-dsqrt(3.0D0)/(2.0D0*dcos(3.0D0*o)*j2**(3.0D0/2.0D0))*dfdo

      do 30 i=1,6
        a(i)=c2*a2(i)+c3*a3(i)
30 continue

      return
      end

```

```

C.....
c   Subroutine FV_DER returns flow-vector derivative wrt full Cauchy .
c   stress .
c .
c   in {stress}           - full stress vector .
c       j2                - second deviatoric stress invariant .
c       d2fd2a-d2fdado    - yield surface derivatives wrt A (sqrt(j2)) .
c                           and theta .
c       o                  - theta .
c       c2,c3             - flow vector coefficients .
c       {a2},{a3}         - flow vector sub-vectors .
c   out [b]               - flow vector derivative .
C.....
      subroutine FV_DER (stress,j2,d2fd2a,d2fdoda,dfdo,d2fd2o,d2fdado,
&                      o,c2,c3,a2,a3,b)

      implicit none

      real*8  stress(6),s(6),j2,d2fd2a,d2fdoda,dfdo,d2fd2o,d2fdado,
&           o,c2,c3,b(6,6),a2(6),a3(6),s11,s22,s33,s12,s13,s23,
&           a2a2(6,6),a2a3(6,6),a3a2(6,6),a3a3(6,6),ss(6,6),b1(6,6),
&           delta(6,6),b2(6,6),c22,c33,c23,c32,volstrs

      integer i,j

      volstrs=(stress(1)+stress(2)+stress(3))/3.0D0
      do 5 i=1,3
         s(i)=stress(i)-volstrs
         s(i+3)=stress(i+3)
5      continue
      s11=s(1)
      s22=s(2)
      s33=s(3)
      s12=s(4)
      s13=s(5)
      s23=s(6)

c ... modify {s} to ensure correct TENSOR multiplication
      do 10 i=1,3
         s(i+3)=s(i+3)*2.0D0
10     continue

c ... calculate [a2a2],[a2a3],[a3a2],[a3a3] & [SS] matrices
      call MATMUL(a2,a2,a2a2,6,1,6)
      call MATMUL(a2,a3,a2a3,6,1,6)
      call MATMUL(a3,a2,a3a2,6,1,6)
      call MATMUL(a3,a3,a3a3,6,1,6)
      call MATMUL(s,s,ss,6,1,6)

c ... [b1]
      do 20 i=1,6
         do 20 j=1,6
            delta(i,j)=0.0D0
20     continue
      do 30 i=1,3
         do 30 j=1,3
            delta(i,j)=-1.0D0/3.0D0
30     continue
      do 40 i=1,3
         delta(i,i)=2.0D0/3.0D0
         delta(i+3,i+3)=2.0D0
40     continue
      do 50 i=1,6
         do 50 j=1,6
            b1(i,j)=delta(i,j)/(2.0D0*dsqrt(j2))-
&                ss(i,j)/(4.0D0*j2**(3.0D0/2.0D0))
50     continue

c ... [b2]
      do 60 i=1,6
         do 60 j=1,6
            b2(i,j)=0.0D0
60     continue
      b2(1,1)=s11*2.0D0/3.0D0
      b2(2,2)=s22*2.0D0/3.0D0
      b2(3,3)=s33*2.0D0/3.0D0
      b2(4,4)=s33*(-2.0D0)

```

```

b2(5,5)=s22*(-2.0D0)
b2(6,6)=s11*(-2.0D0)
b2(1,2)=s33*2.0D0/3.0D0
b2(1,3)=s22*2.0D0/3.0D0
b2(1,4)=s12*2.0D0/3.0D0
b2(1,5)=s13*2.0D0/3.0D0
b2(1,6)=s23*(-4.0D0/3.0D0)
b2(2,1)=b2(1,2)
b2(2,3)=s11*2.0D0/3.0D0
b2(2,4)=s12*2.0D0/3.0D0
b2(2,5)=s13*(-4.0D0/3.0D0)
b2(2,6)=s23*2.0D0/3.0D0
b2(3,1)=b2(1,3)
b2(3,2)=b2(2,3)
b2(3,4)=s12*(-4.0D0/3.0D0)
b2(3,5)=s13*2.0D0/3.0D0
b2(3,6)=s23*2.0D0/3.0D0
b2(4,1)=b2(1,4)
b2(4,2)=b2(2,4)
b2(4,3)=b2(3,4)
b2(4,5)=s23*2.0D0
b2(4,6)=s13*2.0D0
b2(5,1)=b2(1,5)
b2(5,2)=b2(2,5)
b2(5,3)=b2(3,5)
b2(5,4)=b2(4,5)
b2(5,6)=s12*2.0D0
b2(6,1)=b2(1,6)
b2(6,2)=b2(2,6)
b2(6,3)=b2(3,6)
b2(6,4)=b2(4,6)
b2(6,5)=b2(5,6)

c ... C22, C33, C23, C32

c22=d2fdoda*dtan(3.0D0*o)/dsqrt(j2)+d2fd2a+
& 3.0D0*dtan(3.0D0*o)/(j2*(dcos(3.0D0*o))**2)*dfdo+
& dtan(3.0D0*o)/j2*dfdo+d2fd2o*(dtan(3.0D0*o))**2/j2-
& dtan(3.0D0*o)/dsqrt(j2)*d2fdado

c33=3.0D0*(3.0D0*dfdo*dtan(3.0D0*o)+d2fd2o)/
& (4.0D0*(dcos(3.0D0*o))**2*j2**3)

c23=dsqrt(3.0D0)/(2.0D0*dcos(3.0D0*o)*j2*(3.0D0/2.0D0))*
& (d2fd2o*dtan(3.0D0*o)/dsqrt(j2)-d2fdoda)+
& 3.0D0*dsqrt(3.0D0)/(2.0D0*(dcos(3.0D0*o))**3*j2**2)*dfdo

c32=c23

c ... flow vector derivative
do 70 i=1,6
do 70 j=1,6
b(i,j)=c2*b1(i,j)+c3*b2(i,j)+c22*a2a2(i,j)+
& c23*a2a3(i,j)+c32*a3a2(i,j)+c33*a3a3(i,j)
70 continue

return
end

C.....
c Subroutine TANMOD: Returns TANGENT MODULUS .
c .
c in lambda - plasticity modulus .
c e,v,h - material constants .
c {a} - flow vector wrt Cauchy stress .
c {b} - flow vector derivative wrt Cauchy stress .
c out [ddsdde]- tangent modulus .
C.....
subroutine TANMOD (lambda,e,v,h,a,b,ddsdde)

implicit none

real*8 e,h,v,lambda,c(6,6),ddsdde(6,6),
& ident(6,6),a(6),b(6,6),d(6,6),
& daad(6,6),ada(6,6),cb(6,6),icb(6,6),
& invicb(6,6),da(6,1),atd(1,6)

integer i,j

```

```

c ... Load [c], elastic constitutive matrix
  do 10 i=1,6
    do 10 j=1,6
      c(i,j)=0.0D0
  10 continue
  do 20 i=1,3
    do 20 j=1,3
      c(i,j)=v
  20 continue
  do 30 i=1,3
    c(i,i)=1.0D0-v
    c(i+3,i+3)=(1.0D0-2.0D0*v)/2.0D0
  30 continue
  do 40 i=1,6
    do 40 j=1,6
      c(i,j)=c(i,j)*e/(1.0D0+v)/(1.0D0-2.0D0*v)
  40 continue

c ... Define [I]
  do 50 i=1,6
    do 50 j=1,6
      ident(i,j)=0.0D0
  50 continue
  do 60 i=1,6
    ident(i,i)=1.0D0
  60 continue

c ... Calculate [D]

  call MATMUL(c,b,cb,6,6,6)

  do 70 i=1,6
    do 70 j=1,6
      icb(i,j)=ident(i,j)+lambda*cb(i,j)
  70 continue

  call MATINV(icb,invicb)
  call MATMUL(invicb,c,d,6,6,6)

c ... Calculate [ddsdde]
  call MATMUL(d,a,da,6,6,1)
  call MATMUL(a,d,atd,1,6,6)
  call MATMUL(a,da,ada,1,6,1)
  call MATMUL(da,atd,daad,6,1,6)

  do 80 i=1,6
    do 80 j=1,6
      daad(i,j)=daad(i,j)/(ada(1,1)+h)
  80 continue

  do 90 i=1,6
    do 90 j=1,6
      ddsdde(i,j)=d(i,j)-daad(i,j)
  90 continue

  return
  end

C.....
c Subroutine ELASTIC:-
c Returns Elastic Constitutive matrix and updated Stress Vector
c
c in {dstran} - incremental strain
c {stress} - stress vector at beginning of increment [Pa]
c e, v - material constants
c out [ddsdde] - elastic constitutive matrix
c {stress} - updated stress vector
C.....
subroutine ELASTIC (ddsdde,dstran,stress,e,v)

  implicit none

  real*8 ddsdde(6,6),dstran(6),stress(6),dstress(6),e,v
  integer i,j

c ... Load [ddsdde]
  do 10 i=1,6

```

```

        do 10 j=1,6
            ddsdde(i,j)=0.0D0
10 continue
        do 20 i=1,3
            do 20 j=1,3
                ddsdde(i,j)=v
20 continue
        do 30 i=1,3
            ddsdde(i,i)=1.0D0-v
            ddsdde(i+3,i+3)=(1.0D0-2.0D0*v)/2.0D0
30 continue
        do 40 i=1,6
            do 40 j=1,6
                ddsdde(i,j)=ddsdde(i,j)*e/(1.0D0+v)/(1.0D0-2.0D0*v)
40 continue

c ... Update {STRESS}
call MATMUL(ddsdde,dstran,dstress,6,6,1)
do 50 i=1,6
    stress(i)=stress(i)+dstress(i)
50 continue

return
end

C.....
c Subroutine MATMUL : Matrix multiplication
c CC(ii,kk)=AA(ii,jj)*BB(jj,kk)
c
c in AA - iixjj matrix
c BB - jjxkk matrix
c out CC - iixkk matrix
C.....
subroutine MATMUL (aa,bb,cc,ii,jj,kk)

implicit none

integer i,j,k,ii,jj,kk
real*8 aa(ii,jj),bb(jj,kk),cc(ii,kk),sum

do 10 i=1,ii
    do 10 k=1,kk
        sum=0.0D0
        do 20 j=1,jj
            sum=sum+aa(i,j)*bb(j,k)
20
10 cc(i,k)=sum

return
end

C.....
c Subroutine MATINV : Calculate inverse of 6x6 matrix
c
c in mat - 6x6 non-singular matrix
c out invmat - inverse of mat
C.....
subroutine MATINV (matx,invmat)

implicit none

real*8 matx(6,6),mat(6,6),invmat(6,6),z
integer i,j,k

do 10 i=1,6
    do 10 j=1,6
        mat(i,j)=matx(i,j)
10 continue

do 20 i=1,6
    do 30 j=1,6
        invmat(i,j)=0.0D0
30 continue
    invmat(i,i)=1.0D0
20 continue

do 40 k=1,6
    do 50 i=1,6
        if (i.ne.k) then
            z=mat(i,k)/mat(k,k)
            do 70 j=1,6

```

```

        mat(i,j)=mat(i,j)-mat(k,j)*z
        invmat(i,j)=invmat(i,j)-invmat(k,j)*z
70      continue
        end if
50      continue
        z=mat(k,k)
        do 60 j=1,6
            mat(k,j)=mat(k,j)/z
            invmat(k,j)=invmat(k,j)/z
60      continue
40      continue

        return
        end
```

University of Cape Town

APPENDIX H

FORTRAN 77 LISTING: ISO-ERROR ROUTINE

```
C .....  
C   This routine produces a matrix for iso-error contour plotting  
C  
C   * in {spoint} - selected stress point on yield surface for  
C                 error plot [MPa]  
C                 k - INTEGER material constant  
C                 c - REAL material constant  
C                 y - material uniaxial yield strength  
C   * out      [m] - 100x100 iso-error matrix in file PLOT.PRN  
C  
C   * Subroutines called:-  
C  
C     -POINT. For given stress increments in the normal and tangent  
C     directions and a starting stress point, this routine calculates  
C     the resultant stress vector and then returns the corresponding  
C     increment strain.  
C  
C     -UMAT+associated subroutines. Karafillis-Boyce Anisotropic  
C     User Material  
C  
C                                     G.D.Thomas 27 May 1996  
C .....  
C   implicit none  
  
C   integer k,nn,i,j,p,n,ntens,nstatv,nprops,ndi,nshr,noel,npt,layer,  
C   & kspt,kstep,kinc,q  
  
C   real*8  f,j2,j3,o,dfda,d2fd2a,d2fdoda,dfdo,d2fd2o,d2fdado,  
C   & a(6),a2(6),a3(6),c2,c3,dn,dt,h,  
C   & e,poisson,str1(6),str1000(6),  
C   & dot(1,1),error,dstran(6),nmax,tmax,  
C   & spoint(6),c,y,stress(6),m(100,100),  
C   & statev,ddsdde,sse,spd,scd,rpl,ddsddt,drplde,drpldt,  
C   & stran,time,dtime,temp,dtemp,predef,dpred,  
C   & props,coords,drot,pnewdt,ttime,  
C   & celent,dfgrdo,dfgrd1,tmin,sdif(6),norm(1,1)  
  
C   character*8 cmname  
  
C   dimension statev(11),ddsdde(6,6),ddsddt(6),drplde(6),  
C   & stran(6),time(2),predef(1),dpred(1),  
C   & props(15),coords(3),drot(3,3),dfgrdo(3,3),  
C   & dfgrd1(3,3)  
  
C   nprops=15  
C   nstatv=11  
C   ntens=6  
  
C ... specify iso-error matrix dimension:-  
C   nn=100
```

```

c                               USER INPUT
c .....
c   define stress point in PRINCIPAL STRESS SPACE [MPa]
c   and material constants:-
c   spoint(1)=-293.00D0
c   spoint(2)=-293.00D0
c   spoint(3)=00.00D0
c
c   e=73.0D9
c   poisson=0.33
c   y=293.0D6
c   h=5.0D8
c
c   k=6
c   c=0.3D0
c .....
c   y=y/1.0D6
c   h=h/1.0D6
c
c   open (unit=10,file='plot.prn',status='unknown',
c   &      access='sequential')
c ... ZERO {stress},{str1},{str1000},total {strain}, total {plastic strain}
c   & {spoint} shear terms:-
c   do 10 p=1,6
c       stress(p) =0.0D0
c       str1(p)   =0.0D0
c       str1000(p)=0.0D0
c       stran(p)  =0.0D0
c       statev(p) =0.0D0
c   10 continue
c   spoint(4)=0.0D0
c   spoint(5)=0.0D0
c   spoint(6)=0.0D0
c ... von Mises Equivalent Stress & Equivalent Plastic Strain
c   statev(7)=0.0D0
c   statev(8)=0.0D0
c ... Boyce Effective Stress & Equivalent Plastic Strain
c   statev(9)= 0.0D0
c   statev(10)=0.0D0
c   statev(11)=0.0D0
c ... set up props matrix:-
c   E, poisson, H, Y, k, c, lun
c   props(1)=e
c   props(2)=poisson
c   props(3)=h*1.0D6
c   props(4)=y*1.0D6
c   props(5)=k
c   props(6)=c
c   props(7)=166
c ... IPE Transformation Tensor [L] parameters: cc, alpha1, alpha2,
c   gamma1, gamma2, gamma3
c   props(8)=2.0D0/3.0D0
c   props(9)=1.0D0
c   props(10)=1.0D0
c   props(11)=3.0D0/2.0D0
c   props(12)=3.0D0/2.0D0
c   props(13)=3.0D0/2.0D0
c ... determine NORMAL {a} to yield surface at selected stress point:-
c   call YF(spoint,k,c,y,f,j2,j3,o)
c   write(6,*) 'f0=',f
c   if (dabs(f) .gt. 1.0D-2 ) then
c       write(6,*) 'WARNING: Stress point not on Yield Surface!'
c       stop
c   end if
c   call DERIVS(f,y,o,dsqrt(j2),k,c,dfda,d2fd2a,d2fdoda,dfdo,
c   &          d2fd2o,d2fdado)
c   call FVECTOR(spoint,j2,dfda,dfdo,o,a,a2,a3,c2,c3)
c   if ((dabs(a(4))+dabs(a(5))+dabs(a(6))) .gt. 1.0D-6) then
c       write(6,*) 'WARNING :Flow vector has shear components'
c       stop

```

```

endif
c ... STRESS RANGE for plots (expressed as ratio of stress/y):-
      nmax=6.0D0
      tmin=-3.0D0
      tmax=3.0D0

c ... NORMAL & TANGENTIAL stress INCREMENTS [MPa]:-
      dn=nmax/nn*y
      dt=(tmax-tmin)/nn*y

c ... for each normal and tangent stress increment complete the stress
c return for n=1 and n=1000 and then calculate error:-
      n=1000
      do 20 i=0,nn-1
        do 20 j=0,nn-1
          call POINT(dn*(i),tmin*y+dt*(j),spoint,
&                   a,e,poisson,dstran)
          call UMAT(str1,statev,ddsdde,sse,spd,scd,rpl,ddsddt,
&                 drplde,drpldt,stran,dstran,time,ttime,temp,
&                 dtemp,predef,dpred,cmname,ndi,nshr,ntens,nstatv,
&                 props,nprops,coords,drot,pnewdt,celent,dfgrdo,
&                 dfgrdl,noel,npt,layer,kspt,kstep,kinc)

c ... reset {statev} and {stran} to ZERO:-
      do 25 p=1,11
        statev(p)=0.0D0
25      continue
      do 26 p=1,6
        stran(p)=0.0D0
26      continue

      do 30 p=1,6
        dstran(p)=dstran(p)/n
30      continue

      do 40 p=1,n
        call UMAT(str1000,statev,ddsdde,sse,spd,scd,rpl,
&                 ddsddt,drplde,drpldt,stran,dstran,time,dtime,temp,
&                 dtemp,predef,dpred,cmname,ndi,nshr,ntens,nstatv,props,
&                 nprops,coords,drot,pnewdt,celent,dfgrdo,dfgrdl,noel,
&                 npt,layer,kspt,kstep,kinc)

        do 50 q=1,6
          stran(q)=stran(q)+dstran(q)
50        continue

40      continue
      do 45 q=1,6
        sdif(q)=str1000(q)-str1(q)
45      continue
      call MATMUL(sdif,sdif,norm,1,6,1)
      call MATMUL(str1000,str1000,dot,1,6,1)

      error=dsqrt(norm(1,1)/dot(1,1))*100.0D0
2000     m(i+1,nn-j)=error
      write(6,*) i+1,j+1,error
c ... reset {statev} & {stran} to ZERO:-
      do 35 q=1,11
        statev(q)=0.0D0
35      continue
      do 36 q=1,6
        stran(q)=0.0D0
36      continue

20 continue

      write(10,910) ((m(i,j),i=1,nn),j=1,nn)

900 format (6(d12.5,1x))
910 format (10(f9.2,1x))

      close (unit=10)

      stop
      end

```

```

C.....
c      Subroutine POINT. For given stress increments in the normal and .
c      tangent directions and a starting stress point, this routine .
c      calculates the resultant stress vector and then returns the .
c      corresponding increment strain. .
c      .
c      in      dn      - normal stress increment          [MPa] .
c              dt      - tangential stress increment     [MPa] .
c              {stress0} - initial stress point on yield surface [MPa] .
c              e      - elastic modulus .
c              poisson - poisson ratio .
c              {a}    - flow vector .
c      out    {dstran} - strain vector .
C.....
      subroutine POINT(dn,dt,stress0,a,e,poisson,dstran)

      implicit none

      real*8 dn,dt,stress0(6),dstran(6),a(6),const,normal(3),poisson,
&          tangent(3),e,stress(6),d(6,6),dummy(6),dinv(6,6)

      integer p

      do 10 p=1,6
         dummy(p)=0.0D0
10    continue

      if (dabs(a(1)) .lt. 1.0D-4) then
         normal(1)=0.0D0+stress0(1)
         normal(2)=1.0D0/dsqrt(2.0D0)*dn+stress0(2)
         normal(3)=-1.0D0/dsqrt(2.0D0)*dn+stress0(3)
      else
         const=1.0D0/dsqrt(2.0D0*(a(1)**2+a(2)**2+a(1)*a(2))
&          /(a(1)**2))
         normal(1)=dn*const+stress0(1)
         normal(2)=a(2)/a(1)*dn*const+stress0(2)
         normal(3)=-(a(1)+a(2))/a(1)*dn*const+stress0(3)
      end if
      if ( dabs(2.0D0*a(2)+a(1)) .lt. 1.0D-4) then
         tangent(1)=0.0D0+stress0(1)
         tangent(2)=1.0D0/dsqrt(2.0D0)*dt+stress0(2)
         tangent(3)=-1.0D0/dsqrt(2.0D0)*dt+stress0(3)
      else
         const=1.0D0/dsqrt(6.0D0*(a(1)**2+a(2)**2+a(1)*a(2))
&          /(2.0D0*a(2)+a(1))**2)
         tangent(1)=dt*const+stress0(1)
         tangent(2)=-dt*const*(2.0D0*a(1)+a(2))/(2.0D0*a(2)+a(1))
&          +stress0(2)
         tangent(3)=-dt*const*(a(2)-a(1))/(2.0D0*a(2)+a(1))+stress0(3)
      end if

c ... setup stress vector for return [Pa]:-
1000 do 20 p=1,3
         stress(p)=(normal(p)+tangent(p)-stress0(p))*1.0D6
         stress(p+3)=0.0D6
20    continue

c ... determine strain vector for UMAT:-
      call ELASTIC(d,dummy,dummy,e,poisson)
      call MATINV(d,dinv)
      call MATMUL(dinv,stress,dstran,6,6,1)

900 format(d12.5,1x,d12.5,1x,d12.5,1x,d12.5,1x,d12.5,1x,d12.5)

      return
      end

```

APPENDIX I

ABAQUS V5.4 INPUT FILE: DEEP DRAWING PROBLEM

```
*HEADING, UNSYMM
ANISO :k=3,c=0.3513
**
*WAVEFRONT MINIMIZATION,NODES,METHOD=2
1,22073
**
*RESTART,WRITE, OVERLAY
**
*NODE
1, -0.004243, -0.004243
9, 0., -0.006
17, 0.004243, -0.004243
801, -0.006, 0.
817, 0.006, 0.
1601, -0.004243, 0.004243
1609, 0., 0.006
1617, 0.004243, 0.004243
**
*NGEN, NSET=BOT
1, 9, 1
9, 17, 1
*NGEN, NSET=TOP
1601, 1609, 1
1609, 1617, 1
*NGEN, NSET=CENTRE
801, 817, 1
**
*NFILL, NSET=MID
BOT, CENTRE, 8, 100
CENTRE, TOP, 8, 100
**
**
*NODE
2161, -0.004243, -0.004243
2193, 0., -0.006
2225, 0.004243, -0.004243
2129, -0.006, 0.
2001, 0.006, 0.
2257, 0.006, 0.
2097, -0.004243, 0.004243
2065, 0., 0.006
2033, 0.004243, 0.004243
14001, 0.0275, 0.
14257, 0.0275, 0.
**
*NGEN, NSET=OUTER, LINE=C
14001, 14257, 2, , 0., 0., 0., 0., 0., 1.
**
*NGEN
2001, 14001, 600
2033, 14033, 600
2065, 14065, 600
2097, 14097, 600
2129, 14129, 600
2161, 14161, 600
2193, 14193, 600
```

```

2225, 14225, 600
2257, 14257, 600
**
*NGEN, NSET=ANNULUS
2001, 2033, 8
2033, 2065, 8
2065, 2097, 8
2097, 2129, 8
2129, 2161, 8
2161, 2193, 8
2193, 2225, 8
2225, 2257, 8
**
*NGEN, NSET=ANNULUS
2601, 2633, 4
2633, 2665, 4
2665, 2697, 4
2697, 2729, 4
2729, 2761, 4
2761, 2793, 4
2793, 2825, 4
2825, 2857, 4
**
*NGEN, NSET=ANNULUS
3201, 3233, 2
3233, 3265, 2
3265, 3297, 2
3297, 3329, 2
3329, 3361, 2
3361, 3393, 2
3393, 3425, 2
3425, 3457, 2
**
*NGEN, NSET=INNER
3201, 3233, 2
3233, 3265, 2
3265, 3297, 2
3297, 3329, 2
3329, 3361, 2
3361, 3393, 2
3393, 3425, 2
3425, 3457, 2
**
*NFill, NSET=ANNULUS
INNER, OUTER, 36, 300
**
*NSET, NSET=BLANK
MID, ANNULUS
**
*NCOPY, OLD SET=BLANK, NEW SET=BLANK, SHIFT, CHANGE NUMBER=20000
0., 0., 0.00027
0., 1., 0.
**
**
*NSET, NSET=YCONST, GENERATE
809, 817, 2
2001, 14001, 600
20809, 20817, 2
22001, 34001, 300
**
*NSET, NSET=XCONST, GENERATE
809, 1609, 200
2065, 14065, 600
20809, 21609, 200
22065, 34065, 300
**
*ELEMENT, TYPE=C3D8
1, 809, 811, 1011, 1009, 20809, 20811, 21011, 21009
**
*ELGEN, ELSET=BASE
1, 4, 2, 2, 4, 200, 16
**
*ELSET, ELSET=BLANK
BASE
**

```

```

*ELEMENT, TYPE=C3D8
900, 3201, 3801, 3803, 3203, 23201, 23801, 23803, 23203
300, 2001, 2601, 2609, 2009, 22001, 22601, 22609, 22009
600, 2601, 3201, 3205, 2605, 22601, 23201, 23205, 22605
*ELGEN, ELSET=BLANK
300, 8, 8, 8
600, 16, 4, 4
900, 32, 2, 2, 18, 600, 256
**
**
*SURFACE DEFINITION, NAME=BLANKP
BLANK, S2
*SURFACE DEFINITION, NAME=BLANKD
BLANK, S1
*SURFACE DEFINITION, NAME=BLANKH
BLANK, S2
**
**
*NSET, NSET=ZIPBOT, GENERATE
2257, 14257, 600
22257, 34257, 600
*NSET, NSET=ZIPTOP, GENERATE
2001, 14001, 600
22001, 34001, 600
**
*NSET, NSET=ROW1P, GENERATE
2605, 2853, 8
22605, 22853, 8
*NSET, NSET=ROW1A, GENERATE
2601, 2849, 8
22601, 22849, 8
*NSET, NSET=ROW1B, GENERATE
2609, 2857, 8
22609, 22857, 8
**
*NSET, NSET=ROW2P, GENERATE
3203, 3455, 4
23203, 23455, 4
*NSET, NSET=ROW2A, GENERATE
3201, 3453, 4
23201, 23453, 4
*NSET, NSET=ROW2B, GENERATE
3205, 3457, 4
23205, 23457, 4
*MPC
LINEAR, ROW1P, ROW1A, ROW1B
LINEAR, ROW2P, ROW2A, ROW2B
**
*MPC
TIE, 817, 2001
TIE, 1017, 2009
TIE, 1217, 2017
TIE, 1417, 2025
TIE, 1617, 2033
TIE, 1615, 2041
TIE, 1613, 2049
TIE, 1611, 2057
TIE, 1609, 2065
TIE, 1607, 2073
TIE, 1605, 2081
TIE, 1603, 2089
TIE, 1601, 2097
TIE, 1401, 2105
TIE, 1201, 2113
TIE, 1001, 2121
TIE, 801, 2129
TIE, 601, 2137
TIE, 401, 2145
TIE, 201, 2153
TIE, 1, 2161
TIE, 3, 2169
TIE, 5, 2177
TIE, 7, 2185
TIE, 9, 2193
TIE, 11, 2201

```

```

TIE, 13, 2209
TIE, 15, 2217
TIE, 17, 2225
TIE, 217, 2233
TIE, 417, 2241
TIE, 617, 2249
*MPC
TIE, 20817, 22257
TIE, 21017, 22009
TIE, 21217, 22017
TIE, 21417, 22025
TIE, 21617, 22033
TIE, 21615, 22041
TIE, 21613, 22049
TIE, 21611, 22057
TIE, 21609, 22065
TIE, 21607, 22073
TIE, 21605, 22081
TIE, 21603, 22089
TIE, 21601, 22097
TIE, 21401, 22105
TIE, 21201, 22113
TIE, 21001, 22121
TIE, 20801, 22129
TIE, 20601, 22137
TIE, 20401, 22145
TIE, 20201, 22153
TIE, 20001, 22161
TIE, 20003, 22169
TIE, 20005, 22177
TIE, 20007, 22185
TIE, 20009, 22193
TIE, 20011, 22201
TIE, 20013, 22209
TIE, 20015, 22217
TIE, 20017, 22225
TIE, 20217, 22233
TIE, 20417, 22241
TIE, 20617, 22249
**
*NODE, NSET=PUNCH
70000, 0.0, 0.00935, 0.020
*NODE, NSET=HOLDER
80000, 0.0, 0.01685, 0.020
*NODE, NSET=DIE
90000, 0.0, 0.01685, -0.020
**
*RIGID SURFACE, TYPE=AXISYMMETRIC, NAME=DIE, REF NODE=90000, SMOOTH=3.0E-3
0., 0., 0., 0., 0., 10.
START, 0.01685, -0.020
LINE, 0.01685, 0.00
LINE, 0.030, 0.00
**
*RIGID SURFACE, TYPE=AXISYMMETRIC, NAME=HOLDER, REF NODE=80000, SMOOTH=2.0E-3
0.0, 0.0, 0.0, 0., 0., 0.040
START, 0.030, 0.002
LINE, 0.01685, 0.002
LINE, 0.01685, 0.020
**
*RIGID SURFACE, TYPE=AXISYMMETRIC, NAME=PUNCH, REF NODE=70000, SMOOTH=3.0E-3
0., 0., 0.0, 0., 0., 0.070
START, 0.01641, 0.0250
LINE, 0.01641, 0.0065
CIRCL, 0.01191, 0.002, 0.01191, 0.0065
LINE, 0.00, 0.002
**
*CONTACT PAIR, INTERACTION=LUBRIC
BLANKP, PUNCH
BLANKH, HOLDER
BLANKD, DIE
**
*SURFACE INTERACTION, NAME=LUBRIC
*FRICTION
0.00000100000
*SURFACE CONTACT, SOFTENED

```

```

1.E-6, 1.E6
**
*SOLID SECTION, ELSET=BLANK, MATERIAL=A3004
*MATERIAL,NAME=A3004
*USER MATERIAL, CONSTANTS=13, UNSYMM
**ANISOTROPIC MATERIAL CONSTANTS
73.0E9,0.33,5.0E8,293.0E6,3,0.3513,6554,0.6496590997
1.001497,1.1112774,1.5891267,1.5,1.5
**ISOTROPIC MATERIAL CONSTANTS
**73.0E9,0.33,5.0E8,293.0E6,6,0.30,6444,0.66666666667
**1.0,1.0,1.5,1.5,1.5
*DEPVAR
11
**
*BOUNDARY
PUNCH, 1, 2
DIE, 1, 6
HOLDER, 1, 2
HOLDER, 4, 6
PUNCH,4,6
XCONST, 1
YCONST, 2
809, 1, 3
14001, 1, 3
*****
*STEP, NLGEOM, INC=100
Bring holder into contact with blank
*STATIC
0.01, 1., 1.E-6
**
*BOUNDARY
HOLDER, 3, 3, -1.73000100E-3
**
*EL PRINT, FREQUENCY=0
*NODE PRINT, FREQUENCY=0
***PRINT, CONTACT=YES
**
*END STEP
**
*****
*STEP, INC=100, NLGEOM
Replace prescribed holder displacement by applied force
*STATIC
1., 1.0, 1.E-8,
**
*CONTROLS, ANALYSIS=DISCONTINUOUS
*BOUNDARY,OP=NEW
XCONST, 1
YCONST, 2
70000, 1,6
80000, 1, 2
80000, 4, 6
90000, 1, 6
**
*CLOAD
80000, 3, -1.0E3
**
*END STEP
**
*****
*STEP, INC=500, NLGEOM
Displace punch downwards
*STATIC
1.E-2,4.0,1.E-8
**
*BOUNDARY
70000, 3, 3, -0.01585
**
*MONITOR, DOF=1, NODE=14001
*ELPRINT, FREQUENCY=500
SDV9,SDV10,SDV11
**
*NODE FILE,NSET=PUNCH,FREQUENCY=2
RF
**

```

```
*CONTROLS,PARAMETERS=FIELD,FIELD=DISPLACEMENT
2.0E-2,1.0
*CONTROLS,PARAMETERS=TIME INCREMENTATION
10,100
*END STEP
*****
```

University of Cape Town